INFORMATION TO USERS

This manuscript has been reproduced from the microfilm master. UMI films the text directly from the original or copy submitted. Thus, some thesis and dissertation copies are in typewriter face, while others may be from any type of computer printer.

The quality of this reproduction is dependent upon the quality of the copy submitted. Broken or indistinct print, colored or poor quality illustrations and photographs, print bleedthrough, substandard margins, and improper alignment can adversely affect reproduction.

In the unlikely event that the author did not send UMI a complete manuscript and there are missing pages, these will be noted. Also, if unauthorized copyright material had to be removed, a note will indicate the deletion.

Oversize materials (e.g., maps, drawings, charts) are reproduced by sectioning the original, beginning at the upper left-hand corner and continuing from left to right in equal sections with small overlaps. Each original is also photographed in one exposure and is included in reduced form at the back of the book.

Photographs included in the original manuscript have been reproduced xerographically in this copy. Higher quality 6" x 9" black and white photographic prints are available for any photographs or illustrations appearing in this copy for an additional charge. Contact UMI directly to order.

UMI®

Bell & Howell Information and Learning
300 North Zeeb Road, Ann Arbor, MI 48106-1346 USA
800-521-0600

Molecular Dynamics Simulation:
An Investigation into the Short Range Structure of Metaphosphate Glasses

Elizabeth Sourial

A Thesis
in
The Department
of
Chemistry and Biochemistry

Presented in Partial Fulfillment of the Requirements
for the Degree of Master of Science at
Concordia University
Montreal, Quebec, Canada

September 1998

ABSTRACT

Molecular Dynamics Simulation:
An Investigation into the Short Range Structure of Metaphosphate Glasses

Elizabeth Sourial

An investigation into the local environment of three metaphosphate glasses using molecular dynamics simulations is presented. The short range structure of the phosphate and metal networks were determined from pair, cumulative and bond angle distribution functions as well as identifying the types of oxygen ions found within the networks. The short range structure was validated by comparing the results obtained from the simulations to structural properties determined experimentally and found in the literature.

The phosphate network was found to consist of long linear chains of PO_4 tetrahedral units. This type of structure exists in the three metaphosphate glasses, indicating that the modifier has little effect on the structure of the phosphate backbone.

A study of the metal networks revealed that the modifier's field strength plays a significant role in determining the short range order of the metal ions. Results indicate that the lead network has the highest degree of disorder since the lead ion occupies several different local environments compared to the local environments of the magnesium or zinc ions.

Finally, a three body Born-Mayer-Huggins potential model was used to simulate the structure of P_2O_5. This was achieved by developing the pair potential parameters for the P-O and P-P pair and comparing the structure of the simulated crystal to that of the

static P_2O_5 crystal. The P_2O_5 glass was simulated using both the two body potential model as well as the three body model with the developed potential parameters. Results indicate that the three body model improved the short range order of the phosphorus ions.

ACKNOWLEDGEMENTS

I would like to express my gratitude to those persons who made the completion of this thesis possible.

My research supervisor, Dr. J. A. Capobianco, for his guidance and advice.

The members of my thesis committee:

Dr. L. Colebrook

Dr. M. Lawrence

I am also grateful to Dr. Garofalini, for allowing us to use his three body potential.

I would like to extend my warmest thanks to Tania Peres for her untiring support and infinite technical discussions.

Lastly, I wish to thank my family for their encouragement and patience.

TABLE OF CONTENTS

LIST OF FIGURES

LIST OF TABLES

CHAPTER 1

1.0 INTRODUCTION

The chemistry of glasses has been under investigation for over 5000 years and has its roots in ancient Mesopotamia and Egypt. The glassmakers used raw materials such as sea sand, marine shells, and seaweed to extract the essential oxides: SiO_2 and Na_2O. The first glasses produced were sodium glasses. The first decisive change in glass production was the invention of the glass blower's pipe, which occurred around the first century B. C. The next turning point in the history of glass was the introduction of machine production of glass. Many new glasses were developed of which vitreous silica is probably the best known. The study of amorphous phosphates began with the pioneering work of Berzelius and Graham [1] in the early 19^{th} century. Numerous other glass formulations with other elements were tested such as glasses containing B_2O_3. Soon, investigations were aimed at establishing a connection between the composition and the structure of glass. Today, glasses are still being extensively studied as a result of their numerous applications such as communication lasers and smart windows [2,3].

In order to exploit glasses for various applications a detailed understanding of their microstructure is necessary. This will allow the development of a variety of glasses with specific properties that can be used in diverse areas such as nuclear fuel waste immobilization [4], glass lasers [5], and optical fiber amplifiers [6]. Generally, glasses can be defined as solids having a uniform local geometrical arrangement at short distances but lack periodic arrangement at longer distances. In order to provide detailed information on

glass structure various experimental methods such as X-ray and Raman spectroscopy have been employed [7-13]. However, these techniques only reveal average structural characteristics provided by radial distribution functions. Another experimental technique used to study the structure of glasses is Extended X-ray Absorption Fine Structure (EXAFS) [14,15]. EXAFS provides an advantage over other experimental techniques in that it can study the local structure without interference from neighboring atoms. However, even in EXAFS mathematical manipulations to retrieve the structural information such as interatomic bond distances and coordination numbers can conceal the finer details of the structure.

To resolve these problems, we have turned to computational techniques that can provide detailed structural information at the atomic level. Computer simulations are now able to make accurate predictions of the atomic structure of diverse systems such as zeolite catalysts [16] and DNA [17]. However, amorphous materials still represent one of the greatest challenges of such techniques. In this thesis, the application of computer techniques for the study of metaphosphate glasses will be investigated. This will provide a precise understanding of the microstructure in metaphosphate glasses as well as to understand the influence of each element on the metaphosphate glass structure.

1.1 THE STRUCTURE OF GLASSES

Glasses are characterized by certain well defined properties that are common to all glasses but different from those of liquids and crystals. X-ray and neutron experiments show that glasses lack long range periodicity and that they resemble liquids and not crystalline solids in their atomic distributions. This is illustrated in Figure 1.1.1 in which the radial distribution function of a hypothetical material in the glassy state is compared to that in the liquid and the crystalline states [18]. Unlike crystals, glasses do not have a sharp melting point but possess the rigidity characteristic of crystals and the fluidity of the liquid state.

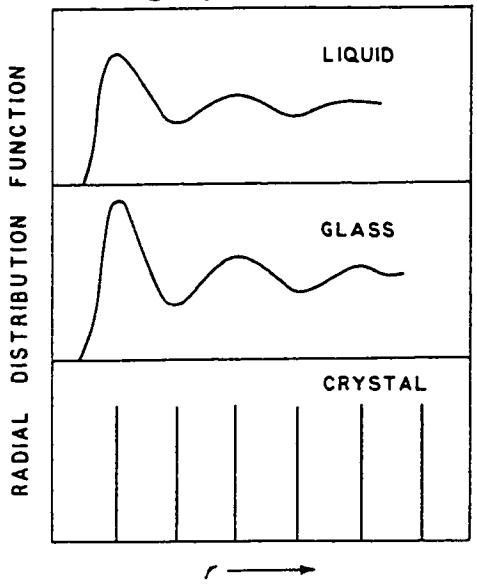

Figure 1.1.1 Comparison of the radial distribution functions of a glass, crystal and liquid After Ref. 18.

Glasses can be defined in several ways. Structurally glasses are defined as "amorphous solids without periodicity in the arrangement of atoms and long range order" [19]. Glasses may also be defined physicochemically as "non-crystalline solids obtained by freezing a

supercooled liquid" [19]. The physicochemical definition is of particular interest since it also describes the process of glass formation.

1.1.1 THE PROCESS OF GLASS FORMATION

The relationship between a liquid, crystal and a glass can be explained by the volume-temperature diagram shown in Figure 1.1.1.1. The process of glass formation begins at high temperatures where a liquid melt is present at A. As the temperature decreases its volume decreases steadily along AB. If the rate of cooling is slow, crystallization will take place at the freezing point (T_f) which is accompanied by a sharp drop in the volume from B to C. Having crystallized, the solid will then continue to decrease in volume along CD as the temperature is cooled. However, if the rate of cooling is sufficiently rapid, crystallization will not take place at T_f and the volume of the now "supercooled" liquid will decrease along BE. At a certain temperature Tg, the slope of the volume-temperature graph will change significantly and continue to decrease along EF, almost parallel to that of the crystalline path CD. It is only below the glass transition temperature that the material is considered to be a glass. Having reached point E, the system is no longer in equilibrium. This can be explained by the following: As the system is cooled, the atoms seek a minimum energy configuration. The time taken for the system to find its energy minimum is called the relaxation time. As the temperature is lowered the relaxation time increases. An unstable state will eventually find its equilibrium state, minimum energy, provided that sufficient time is given for the atoms to find their equilibrium state. Such a process will create a more ordered system (crystals). However, if

the system is cooled very rapidly such that the atoms are unable to find their minimum energy or equilibrium state, only local relaxation will occur and the system will have short range order (glasses). Furthermore, as the system is cooled and its volume decreases, the viscosity of the liquid will continuously increase until it reaches a certain point that the viscosity has become so high that establishing an equilibrium is no longer possible. This is representative of the glassy state.

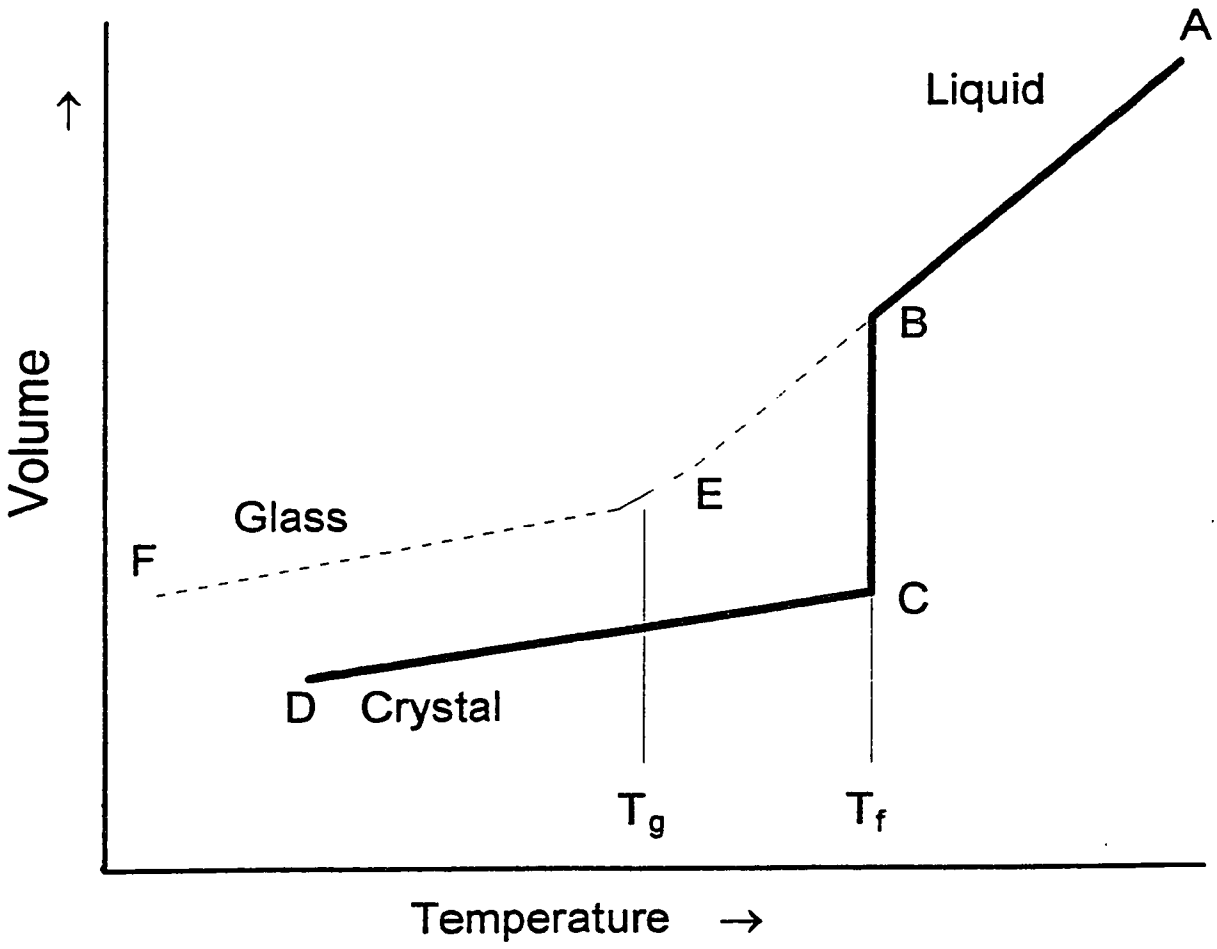

Figure 1.1.1.1 Relationship between the glassy, liquid and solid states.

1.1.2 NETWORK HYPOTHESIS

If one starts from the principle that liquids have a disordered structure, then the same must be true for a glass, which is in essence a frozen liquid. From this, several hypothesis about the structure of glass and the conditions for their formation have been developed. The most significant of these developed by Zachariasen [20] who observed that the energy difference between a glass and a crystal of the same composition is very small. This will result in a similar bonding structure in the glass and in the crystal. For example, PO_4 tetrahedra are observed in both crystalline and glass phosphate structures but in the crystal these tetrahedra are arranged regularly while in the glass they form a random network. This relationship will become more evident in Chapter 5. Figure 1.1.2.1 shows a schematic representation of a hypothetical crystalline and glass structure.

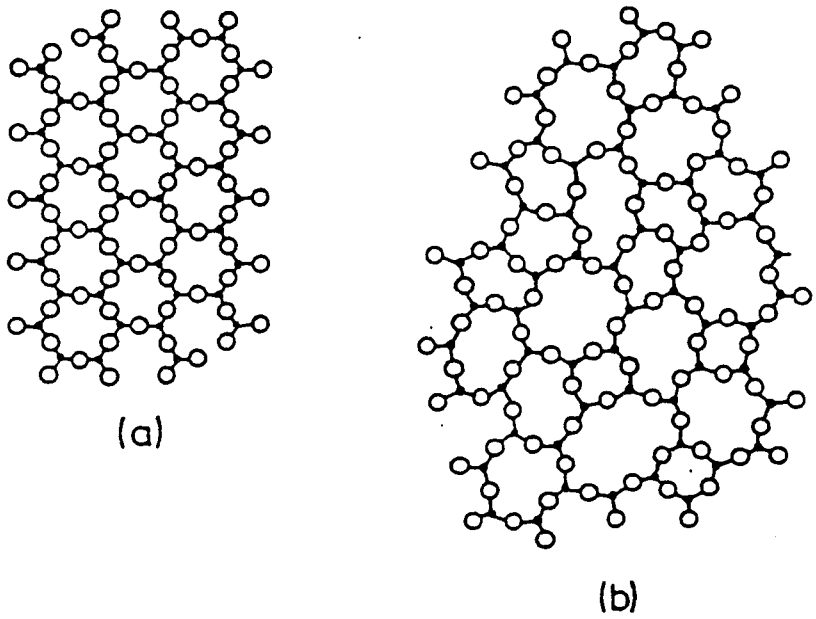

Figure 1.1.2.1 Two-dimensional structural representation of a a) hypothetical crystal and b) hypothetical glass.

From these observations, Zachariasen proposed that an oxide must satisfy the following conditions in order to form a glass:

1) The coordination number of the cation must be small

2) An oxygen ion may not be linked to more than two cations

3) The oxygen polyhedra may share only corners not edges or faces

4) At least three of the corners of every oxygen polyhedron must be shared by other polyhedra

Furthermore, Zachariasen postulated that the non-periodic arrangement of the glass formers will have slight variations in their bond lengths and bond angles while maintaining a defined geometry. Various oxides including P_2O_5 fulfill these conditions. However, the formation of glasses is also possible with the incorporation of several other components such as in binary systems $MO{\cdot}P_2O_5$ where M is a metal ion. The basis of glass formation is the backbone network, which in the example given previously comprises of PO_4 tetrahedrons. Cations that can form network building polyhedra are called network formers. Network formers include Si, B and P atoms. Those cations that break up the network are called network modifiers. Network modifiers include alkalis, alkaline earth and other metal cations such as Mg, Zn and Pb [21]. These modifiers can not form glasses themselves. An example of how these metal ions modify the glass network is shown in Figure 1.1.2.2.

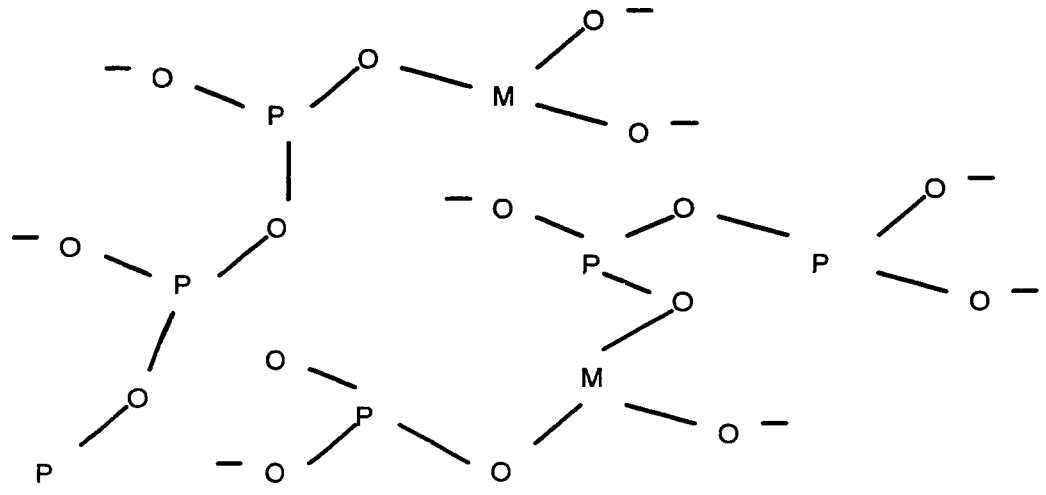

Figure 1.1.2.2 A schematic representation of the modifier effect on a phosphate network.

Zachariasen postulated that these cation modifiers are randomly distributed throughout the glass network. The introduction of a metal significantly changes the glass structure. In pure P_2O_5 glass, the oxygen atoms act only as bridges between neighboring P^{5+} ions to form P-O-P links and are known as bridging oxygens. The addition of a metal will break the phosphorus-oxygen bond forming the network and produce bridges of the type P-O-M, these oxygens are nonbridging oxygens. The formation of nonbridging oxygens

represents the most important influence of the modifiers. The effect of network modifiers is to cause a weakening of the glass structure since the network former determines the strength of the glass. Consequently, the modifying strength of these cations plays an important role in the determination of glass structure, this will become more evident in Chapter 5. Also, with increasing concentration of metal oxide, the phosphate backbone network is more and more disrupted. As metal oxide is added to P_2O_5, the phosphate structural groups pass from the metaphosphate to pyrophosphate and to orthophosphate compositions. That is the MO/P_2O_5 ratio passes from 1 to 2 and finally to 3.

1.2 MOLECULAR DYNAMICS

The study of amorphous materials using experimental and theoretical techniques has a long and rich history. The study of amorphous materials may be approached from various aspects [22], in this thesis we are concerned with the structural and atomic arrangements of the glassy state. Experimentalists have worked to improve the understanding of structure that characterize various glasses. However, to date, experimental methods cannot yield accurate structural information at the atomic level since they can only provide average structural information such as radial distribution functions (RDFs) provided by diffraction methods or very local information derived from extended X-ray absorption fine structure (EXAFS) and nuclear magnetic resonance (NMR) experiments.

One of the major developments in science over the past 40 years concerns the application of computational techniques for the modeling of the structures and properties

of matter at the atomic level. These computer models give detailed information about the structural and dynamic properties of the system. To this end, molecular dynamics (MD) simulation has proven to be a useful method for analyzing the glassy state. This began with the pioneering work of Woodcock, Angell and Cheeseman [23] on the simulation of vitreous silica. Since, there have been numerous MD simulations on vitreous silica [24-27] using both two (Born-Mayer-Huggins) and three body potential models [28-30]. However, little work has been done on simulating phosphate glasses. Consequently, this thesis will focus on the application of molecular dynamics for the modeling of metaphosphate glasses using a two body Born-Mayer-Huggins potential model and will also initiate the development of the parameters to be used in a three body potential model developed by Feuston and Garofalini [31].

1.2.1 THE MODEL FOR MOLECULAR DYNAMICS

Molecular dynamics simulations compute the motion (positions and velocities) of individual molecules in models of solids, liquids or gases. Molecular dynamics is based on the fact that the behavior of a system can be computed if a set of initial conditions (atomic coordinates and velocities) and the forces of interaction that govern the system, are known. The model for molecular interactions is contained in an intermolecular potential energy function. Therefore, the potential function describes the interactions between molecules. In most simulations the intermolecular potential energy function is taken to be the sum of the isolated pair interactions (also called pairwise additivity). Therefore, the first task in modeling is to develop a potential energy function suitable for the system

investigation. In this thesis, a two body Born-Mayer-Huggins potential model developed by Mitra et al. [26] was employed and will be described in detail in Section 3.1. Having developed a model, the molecular dynamics simulation is then concerned with the calculation of the molecular trajectories and the analysis of these trajectories to obtain the properties of interest, which will be described in more detail in Section 3.2.

The molecular model developed by Mitra et al. [32] was developed for the study of silicon dioxide glass. With the use of a Born-Mayer-Huggins pair potential, the authors showed that the ionic model reproduced the structural features consistent with those found experimentally. The validity of the potential model can be seen by the comparison of the simulated radial distribution function with that reported by Woodcock et al. [23] whereby the Si-O peak positions and coordination numbers were in good agreement. For example, they showed a tetrahedral arrangement for the Si-O atomic pair. This demonstrated that the inclusion of covalency in the potential model was not necessary for the correct simulation of the tetrahedral network. Therefore, this model is applicable for the simulation of phosphate systems, which also exhibits a partial covalent character for the P-O bonds. However, some discrepancies were observed using the two body potential model such as a broader O-Si-O bond angle distribution and a higher Si-O-Si bond angle in the simulated glass.

Improvements to this potential model were made by Newell et al. [33] by the inclusion of a three body interaction term which accounts for the partial covalent character of the Si-O bond. Using the three body potential model the authors report an increase in the short range order with a narrower O-Si-O bond angle distribution as well as fewer number of bond defects. The use of a three body potential model for the study of

phosphate glasses has not, to our knowledge, been reported in the literature. Section 5.5 of this thesis will show the development of the necessary parameters used to simulate P_2O_5 glass.

1.2.2 MODELING VERSUS SIMULATION

Before proceeding to Chapter 3, which discusses in more detail the potential model and the simulation procedure used in this thesis, it is important to clarify the difference between a model and a simulation. A **model** attempts to remove any interactions that has little effect or no effect on the values (both input and output) being studied. Consequently a model is simpler than the actual system being studied. For example, in this thesis the systems under investigation are metaphosphate glasses. In a "real' metaphosphate glass, there are complex physical and chemical properties that exist such as their covalent and ionic contributions, electronic charge distribution and polarizability. However, the simulated glass is based only on the ionic contribution between two point charged particles, defined by the potential. These characteristics are only a part of what is present in the "real" metaphosphate glass and thus the model can not mimic all of the properties associated with the "real' glass and is therefore simpler than the system it mimics.

In contrast, a **simulation** is more complicated than the system it is simulating. A simulation imposes constraints such that the values of the output that are being calculated are consistent with those found in the "real" system. For example, computationally this could be achieved by varying the time steps, cooling procedure or thermalization steps. Necessarily, the simulation need not be related to the simulation of a "real" system. That

is, a computational simulation for making a glass does not have to mimic the procedure used to make a "real" glass [34].

In this thesis, a molecular dynamics simulation of various metaphosphate glasses has been performed. The model producing the glass is simpler than a "real" metaphosphate glass because the atoms that comprise the "real" metaphosphate glass are not perfect spheres and their interactions are not merely pairwise. A simulation using the Born-Mayer-Huggins potential model is used to obtain the simulated glass structure.

1.3 THE STRUCTURE OF PHOSPHATE GLASS

As seen in Section 1.1.2, phosphate glasses are made up of a disordered three dimensional phosphate network which is broken up by the presence of cation modifiers. The extent to which the phosphate structure will be broken is dependent on the type of cation modifier present in the glass. To fully understand the effect of the cation modifier on the phosphate system, a fundamental description of the phosphate backbone structure is necessary.

In the single component glass, P_2O_5, a pentavalent phosphorus atom exists and the structure is based on a tetrahedral bond configuration. It is the tetrahedral PO_4 unit that the term phosphate refers to and which forms the basic structure of the glasses studied in this thesis. Detailed X-ray diffraction studies on phosphates [35] have described the basic structure to consist of these PO_4 units linked together by mutual sharing of corners only. No cases of two tetrahedra sharing an edge have been discovered. This observation is

consistent with Zachariasen's Random Network Model (Section 1.1.2). Figure 1.3.1 illustrates how two PO_4 units are corner shared.

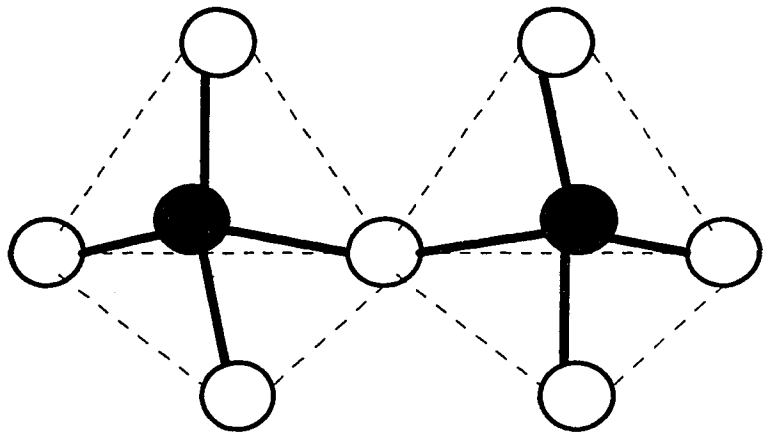

Figure 1.3.1 Corner sharing PO_4 tetrahedral units After Ref. 35.

In accordance with the pentavalent character of phosphorus any single tetrahedron can share a maximum of three of its corners with neighboring tetrahedra through single phosphorus-oxygen bonds (P-O) while the fourth bond represents that of a phosphorus-oxygen double bond (P=O) and is not connected to other tetrahedral units. The structural properties of vitreous P_2O_5 were also investigated by Van Wazer [36-39] and his results revealed two phosphorus-oxygen bond lengths. The first at 1.49 Å representing the double bonded oxygen and the second at 1.56 Å indicative of the P-O single bonds. Although the basic structure of phosphate glasses is known, there are discrepancies that arise at the metaphosphate composition.

An anomalous behavior has been ascribed to the magnesium and zinc metaphosphate glasses, because for these metaphosphate glasses, the dependence of some physical properties (such as refractive index and density) on the metal oxide concentration shows a great deal of variation at the metaphosphate composition [40]. Previous researchers believed this "Phosphate Anomaly" was due to a change in the coordination number of the metal ion from 4 to 6 [41,42]. The discrepancies observed in the short range order of the magnesium and zinc metaphosphate glasses make them interesting to study.

1.4 STATEMENT OF THE PROBLEM

In this thesis, the short range order of three metaphosphate glasses ($Mg(PO_3)_2$, $Zn(PO_3)_2$, and $Pb(PO_3)_2$) will be investigated using computer simulations. This will be achieved by simulating the metaphosphate glasses using a two body Born-Mayer-Huggins potential model. Structural properties such as pair and cumulative distribution functions will be calculated. Subsequently, analysis of the phosphate backbone will be undertaken and insight into the effect of the cation modifier on the phosphate backbone structure will be determined.

To provide a more in depth investigation of the effect of the modifiers, a study of the metal network will be performed. This will permit the examination of the local environment surrounding each cation modifier. The structural properties obtained from the simulations will be compared to those determined experimentally. Assuming a good agreement between the simulated and laboratory metaphosphate glasses, conclusions pertaining to the effect of the modifier on metaphosphate glass structures may be drawn.

Finally, we will show how improvements in the short range order of phosphate glasses may be achieved by employing a three body potential model.

CHAPTER 2

2.0 THEORY

2.1 COMPUTER SIMULATION METHOD

A computer simulation is applied to the model that describes the interactions of the atoms that make up the material of interest. In most simulations the intermolecular potential energy function is taken to be the sum of the isolated pair interactions, this is called the pairwise additivity and is based on solving the Newtonian equations of motion. The first objective of a molecular dynamics simulation is to generate positions and velocities. The ions of the ensemble N which interact according to the potential energy function, will move according to Newton's Second Law and generate time dependent positions $x_i(t)$. It's velocity will also change with time thus establishing time dependent velocities $v_i(t)$. The positions of the N ions in the ensemble at a time t, generates a configuration. This configuration may be subsequently used for data analysis (Section 3.2).

In addition to understanding the interactions between the ions in the ensemble, it is also important to describe the interactions between the ions and their surroundings, this encompasses the boundary conditions. The forces between the ions may be sufficient to hold the system together during the course of the simulation, otherwise the ions may be confined by a potential representing a cube. One of the problems during a simulation is that the ions which lie at the surface of the cube experience different forces than the ions which are in the bulk. This can be overcome by implementing periodic boundary

conditions. The cubic box is replicated throughout space to form an infinite lattice. During the simulation, as the ion moves in the original box, its periodic image in each of the neighboring cubes will move in the same manner. Thus as an ion leaves the cube, one of its images will enter through the opposite face [43]. The use of periodic boundary conditions removes the effects of unwanted surface effects as well as to limit molecular dynamics to the study of short range phenomena. Molecular dynamics simulations are also limited by the speed and storage constraints of available computers. Because of the size limitations, simulations are normally confined to systems of ions that interact with short range forces. The speed limitations, confines study to those occurring in short intervals in the range of less than 1000 ps.

2.2 ANALYSIS METHODS

In this section, the methods used to understand and predict the structures of the metaphosphate glasses will be discussed. In order to comprehend the structure of a glass the bonding relationships between the atoms must be investigated. One such method is by establishing the chemical bond strength of the atoms in the solid. Assessing the bond strength can be done through electronegativity values, degree of ionicity and covalency, and finally by considering the field strength of an atomic pair [44].

2.2.1 ELECTRONEGATIVITY

In most cases chemical bonds are neither purely ionic nor purely covalent but rather partially covalent or partially ionic. This is a result of the unequal sharing of the bonding electrons due to the atom's electronegativity. The electronegativity of the atom provides good insight into the type of bonding that will occur. Atoms with very different electronegativities (a difference of 2.0 or more) will tend to form ionic bonds while those with similar electronegativities will form covalent bonds. The electronegativities to be considered in this thesis are Mg = 1.2, Zn = 1.6, Pb = 1.9, P = 2.1 and O = 3.5. These electronegativity values can be used to ascertain the extent of attraction of the atom for the electrons. The larger the electronegativity differences between two atoms, the greater the partial ionic character of a bond. Using a table relating the percent ionic character of a bond to a difference in electronegativity [19], the percent ionic character of the metal-oxygen atomic pairs discussed in this thesis were determined and are summarized in Table 2.2.2.1.

2.2.2 FIELD STRENGTH

The strong electrostatic forces of attraction among ions can also be represented by Coulomb's Law. According to Coulomb's Law, the force of attraction, F, between two oppositely charged ions with valences z_1 and z_2 is directly proportional to the product of the charges and inversely proportional to the square of the distance, r, separating them.

The value of this attractive force is termed the field strength value and is represented by the following equation:

$$F = \frac{z_1 z_2 e^2}{r^2} \qquad (2.2.2.1)$$

If one considers a system in which one of the ions is always the same such as oxide glasses then in the above equation e^2 and z_2 are constant, where e is the elementary charge and z_2 is the charge of the oxygen ion. Consequently, the quantity z_1/r^2 describes the field strength of ion 1. Since the field strength values reported in this thesis were developed in such a manner, they are applicable to the metaphosphate glasses under investigation. Table 2.2.2.1 shows the field strength values which were calculated by Dietzel [19] for the cations studied in this thesis.

Table 2.2.2.1

FIELD STRENGTH AND PERCENT IONIC CHARACATER VALUES FOR THE ELEMENTS IN THE METAPHOSPHATE GLASSES

Element	Field Strength (C^2/nm^2)	Ionic Character (%)
Mg	0.51	64
Zn	0.59	51
Pb	0.32	40
P	2.08	32

The field strength of cation network formers lie between 1 to 2, while cations with very low field strengths up to 0.35 represent strong network modifiers, such as the lead ion. Network formers (Si, B, Ge, P) are oxides which are capable of forming a single component glass while network modifiers (Na, Pb, Ca) modify the properties of the single component glass. In between these regions there are several cations such as Mg and Zn with intermediate values. Therefore, it can be anticipated that these cations will have transitional behavior between that of a network former and a network modifier [19].

CHAPTER 3

3.0 COMPUTATIONAL PROCEDURE

3.1 TWO BODY POTENTIAL MODEL

The molecular dynamics method used to perform the simulations is based on solving the Newtonian equations of motion. The force law used in the present calculation is derived from the pairwise ionic spherical potential that includes the Pauling repulsive term. It is the same form described by Mitra et al. [45] and is found to be:

$$F(r_{ij}) = \frac{(q_i q_j)e^2}{4\pi\varepsilon_o r_{ij}^2}\left[1 + sign(q_i q_j).\left(\frac{\sigma_i + \sigma_j}{r_{ij}}\right)^n\right] \qquad (3.1.1)$$

where the first term represents the short range repulsive component and the second term represents the long range Coulombic interactions. The parameters q_i and q_j are the ionic charges, e is the electronic charge, ε_o is the permittivity in vacuum, σ_i and σ_j are the ionic radii (in Angstroms) of atoms i and j, r_{ij} is the distance between atoms i and j in Angstroms and n (unitless) is a measure of the hardness of repulsion between the ions [26,32,45]. The sign function returns a value of –1 or +1 depending on the sign of the operand (q_iq_j). The charges, radii and n were determined empirically. The instantaneous force acting on each atom at a specific time was determined over a range of atomic neighbors within a 5.5 Å radius. This length is large enough to include the neighbors of importance (approximately

increase will not cause an effect on the structural properties of the glass. The associated potential is found to be:

$$V(r_{ij}) = \frac{-(q_i q_j)e^2}{4\pi\varepsilon_o}\frac{1}{r_{ij}}\left[1 + sign(q_i q_j).\frac{(\sigma_i + \sigma_j)^n}{n+1}\frac{1}{r_{ij}^n}\right] \qquad (3.1.2)$$

Once the instantaneous force on each atom was computed at every timestep (1 timestep = 1.0 $x10^{-15}$ s), new atomic positions and velocities were calculated using the Verlet algorithm [46] which introduces a simple finite difference formula for the second order derivative

$$x_i(t + \Delta t) = 2x_i(t) - x_i(t - \Delta t) + \left(\frac{\Delta t^2}{m_i}\right)F_i(t) \qquad (3.1.3)$$

the velocity is then calculated from the first order derivative of equation 3.1.3 which gives equation 3.1.4:

$$v_i(t) = \frac{\left(x_i(t + \Delta t) - x_i(t - \Delta t)\right)}{2\Delta t} \qquad (3.1.4)$$

3.2 DATA ANALYSIS OF MD RESULTS

To ensure that the simulation of the glasses proceeded without faults, properties such as the instantaneous energy and temperature of the ensemble were verified throughout the run.

3.2.1 INSTANTANEOUS TEMPERATURE AND ENERGY

The instantaneous temperature of the atomic ensemble can be found from the total kinetic energy, which incorporates the Maxwellian velocity distribution at a given moment. The average velocity of the atoms (v_L) of a given atomic type L can be calculated from the following equation:

$$\bar{v}_L = \sum_{n_L} \left[(v_x)_{n_L} + (v_y)_{n_L} + (v_z)_{n_L} \right] \qquad (3.2.1.1)$$

where n_L is the number of atoms of each atomic type and v_x, v_y, v_z are the x, y, and z components of the velocity. From the velocities the total kinetic energy of the ensemble, E_k, can be computed according to

$$E_k = \frac{1}{2} \sum_L m_L \bar{v}_L^{\,2} \qquad (3.2.1.2)$$

where m_L is the mass of atomic type L. Using the instantaneous kinetic energy, the instantaneous temperature can then be approximated from the Maxwell-Boltzmann distribution by the following relationship

$$T = \frac{2}{3}\frac{E_k}{kN} \tag{3.2.1.3}$$

where k is the Boltzmann constant and N is the number of atoms in the ensemble. The instantaneous temperature is subsequently used to scale the atomic velocities such that the desired temperature is maintained.

The instantaneous energy of the ensemble can be found by summing the instantaneous total kinetic energy and the instantaneous total potential energy.

$$E = \left(\frac{1}{2}\sum_i m_i v_i^2 \right) + \left(\sum_{i,j \neq i} V(r_{ij}) \right) \tag{3.2.1.4}$$

where $V(r_{ij})$ is the potential energy found by equation 3.1.2

3.2.2 PAIR AND CUMULATIVE DISTRIBUTION FUNCTIONS

The pair and cumulative distribution functions (PDF and CDF respectively) were calculated and averaged throughout the quench procedure at every 1 000 time step and are derived from the time averaged positions of the atoms. The pair distribution function is defined as the number of atoms at a distance between r and r+Δr from a central atom averaged over all central atoms. For each pair of ionic species, i and j, the pair distribution function (PDF) were obtained by solving the following equation

$$g_{ij}(r) = \frac{V n_{ij(r)}}{N_i N_j 4\pi r^2} \qquad (3.2.2.1)$$

where $n_{ij(r)}$ is the time averaged number of ion pairs between i and j within a distance of r-Δr/2 to r+Δr/2, N_i and N_j are the number of atoms i and j respectively in the cell and V is the volume of the cell. The calculations of $g_{ij(r)}$ are made over hundreds of time steps to ensure an average value of $g_{ij(r)}$. The cumulative distribution function (CDF) can be calculated from the pair distribution functions and describe the coordination numbers of the atomic pair. The CDFs describe the average number of atoms of type j surrounding an atom of type i in a sphere of radius r.

$$N_{i(r)} = \sum_{r=0}^{r} \frac{n_{ij}(r)}{N_i} \qquad (3.2.2.2)$$

3.2.3 BOND ANGLE DISTRIBUTIONS

The bonding geometries of the ions in the simulated phosphate systems were analyzed by calculating the type of neighbor for each ion and the bonding angles between these neighbors. The angle between three adjacent atoms can be defined by the following equation

$$\cos\Theta = \frac{\vec{r}_{ik} \cdot \vec{r}_{jk}}{\left|\vec{r}_{ik}\right|\left|\vec{r}_{jk}\right|} \qquad (3.2.3.1)$$

where r_{ik} and r_{jk} are the directionality vectors between atom k and two of its neighbors i and j. This angle and the two vectors are represented by Figure 3.2.3.1

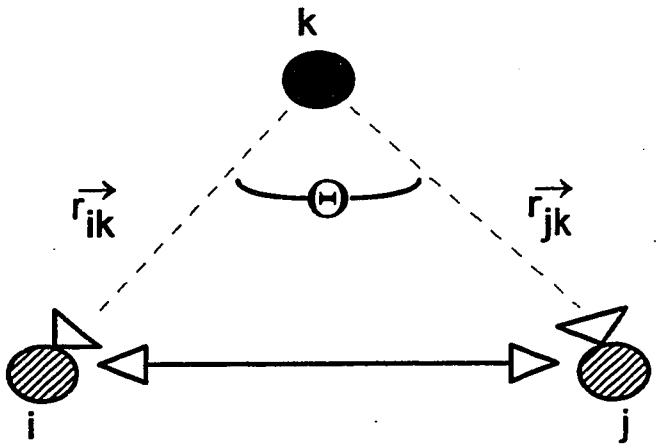

Figure 3.2.3.1 Pictorial representation of the angle Θ between three atoms i, j and k.

The distributions of bond angles can be defined as:

$$a_{ikj}(r_{ij},\Theta) = \frac{1}{n_o 2\pi^2 \sin\Theta} \frac{d\langle n(r_{ij},\Theta)\rangle}{dr_{ij} d\Theta} \qquad (3.2.3.2)$$

where $a_{ikj}(r_{ij},\Theta)$ represents the probability of finding a third ion k in a volume element ($2\pi^2 \sin\Theta\ dr_{ij}\ d\Theta$), where Θ denotes the angle defined by equation 3.2.3.1 and r_{ij} is the distance between atoms i and j.

3.3 THREE BODY POTENTIAL MODEL

The three body potential model used in this thesis was developed by Feuston and Garofalini [31] and was shown to be highly successful in the simulation of a sodium trisilicate glass [33]. The two body term describes the interactions between the atom pairs and consists of a modified Born-Mayer-Huggins ionic potential and is of the form:

$$V_{ij}^{2} = A_{ij} \exp\left(\frac{-r_{ij}}{\rho_{ij}}\right) + \frac{Z_i Z_j e^2}{r_{ij}} erfc\left(\frac{r_{ij}}{\beta_{ij}}\right) \qquad (3.3.1)$$

where r_{ij} is the distance between atoms i and j, Z is the formal ionic charge of the atoms, A_{ij} is the short range repulsion coefficient used to determine bond lengths, β_{ij} and ρ_{ij} are adjustable parameters for the different atomic pairs. This function has been shown to

reproduce the experimentally determined radial distribution function and bond angle distribution for bulk silica [27,47]. A representation of the force function, which is simply the derivative of the potential energy function, is shown in Figure 3.3.1.

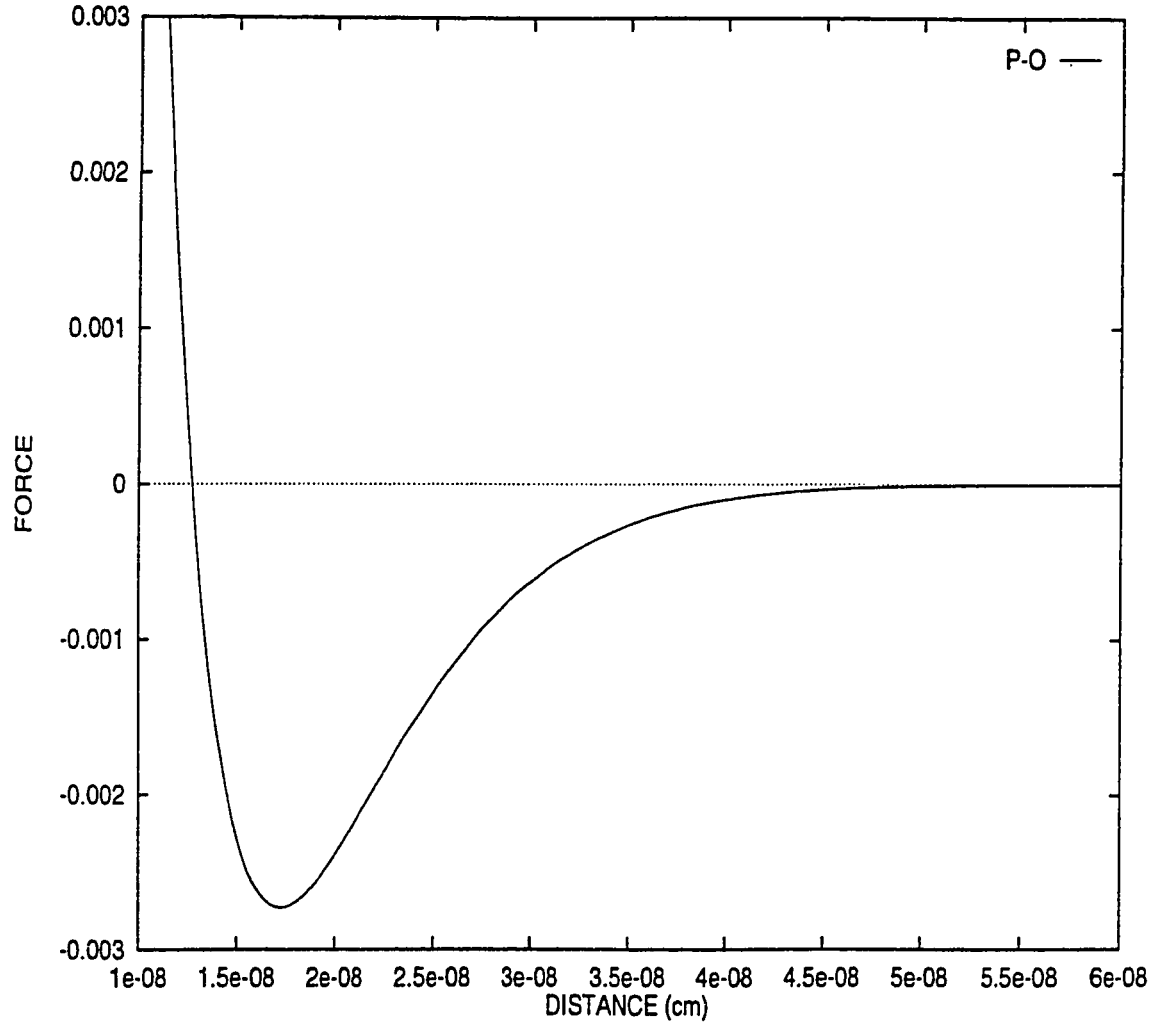

Figure 3.3.1 Representation of the P-O interionic force used in this thesis.

The three-body potential energy term is represented by the following equation:

$$V_3(r_{ij}, r_{ik}, \theta_{jik}) = \left[\lambda_{jik} \exp\left(\frac{\gamma_{ij}}{r_{ij} - r_i^c} - \frac{\gamma_{ik}}{r_{ik} - r_i^c} \right) * \left(\cos\theta_{jik} + \frac{1}{3} \right)^2 \right] \quad (3.3.2)$$

where $\cos\theta_{jik}$ is the angle subtended by r_{ij} and r_{ik} with the vertex at i, i is the central atom with nearest neighbors j and k, λ_{jik},γ_{ij}, γ_{ik} and r_i^c are constants. These constants were not modified from their original values, which were developed for SiO_2 [31], since they were designed to reproduce the tetrahedral geometry about the Si atoms which is also required for the P atoms in this thesis. The function $V_3(r_{ij},r_{ik},\theta_{jik})$ determines the three body contribution that comes from the three atoms i, j and k with i as the central atom and j, k as two of its covalently bonded neighbors. Integration of the Newtonian equations of motion for the ensemble was accomplished using a Gear predictor algorithm [34] with a time step of 1.0 fs (1.0 x 10^{-15} s). The Gear algorithm is composed of three steps: prediction, evaluation and correction. It does so by using the current position x(t) and velocity v(t) to:

1) Predict the position x(t+Δt) and velocity v(t+Δt) using the following equations

$$x(t + \Delta t) = x(t) + v(t)\Delta t \quad (3.3.3)$$

$$v(t + \Delta t) = v(t) - \frac{1}{t^2} x(t)\Delta t \quad (3.3.4)$$

2) Evaluate the force at t+Δt:

$$\frac{f(t+\Delta t)}{m} = -\frac{1}{t^2}x(t+\Delta t) \tag{3.3.5}$$

3) Correct the predicted positions and velocities according to:

$$x(t+\Delta t) = x(t) + v(t+\Delta t)\Delta t \tag{3.3.6}$$

$$v(t+\Delta t) = v(t) - \frac{1}{t^2}x(t+\Delta t)\Delta t \tag{3.3.7}$$

The adjustable parameters used in the MD simulation that best reproduced the vitreous P_2O_5 structure are given in Table 3.3.1.

Table 3.3.1

BMH PAIR POTENTIAL PARAMETERS USED IN THE MD SIMULATION OF P_2O_5

Atomic Pair	A_{ij} (ergs x 10^{-8})	β_{ij} (cm x 10^{-7})	ρ_{ij} (cm x 10^{-8})
P-O	0.23	0.21	0.31
P-P	0.32	0.07	0.45
O-O	0.07	0.23	0.29

No adjustments were made to the pair potential parameters for the O-O pair since they had already been developed for SiO_2 [31,47]. While for the P-P and P-O pair, a parameter search was performed by allowing the crystalline P_2O_5, to run with the given set of parameters at 300 K for 10 000 time steps. In doing so, the stability of the crystal was inspected by verifying any fluctuations in temperature and pressure throughout the run. To further test the validity of the potential we compared room temperature structural properties such as the pair and cumulative distribution functions with available experimental data (will be discussed in greater detail in Section 5.5.1). The cutoff distance was increased from 5.5 Å to 8.0 Å in order to account for the long range interactions that play an important role in modeling the features of the glass.

3.3.1 PICTORIAL REPRESENTATION

Pictorial representations in this thesis have been obtained from the final configuration of each metaphosphate glass. The ions were then represented by a program developed by Professor Garofalini at the Molecular Dynamics Laboratory Institute of Engineered Materials – Rutgers University. This technique allowed the visualization of the approximately 4 000 ions in the three metaphosphate glasses as well as the crystal and glass structures for P_2O_5. The software allows the user to define the types of ions and cutoff distances chosen between the ions. This permits the visualization of only the phosphate backbone for instance, or to isolate a particular ion with only its nearest neighbors showing.

CHAPTER 4

4.0 EXPERIMENTAL

4.1 PREPARATION OF THE SIMULATED GLASSES

4.1.1 TWO BODY SIMULATION PROCEDURE

All of the simulations were performed using Mitra's potential [26,32,45] and were carried out at constant volume on an Indy or Indigo 2 Silicon Graphics workstation. Certain parameters defined in equation 3.1.1 were common to all of the simulations. Charges, radii and n were determined empirically such that they reproduced the observed short range structure of the laboratory glasses. Table 4.1.1.1 summarizes the parameters used in the simulation of $Mg(PO_3)_2$, $Zn(PO_3)_2$, $Pb(PO_3)_2$ and P_2O_5.

The initial set of atomic positions used to simulate each of the glasses were obtained from the corresponding crystalline unit cell of $Mg(PO_3)_2$, $Zn(PO_3)_2$, $Pb(PO_3)_2$ and P_2O_5. To obtain the liquid melt the respective crystals were heated from 300 K to 15 000 K within 30 000 time steps (where each time step is 1fs = $1.0x10^{-15}$). At 15 000 K all the atoms have completely random positions and velocities. The system was thermalized for an additional 50 000 time steps and subsequently cooled in a stepwise manner to room temperature (300 K).

Table 4.1.1.1

POTENTIAL PARAMETERS COMMON TO ALL SIMULATIONS

Element	Ionic Radius (Å)	Ionic Charge (q)
O	1.20	-1.14
P	0.15	2.84
Mg	0.66	1.10
Zn	0.71	1.10
Pb	0.99	1.14

The cooling procedure involved 6 temperature steps: 7 500, 5 000, 2 500, 1 250, 600 and 300 K. The cooling procedure for each temperature step was achieved within 30 000 time steps and the glass was thermalized for 50 000 time steps before being cooled to the next temperature step. The total quench time was thus accomplished in 530 000 time steps (530 ps).

Throughout the simulation, the ions of the ensemble were enclosed in a cubic box to which periodic boundary conditions were imposed to eliminate the possibility of surface effects. The size of the box at 300 K was adjusted to give the correct room temperature density for the three metaphosphate glasses and the phosphate glass. The room temperature densities of the glasses were obtained from the literature [48]. The compositions of the four simulated glasses are found in Table 4.1.1.2. This table describes for each glass the 1) number of ions for each ion type that was used in the simulation 2) the oxygen molar volume in cm^3/mol O 3) the length of the box side in Ångstroms and 4) the simulated density in g/cm^3.

Table 4.1.1.2

SIMULATION PARAMETERS FOR $Mg(PO_3)_2$, $Zn(PO_3)_2$, $Pb(PO_3)_2$ AND P_2O_5

	$Mg(PO_3)_2$	$Zn(PO_3)_2$	$Pb(PO_3)_2$	P_2O_5
Number of O ions	2880	2688	2880	1600
Number of P ions	960	896	960	640
Number of M ions	480	448	480	-
Oxygen molar volume (cm^3/mol O)	12.52	13.06	12.89	9.86
Length of box (Å)	39.121	38.773	39.502	29.697
Density (g/cm^3)	2.427	2.850	4.740	2.880

Throughout the quench procedure, pair, cumulative and bond angle distribution functions were calculated. However, the structural parameters presented in this thesis are given for the temperature step at 300 K. An averaging of the pair distribution function and cumulative distribution and bond angle distribution functions was done for the last 50 000 time steps of each temperature run. The distribution functions reported have step increments of 0.01 nm for the PDF and CDF and of 1^0 for the bond angle distribution.

4.1.2 THREE BODY SIMULATION PROCEDURE

The 1792 ions used in the simulation of P_2O_5 glass were enclosed in an orthorhombic system with the periodic boundary conditions applied. Simulation parameters specific to those using the three body potential model are summarized in Table 4.1.2.1. As with the two body potential model, the volume of the system was adjusted in order to give the correct room temperature density of the glass.

Table 4.1.2.1

SIMULATION PARAMETERS FOR VITREOUS P_2O_5

Three Body Simulation Parameters	
Number of O ions:	1280
Number of P ions:	512
Charge on the O ions:	-2
Charge on the P ions:	+5

The initial set of atomic coordinates was derived from the crystalline unit cell for P_2O_5 [49]. The initial configuration was melted by heating from 300 K to 15 000 K. The velocities were scaled according to the Gear predictor algorithm, the system was then allowed to run at constant energy for 10 000 time steps ($\Delta t = 1.0 \times 10^{-15}$s). This step ensured randomization of the initial configuration. The system was then cooled to room

temperature in a series of eight temperature steps; 8 000, 7 000, 6 000, 4 000, 3 000, 2 000, 1 000 and 300 K. Throughout the cooling and at each temperature step, the velocities were scaled for 2 ps and then continued at constant energy for another 8 ps. However, at 4 000 and 3 000 K the system was run for 20 ps with an equilibrium period of 4 000 time steps in order to allow for further structural relaxation. The total quench time of the run was 0.11 ns.

As with the two body potential model, the structural properties (pair, cumulative distribution functions and bond angle distributions) presented in this thesis using the three body potential model represent those at 300 K.

CHAPTER 5

5.0 RESULTS AND DISCUSSION

The main emphasis of this work was to describe the short range order of magnesium, zinc and lead metaphosphate glasses using MD computer simulation technique. A detailed analysis of the short range order was accomplished in three steps. Firstly, the phosphate backbone structure was examined for the three metaphosphate glasses in order to determine whether the type of modifier present has an effect on the local order of the phosphate network. This will be the focus of Section 5.1. The study is then extended to investigate the structural features of the metal network (Section 5.3) and finally Section 5.5 discusses how improvements in simulating the short range order of phosphates may be achieved by employing a three body potential model.

When describing the short range order of metaphosphate glasses, it is common to refer to the local environment of the ions. The environment describes not only the ion's local geometry but also the type of ligands. Several different environments, for a particular ion, may exist within a metaphosphate glass. This definition becomes important when comparisons of the local structure of the metaphosphate glasses will be discussed. In addition, comparisons between the results obtained from the simulations and experimental results found in the literature will be made whenever possible.

5.1 INVESTIGATION OF THE PHOSPHATE BACKBONE NETWORK

The short range order of the phosphate backbone was verified by examining the room temperature pair distribution functions (PDFs) and cumulative distribution functions (CDFs) for the phosphorus-oxygen (P-O), phosphorus-phosphorus (P-P) and oxygen-oxygen (O-O) pairs. In addition, the O-P-O and P-O-P bond angle distributions (BADs) were calculated and the different types of oxygen ions present within the phosphate network identified.

5.1.1 THE PHOSPHORUS-OXYGEN PAIR

The P-O pair distribution functions are shown in Figures 5.1.1.1a, 5.1.1.1b, and 5.1.1.1.c for the magnesium, zinc and lead metaphosphate glasses respectively. The three PDFs show a sharp and well defined first coordination peak that returns to a null value, indicating that a clear distinction exists between the first and second coordination shells. The P-O interionic bond distance, determined from the peak maxima of the first coordination shell, was found to be 1.5 Å (using a cutoff of 2.0 Å) with a full width at half maxima (FWHM) of 0.1 Å for the three metaphosphate glasses. This narrow distribution in conjunction with the clear separation between the first and second coordination shells indicates that a high degree of short range order is present within the phosphate network. The P-O interionic bond distance is in excellent agreement with experimental data obtained by Hoppe et al. [40]. The authors have reported a P-O interatomic bond distance of 1.55 Å and 1.54 Å for $Mg(PO_3)_2$ and $Zn(PO_3)_2$ glasses respectively. Similar results

were obtained by Matz et al. [50] who studied the structure of alkaline earth metaphosphate glasses using neutron diffraction and reported an average P-O interatomic bond distance of 1.53 Å and 1.54 Å for $Mg(PO_3)_2$ and $Zn(PO_3)_2$ glasses respectively. Experimental studies on lead metaphosphate are scarce, however, Musino et al. [51] have investigated the short range order of lead metaphosphate glass using X-ray diffraction and report an average P-O interatomic bond distance of 1.593 Å.

It is also possible to compare the structure of the metaphosphate glasses to their crystal counterpart as a means of determining the expected glass structure. This is due to the fact that the total energy of a glass is comparable to the corresponding crystal and will have a similar atomic arrangement [52]. When comparing the structural results obtained in the simulated metaphosphate glasses to those of the corresponding crystals some similarities were observed. For example, the average crystal P-O bond length for $Zn(PO_3)_2$ has been reported to be 1.54 Å by Avenbuch et al. [53] and 1.54 Å in a $Mg(PO_3)_2$ crystal by Nord et al. [54]. These results are in excellent agreement to the value of 1.5 Å reported in this thesis. Data on lead metaphosphate crystals is not available in the literature.

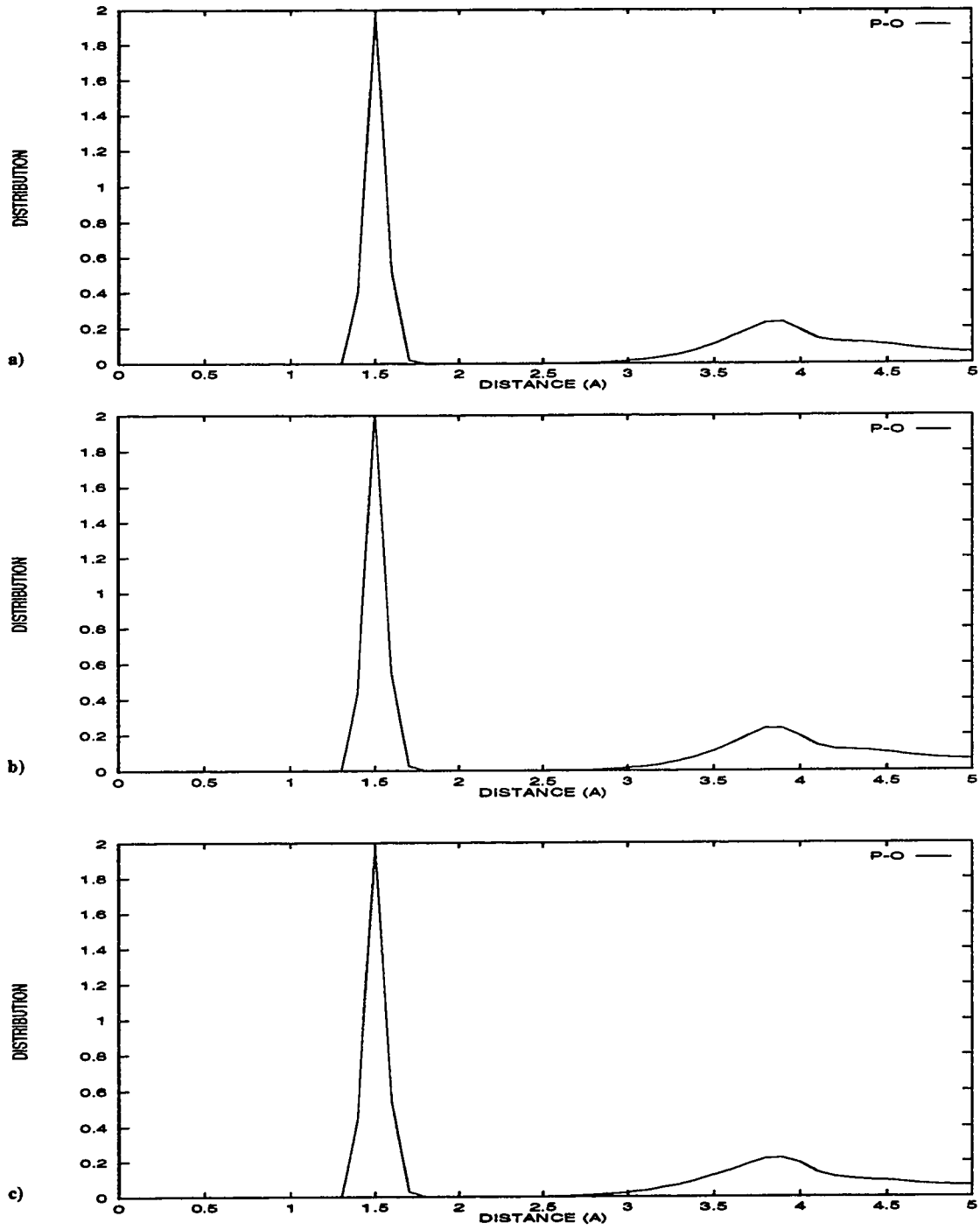

Figure 5.1.1.1 Pair distribution functions for the P-O pair in the a) $Mg(PO_3)_2$, b) $Zn(PO_3)_2$ and c) $Pb(PO_3)_2$ glasses.

The average P-O coordination number (CN) determined from the cumulative distribution functions was found to be 4.0 for the three metaphosphate glasses. The CDFs are shown in Figures 5.1.1.2a, 5.1.1.2b and 5.1.1.2c for the magnesium, zinc and lead metaphosphate glasses respectively. The average coordination numbers (CNs) were calculated at a cutoff radius of 2.0 Å, which corresponds to the first minimum, found between the first and second coordination shells. These results are in excellent agreement with those reported by Musino et al. [51]. The authors have performed theoretical calculations and report a P-O coordination of 4.0 for both magnesium and lead metaphosphate glasses thus confirming the accuracy of our simulations. The CNs obtained from the simulations are also in excellent agreement with those reported by Hoppe et al. [40] who have determined a P-O coordination number of 4.1 and 4.0 in magnesium and zinc metaphosphate glasses respectively. The coordination numbers obtained from the simulations indicate that each phosphorus ion is surrounded by an average of four oxygen ions. These four coordinated structures consist of PO_4 tetrahedral units (further evidence is provided by the O-P-O bond angles in section 5.1.3) which are linked to form the phosphate backbone network for the three metaphosphate glasses. This is consistent with the structure in the corresponding $Mg(PO_3)_2$ and $Zn(PO_3)_2$ crystals, which show that the phosphorus ions are coordinated to four oxygen ions and that the backbone is comprised of PO_4 tetrahedra linked together in an infinite chain [53,54].

The CDFs for the three metaphosphate glasses reveal a plateau in the region from 1.6 Å to 2.9 Å. The plateau occurs over a relatively long distance, which indicates that a high degree of short range order is present in the phosphate backbone network for the three metaphosphate glasses. Furthermore, the PDFs (Figure 5.1.1.1) the CDFs (Figure

5.1.1.2) of the three metaphosphate glasses are comparable, indicating that a similar phosphate backbone structure exists between the three metaphosphate glasses regardless of the type of cation modifier present.

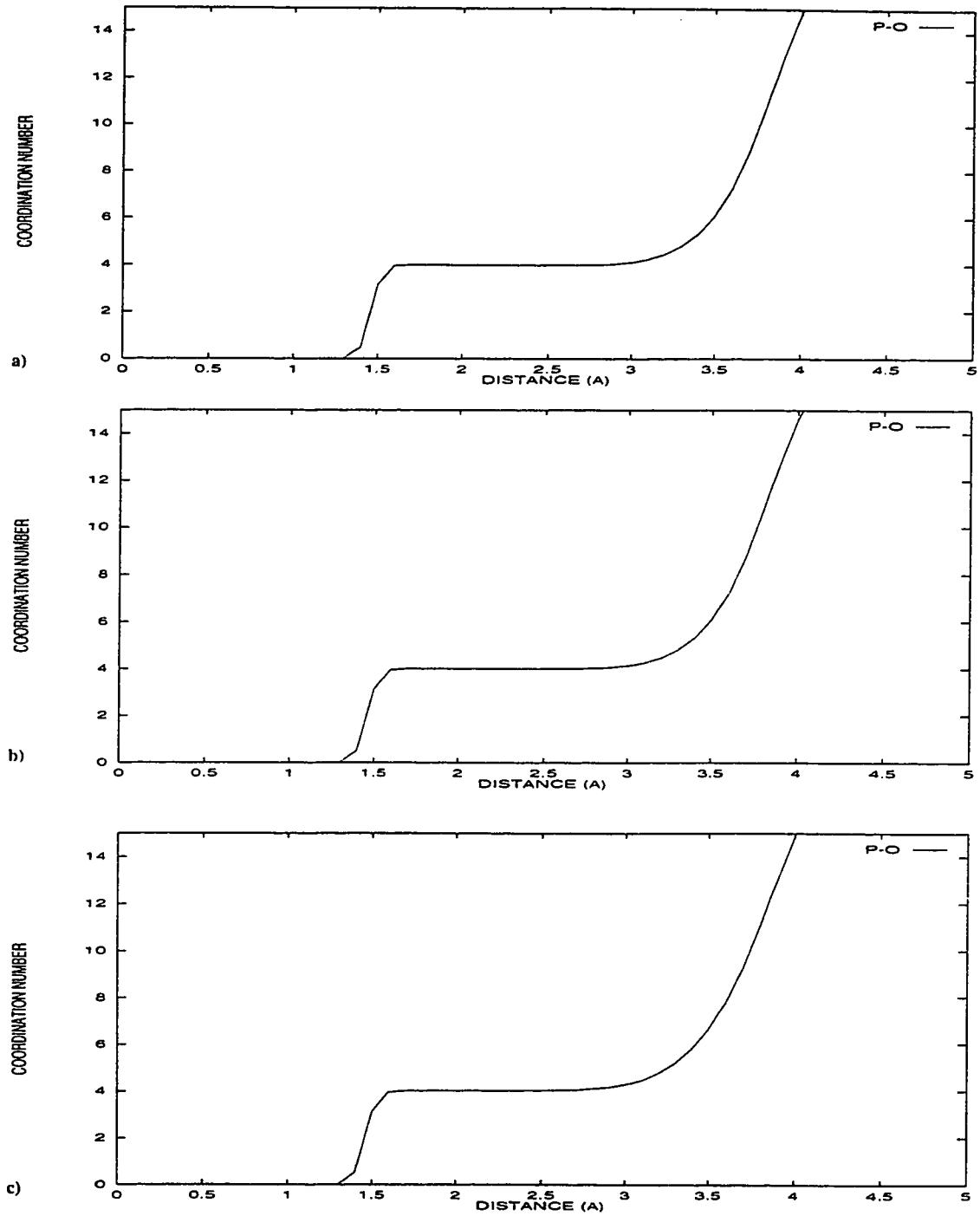

Figure 5.1.1.2 Cumulative distribution functions for the P-O pair in the a) $Mg(PO_3)_2$, b) $Zn(PO_3)_2$ and c) $Pb(PO_3)_2$ glasses.

5.1.2 THE PHOSPHORUS-PHOSPHORUS AND OXYGEN-OXYGEN PAIRS

The phosphorus-phosphorus (P-P) and oxygen-oxygen (O-O) pair and cumulative distribution functions further support the observation that the three metaphosphate glasses have a similar phosphate backbone structure. The room temperature PDFs for the P-P pair are shown in Figures 5.1.2.1a, 5.1.2.1b, and 5.1.2.1c for the magnesium, zinc and lead metaphosphate glasses respectively. An average phosphorus-phosphorus interionic bond distance of 3.0 Å and FWHMs of 0.2 Å (cutoff = 3.4 Å) was found for the three metaphosphate glasses. These results are in excellent agreement with those determined from neutron diffraction studies by Matz et al. [50]. The authors have reported an average P-P interatomic bond distance in the $Mg(PO_3)_2$ and $Zn(PO_3)_2$ glasses of 2.85 Å and 2.92 Å respectively. Results for the lead metaphosphate glass obtained from the simulation are in excellent agreement with those reported by Musino et al. [51] who found an average P-P interatomic bond distance of 2.79 Å using X-ray diffraction. The P-P PDFs for the three metaphosphate glasses also show a well defined first coordination shell since the first peak returns to a null value in all three cases. This indicates that a high degree of short range order is present in the phosphate backbone network of the three metaphosphate glasses and supports previous conclusions (Section 5.1.1) that the phosphate backbone is similar in structure regardless of the type of cation modifier present. This observation has been confirmed by Uchino et al. [55] who have reported that the intensity of the P-O-P symmetric vibration does not change systematically with the type of alkali cation but is the same for all the alkali metaphosphate glasses studied.

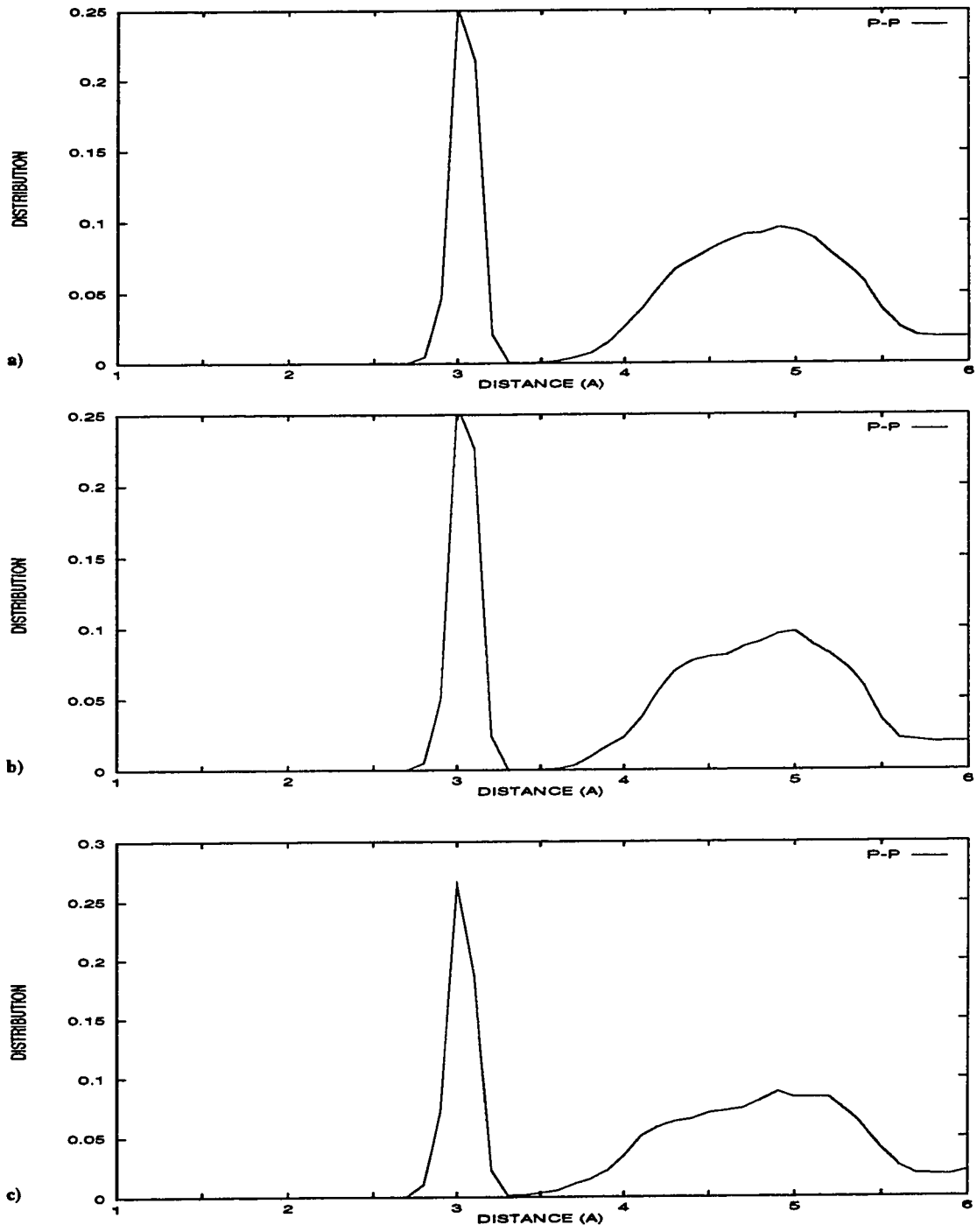

Figure 5.1.2.1 Pair distribution functions for the P-P pair in the a) $Mg(PO_3)_2$, b) $Zn(PO_3)_2$ and c) $Pb(PO_3)_2$ glasses.

From these results, they concluded that the metal ion interacts weakly with the bridging oxygen ions in the phosphate backbone structure [55] thus indicating that the metal ion has little influence on the structure of the phosphate network. Additional evidence supporting their conclusions is obtained from the P-O-P bond angle distributions (section 5.1.3) for the three metaphosphate glasses.

The P-P cumulative distribution functions are shown in Figure 5.1.2.2a, 5.1.2.2b, and 5.1.2.2c and reveal an average coordination of 2.0 for the three metaphosphate glasses. This average coordination of 2.0 indicates that there are two phosphorus ions surrounding each phosphorus ion within a spherical cutoff radius of 3.4 Å. Experimental data is not available in the literature for the lead metaphosphate glass, however, results by Matz et al. [50], reveal that the $Mg(PO_3)_2$ and $Zn(PO_3)_2$ glasses have an average P-P coordination of 2.22 and 1.97 respectively. Matsubara et al. [56] have reported a slightly lower average coordination number of 1.87 for the P-P pair in $Zn(PO_3)_2$ glass. These results are in excellent agreement with the average P-P coordination numbers reported in this thesis.

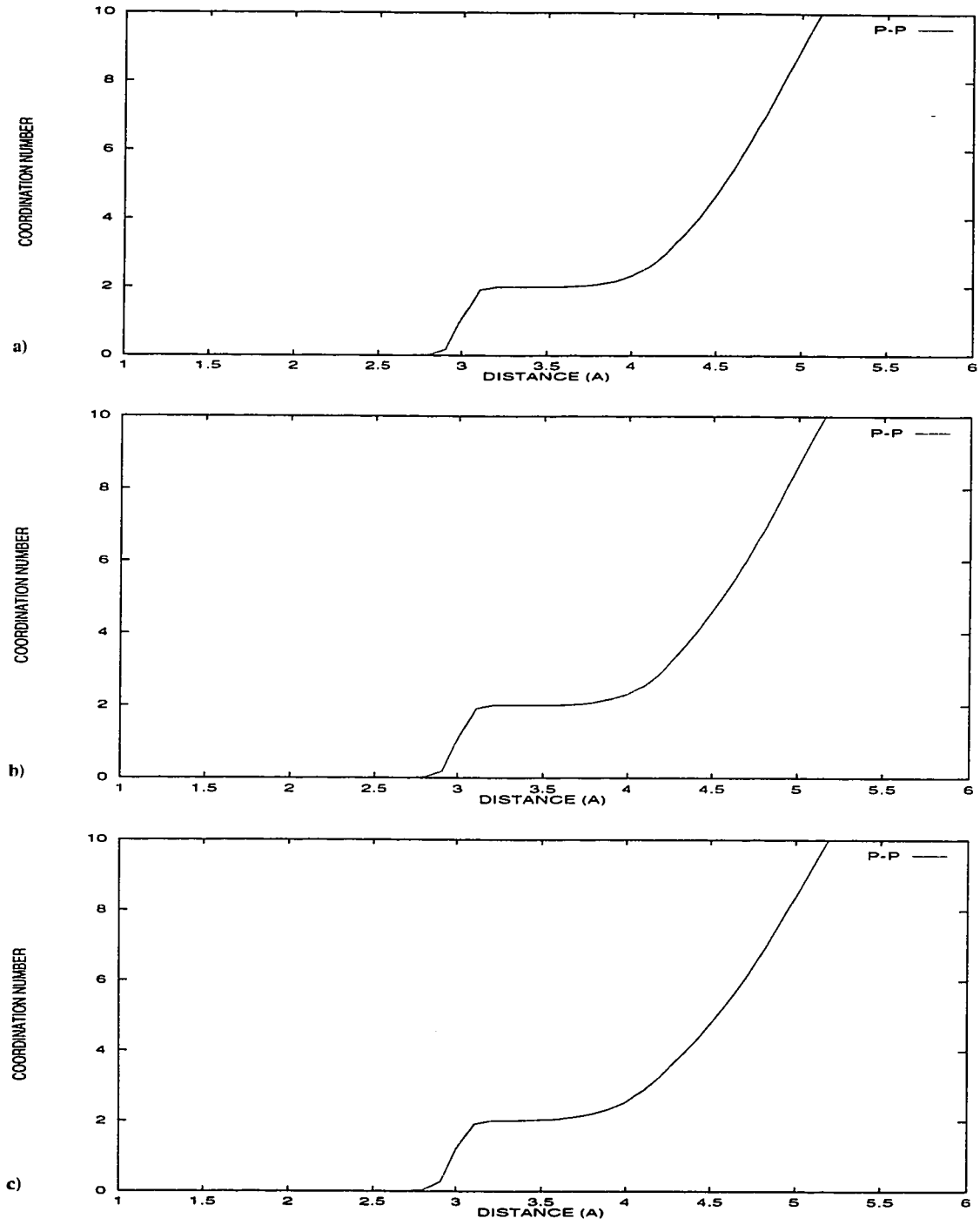

Figure 5.1.2.2 Room temperature cumulative distribution functions of the P-P pair in a) $Mg(PO_3)_2$ b) $Zn(PO_3)_2$ and c) $Pb(PO_3)_2$ glasses.

The P-P CDFs have a plateau ranging from 3.1 Å to 3.9 Å indicating a high degree of short range order in the phosphate backbone network, as was observed from the P-O CDFs (Figure 5.1.1.2), for the three metaphosphate glasses. The similarity of the P-P PDFs and CDFs for the three metaphosphate glasses indicates that the phosphate backbone is similar in structure and is unaffected by the type of cation modifier present in the metaphosphate glass. This supports our previous conclusion (Section 5.1.1) that the cation modifier does not play a significant role in altering the phosphate backbone structure.

The O-O pair distribution functions are shown in Figures 5.1.2.3a, 5.1.2.3b and 5.1.2.3c for $Mg(PO_3)_2$, $Zn(PO_3)_2$, and $Pb(PO_3)_2$ respectively. The O-O interionic bond distance (first coordination shell) was found to be 2.4 Å (cutoff = 2.7 Å) and a FWHM of 0.2 Å for the three metaphosphate glasses. The identical interionic bond distances and FWHMs indicate a similar phosphate backbone structure for the three metaphosphate glasses. The fact that the first peak does not return to a null value implies some overlap between the first and the second coordination shells. Experimental data on the O-O interatomic bond distance has been reported in the literature and all are in excellent agreement with the values reported in this thesis. For example, Hoppe et al. [40] report an O-O interatomic bond distance of 2.53 Å and 2.52 Å in magnesium and zinc metaphosphate glass respectively. In addition, the O-O interionic bond distance obtained from the simulations of the metaphosphate glasses are in good agreement with the O-O bond length of 2.5 Å found in both the $Mg(PO_3)_2$, and $Zn(PO_3)_2$ crystals [53,54].

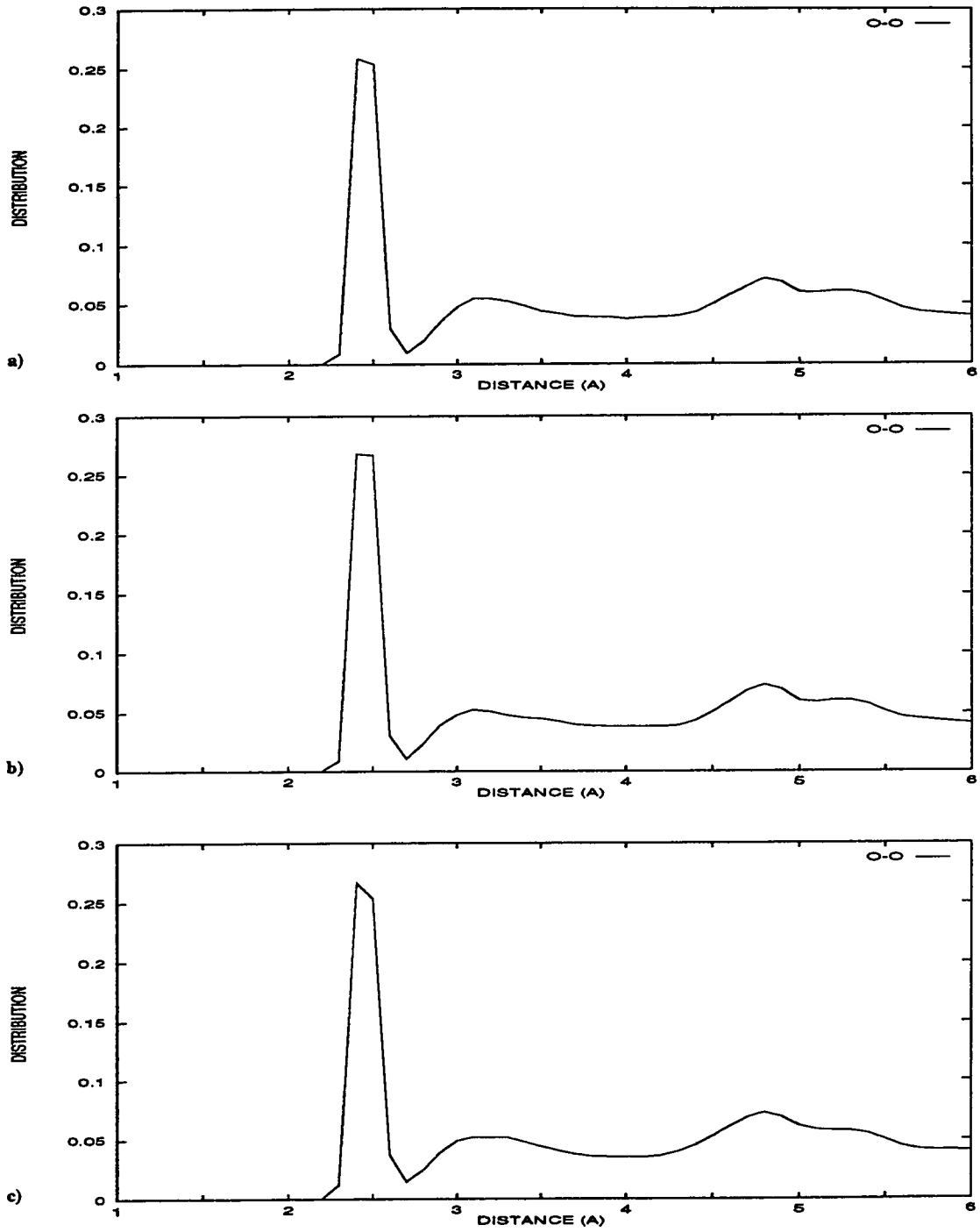

Figure 5.1.2.3 Pair distribution functions for the O-O pair in the a) $Mg(PO_3)_2$, b) $Zn(PO_3)_2$ and c) $Pb(PO_3)_2$ glasses.

The cumulative distribution functions for the O-O pair are shown in Figures 5.1.2.4a, 5.1.2.4b, and 5.1.2.4c for the $Mg(PO_3)_2$ and $Zn(PO_3)_2$ and $Pb(PO_3)_2$ glasses respectively. An average coordination number of 4.0 was found for the magnesium and zinc metaphosphate glasses while the lead metaphosphate glass revealed an average coordination number of 4.2 for the O-O pair. Bionducci et al. [57] have reported a similar average O-O CN of 3.8 for the zinc metaphosphate glass, determined experimentally by neutron diffraction. The similarity in the PDFs and CDFs for the O-O pair among the three metaphosphate glasses indicates that the metal ion does not affect the phosphate backbone structure. A summary of the results pertaining to the structure of the phosphate backbone and a comparison to literature values is shown in Table 5.1.2.1.

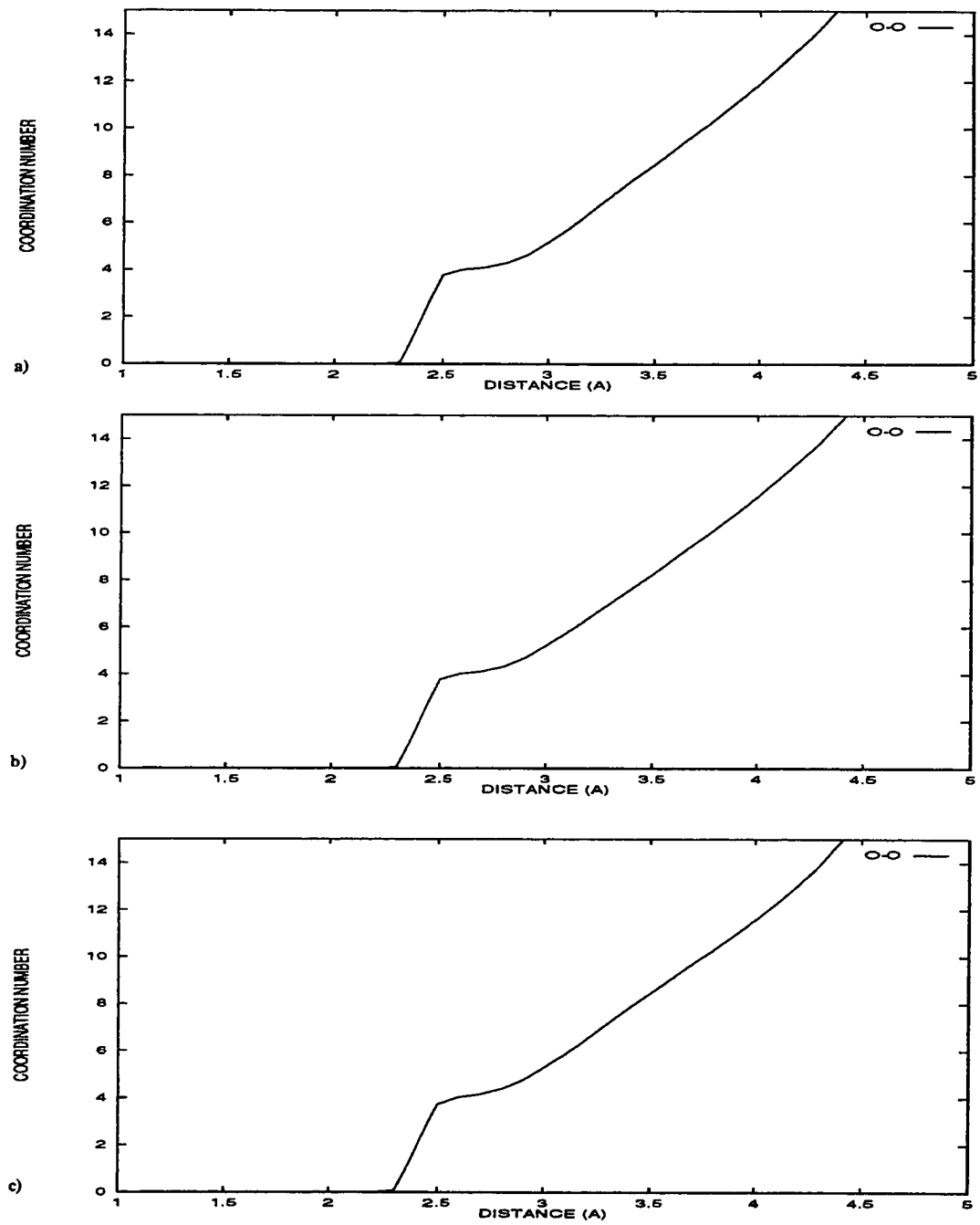

Figure 5.1.2.4 Cumulative distribution functions for the O-O pair in the a) $Mg(PO_3)_2$, b) $Zn(PO_3)_2$ and c) $Pb(PO_3)_2$ glasses.

Table 5.1.2.1

A SUMMARY OF THE BACKBONE STRUCTURE, BOND DISTANCES, r, AND COORDINATION NUMBERS, N

Reference	Glass	r_{P-O} (Å)	N_{P-O}	r_{P-P} (Å)	N_{P-P}	r_{O-O} (Å)	N_{O-O}	Technique
Musino	$Zn(PO_3)_2$	1.56	4.13	2.85	-	-	-	X-ray
et al. [51]	$Pb(PO_3)_2$	1.59	4.03	2.79	-	-	-	diffraction
Matz	$Mg(PO_3)_2$	1.53	4.03	2.85	2.22	2.51	4.70	Neutron
et al. [50]	$Zn(PO_3)_2$	1.54	3.90	2.92	1.97	2.51	4.50	diffraction
Hoppe	$Mg(PO_3)_2$	1.55	4.1	-	-	2.53	4.06	Neutron
et al. [40]	$Zn(PO_3)_2$	1.54	4.0	-	-	2.52	3.95	diffraction
Cervinka	$Mg(PO_3)_2$	1.53	-	3.00	-	2.50	-	X-ray
et al. [59]	$Zn(PO_3)_2$	1.53	-	3.00	-	2.50	-	diffraction
Bionducci	$Zn(PO_3)_2$	1.53	3.82	-	-	2.50	4.13	X-ray
et al. [57]								diffraction
Matsubara	$Zn(PO_3)_2$	1.53	4.19	2.98	1.87	2.48	4.53	X-ray
et al. [56]								Scattering
This	$Mg(PO_3)_2$	1.5	4.0	3.0	2.0	2.4	4.0	
Thesis	$Zn(PO_3)_2$	1.5	4.0	3.0	2.0	2.4	4.0	MD
	$Pb(PO_3)_2$	1.5	4.0	3.0	2.0	2.4	4.2	

5.1.3 BOND ANGLE DISTRIBUTIONS

Knowing the P-O and P-P interionic bond distances it is possible to calculate the tetrahedral angle (O-P-O) as well as the dihedral angle (P-O-P) for the three metaphosphate glasses. The O-P-O bond angles were calculated by determining which oxygen ion pairs fall within the first O-O coordination shell. The interionic bond distance between these oxygen pairs and neighboring phosphorus ions were also calculated. The resulting O-P-O bond angles were computed and averaged over all ions. The O-P-O bond angle distributions are shown in Figure 5.1.3.1a, 5.1.3.1b and 5.1.3.1c for magnesium, zinc and lead metaphosphate glasses respectively. An average bond angle of 109^0 was obtained for the three metaphosphate glasses, which is very close to the theoretical tetrahedral bond angle of 109.5^0. The O-P-O bond angle in the simulated $Mg(PO_3)_2$ and $Zn(PO_3)_2$ glasses is in excellent agreement with the value of the bond angle (109.3^0) found in the corresponding crystals [53,54]. The FWHMs (Figure 5.1.3.1) were found to be 10.5^0, 10.5^0 and 10.6^0 for the $Mg(PO_3)_2$, $Zn(PO_3)_2$ and $Pb(PO_3)_2$ metaphosphate glasses respectively. This relatively narrow distribution is to be expected for a network former with high field strength (2.08) [19]. Elements such as P, Si and B with field strengths between 1 and 2 show a tendency for glass formation and are all network formers. Therefore, the phosphorus ions within the phosphate network will possess a high degree of short range order. This in turn results in a narrow O-P-O bond angle distribution since all the phosphorus ions have similar environments throughout the backbone. More specifically, by investigating O-P-O bond angles in conjunction with the coordination numbers of 4.0, a predominantly PO_4 tetrahedral environment exists for the phosphorus

ions in the three metaphosphate glasses. Furthermore, these PO_4 tetrahedral units form mostly long linear chains connected by bridging oxygen ions that make up the phosphate backbone structure. This will be discussed in more detail in section 5.1.4. Previous researchers using a variety of experimental techniques [9,10,13,58-60] have reported this type of structure in metaphosphate glasses. The similarity in the phosphate backbone structure has also been reported by Rouse et al. [7]. The authors concluded that binary metaphosphate glasses have the same basic structure regardless of the type of metal and consists of polymeric chains of PO_4 tetrahedra bonded to adjacent tetrahedra through bridging oxygen atoms [61].

Despite the good agreement of the simulation results to experimental data, improvements can be made to reduce the FWHM of the O-P-O bond angle. Doing so will further improve the short range order found in the phosphate backbone. This has been achieved by employing a three body potential model and will be the focus of section 5.5.

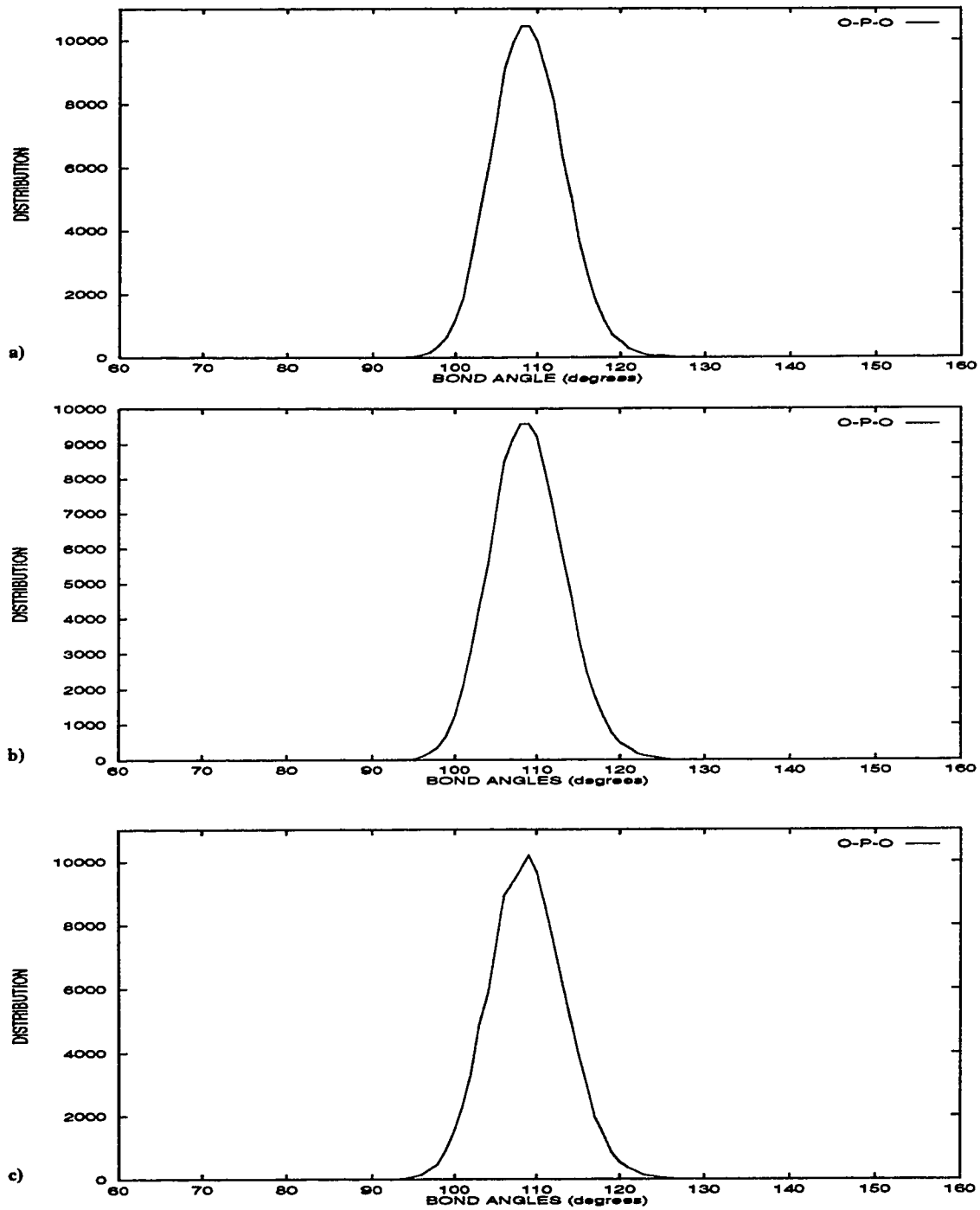

Figure 5.1.3.1 Time averaged O-P-O bond angle distribution functions for the a) $Mg(PO_3)_2$, b) $Zn(PO_3)_2$ and c) $Pb(PO_3)_2$ glasses.

Another important angle is the P-O-P angle, which gives information on the connectivity of the PO_4 tetrahedra. A similar procedure as that used to calculate the O-P-O bond angle distributions was used in calculating the P-O-P bond angle distributions. A cutoff of 3.4 Å was taken to account for the P-P first coordination shell and the oxygen ions bonded to each phosphorus pair were counted and the P-O-P bond angle calculated. The P-O-P bond angle distributions are shown in Figure 5.1.3.2a, 5.1.3.2b and 5.1.3.2c with average values of 166^0, 165^0, and 165^0 for the $Mg(PO_3)_2$, $Zn(PO_3)_2$, and $Pb(PO_3)_2$ glasses respectively. The similar P-O-P bond angle for the three metaphosphate glasses is in agreement with Raman spectroscopy results [55,61] which show that the frequency and intensity of the P-O-P symmetric vibration are approximately the same for all the metaphosphate glasses studied. This indicates that the metal ion interacts weakly with the bridging oxygen ions forming the phosphate tetrahedral chains. Similar results were obtained by Uchino et al. [55] and support the similar P-O-P bond angles observed in this thesis indicating that the phosphate backbone structure is independent of the type of cation modifier present within the metaphosphate glass.

The broader distributions for the P-O-P bond angle in comparison to the O-P-O bond angle distributions (Figure 5.1.3.1) is to be expected due to the disordered nature of the corner sharing tetrahedral units. In addition, Figure 5.1.3.2 shows that bond angles below 120^0 were not observed in the three metaphosphate glasses. This observation is in agreement with neutron diffraction results obtained by Matz et al. [50] who report that P-O-P bond angles below 100^0 were not observed in magnesium and zinc metaphosphate glasses.

A more in depth analysis of the simulation results reveals a larger bond angle in comparison to experimental results [50]. For example, Matz et al. [50] report an average P-O-P bond angle of approximately 140^0 in the magnesium and zinc metaphosphate glasses which is smaller than the values reported in this thesis. This difference indicates some discrepancies in the phosphate backbone structure between the simulated and experimental metaphosphate glasses. Furthermore, the P-O-P bond angle distribution reported by Matz et al. [50] decreases more rapidly at the low angle side than at the larger angle side. This type of distribution is reversed for the P-O-P bond angle distributions obtained from the simulations which decreases more rapidly at the large angle side, compared to the low angle side. Such discrepancies between the simulation and experimental results decreases the local order around phosphorus in comparison to the experimental metaphosphate glass and a three body potential model taking into account the partial covalent character of the P-O bond may improve these results (Section 5.5). In a study of vitreous silica Feuston and Garofalini [31] reduced the average Si-O-Si bond angle from 162^0 obtained using a two body potential model to 154^0 by employing a three body potential model.

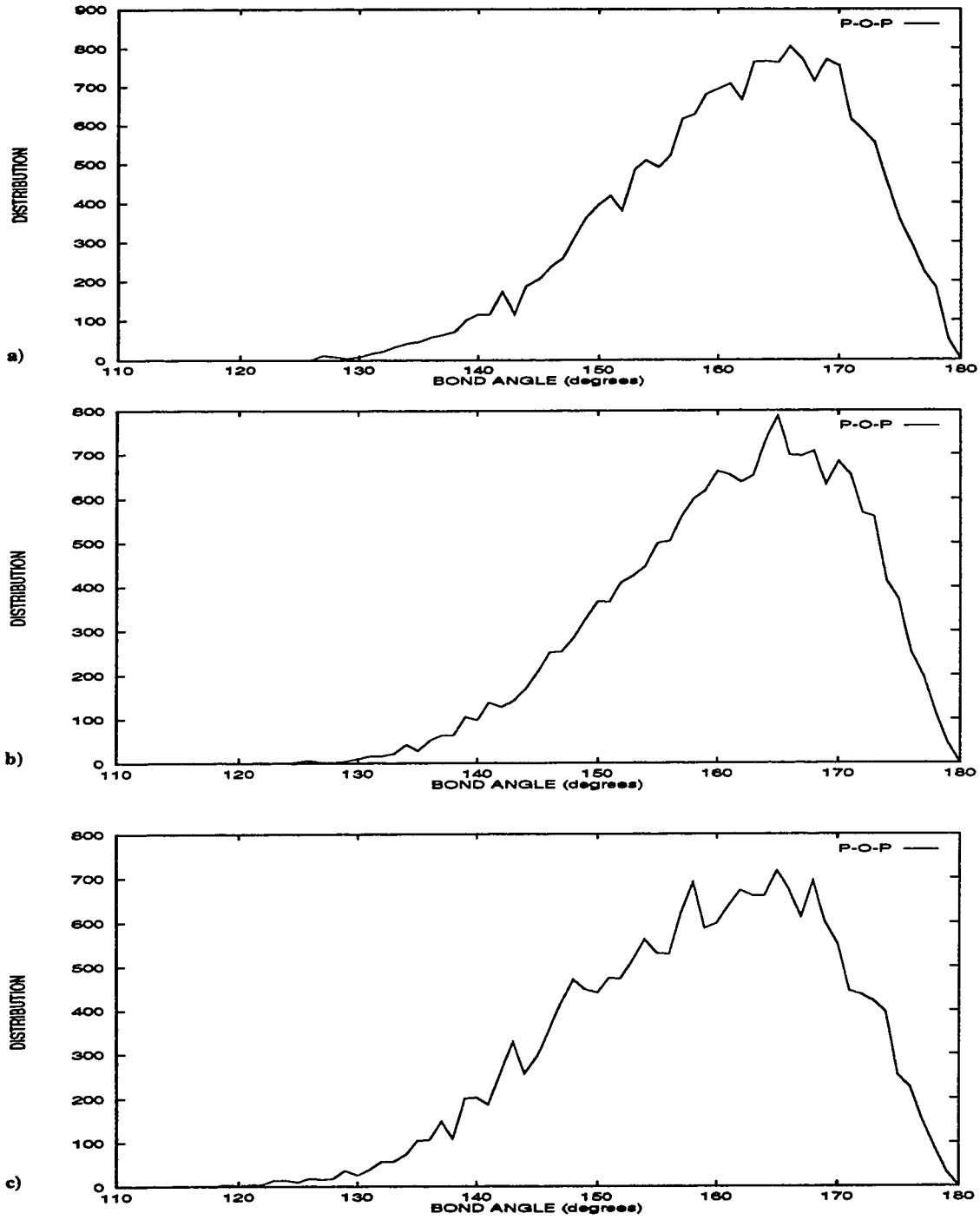

Figure 5.1.3.2 Time averaged P-O-P bond angle distribution functions for the a) $Mg(PO_3)_2$, b) $Zn(PO_3)_2$ and c) $Pb(PO_3)_2$ glasses.

5.1.4 TYPES OF OXYGEN IONS IN THE PHOSPHATE BACKBONE

The subsequent step in analyzing the short range structure of the phosphate backbone involves the identification of bridging oxygens (BO), nonbridging oxygens (NBO) and free oxygens. In this thesis, a bridging oxygen ion is defined as an oxygen ion connected to two similar ions while a nonbridging oxygen ion is connected to two different types of ions. The free oxygens are those which act as individual units and do not contribute to the phosphate backbone. To calculate the NBOs and BOs the number of oxygen ions are counted around each phosphorus ion within a 2.0 Å radius. The value of 2.0 Å is chosen because it is the cutoff point between the first and second coordination shells for the P-O pair. A count is made of the phosphorus ions which fall within the first coordination shell. If there is one P-O link the oxygens are labeled as NBOs, if a second phosphorus ion falls within the cutoff the oxygen is labeled as a BO while the free oxygens are not connected to the phosphate backbone. The results summarizing the types of oxygen ions found are shown in Table 5.1.4.1.

Table 5.1.4.1

TYPES OF OXYGEN IONS FOUND IN THE PHOSPHATE BACKBONE OF THE $Mg(PO_3)_2$, $Zn(PO_3)_2$, AND $Pb(PO_3)_2$ GLASSES

Glass	% BO	% NBO	% Free
$Mg(PO_3)_2$	31.4	62.7	5.9
$Zn(PO_3)_2$	21.2	42.4	36.4
$Pb(PO_3)_2$	33.3	66.7	0.0

In all three metaphosphate glasses, the results reveal a higher percentage of NBO than BO species. Furthermore, there are approximately twice the amount of NBOs compared to BOs in the phosphate backbone structure, which is in agreement with the theoretical values reported by Martin [62] and Gresch et al. [63]. The authors reported that the ratio, BO/NBO, in binary phosphate glasses may be calculated using the following relationship:

$$BO / NBO = 0.5(3 - 4x) \qquad (5.1.4.1)$$

where x is the mole fraction of modifier oxide. In metaphosphate glasses the mole fraction is 0.5 therefore the ratio, BO/NBO, is 1:2 which is in excellent agreement with our simulation results (Table 5.1.4.1). The results obtained for the $Pb(PO_3)_2$ glass show that 33.3 % of the oxygens are present as BO, 66.7 % as NBO and no free oxygens were found. These results indicate that approximately 67 % of the oxygen ions related to the phosphate backbone are bonded to both a metal and a phosphorus ion, while approximately 33 % are bonded to two phosphorus ions. The high percentage of NBOs in comparison to those found in the $Mg(PO_3)_2$ and $Zn(PO_3)_2$ glasses is to be expected since lead has the lowest field strength and therefore the strongest modifier of the three metals. Consequently lead disrupts the phosphate backbone to a higher degree by depolymerizing the network and converting more bridging oxygen ions to nonbridging oxygen ions. The significantly larger ionic radius of the lead ion (0.99 Å) compared to magnesium (0.66 Å) and zinc (0.71 Å) will also contribute to the depolymerization of the phosphate backbone resulting in a higher number of NBOs for the lead metaphosphate glass.

Similarly, the lower percentage of NBOs in the magnesium metaphosphate glass as opposed to those in the lead metaphosphate glass may be attributed to the higher field strength of the magnesium ion (0.51) in comparison to that of the lead (0.32) ion. The higher field strength value renders the magnesium ion a weaker modifier and thus can not disrupt the phosphate network to the same extent. This trend is also observed when comparing the magnesium and zinc metaphosphate glasses whereby the zinc metaphosphate glass has the lowest number of NBOs (42.4 %).

Further studies should be carried out on glasses containing different metal concentrations in order to ascertain the effect on the percentage of bridging and nonbridging oxygens. One would expect that as the concentration of metal increases the fraction of NBOs would also increase because of the greater disruption of the phosphorus network with the increase in the percentage of the metal ions in the glass.

Identification of the bonding type of each oxygen ion allows us to calculate the Q^i distribution. The Q^i distribution is a labeling system for the local environment of phosphorus ions and is defined as a percentual distribution of the number of bridging oxygen ions attached to individual phosphorus ions. Two different types of distributions are possible: the first is a binary distribution in which a maximum of two Q species exists and the second is a statistical distribution with several Q^i species present [64]. All three metaphosphate glasses have several Q^i species present and follow a statistical distribution. The results are summarized in Table 5.1.4. 2

Table 5.1.4.2

Q^i DISTRIBUTION (PERCENTAGE) FOR $Mg(PO_3)_2$, $Zn(PO_3)_2$ AND $Pb(PO_3)_2$ GLASSES

Q^i	$Mg(PO_3)_2$	$Zn(PO_3)_2$	$Pb(PO_3)_2$
Q^4	3.5	3.9	2.9
Q^3	25.2	24.8	21.4
Q^2	44.0	43.8	46.4
Q^1	25.2	25.0	26.1
Q^0	2.1	2.5	3.2

The Q^i distributions confirm that the short range structure of the phosphate network is the same in the three metaphosphate glasses. This has been shown to be the case by (i) the presence of a statistical distribution and (ii) the similarities in the percentage of each type of Q species for the three metaphosphate glasses.

The formation of Q^2 and Q^1 tetrahedral species results from the depolymerization of Q^4 and Q^3 species with the addition of the metal oxide. Therefore, the distribution of Q^i species will be determined by the degree of depolymerization caused by the cation modifier [65]. Since lead has the strongest modifying ability of the three modifiers studied in this thesis, a higher percentage of the lower Q species (Q^2, Q^1 and Q^0) is expected in comparison to those found in the $Mg(PO_3)_2$ and $Zn(PO_3)_2$ glasses. This is shown to be the case (see Table 5.1.4.2). Necessarily, lower percentages of Q^4 and Q^3 species were found in the lead metaphosphate glass in comparison to those in the magnesium and zinc metaphosphate glasses due to the fact that lead has a stronger ability to depolymerize the phosphate network. The similar distribution of Q^i species between the magnesium and zinc metaphosphate glasses indicates that these modifiers have similar effects on the metaphosphate glass structure. This is due to the fact that they have similar field strengths and ionic radii (discussed in greater detail in section 5.3).

The Q^2 species are predominant in the three metaphosphate glasses studied i.e. bonded to two bridging oxygen ions and two nonbridging oxygen ions. The high percentage of Q^2 species has been reported in the literature [66-68]. However when comparing the results obtained from the simulations to those found experimentally by Lai et al. [69] some discrepancies were observed. Using ^{31}P MASS NMR spectroscopy the authors report that in the zinc metaphosphate glass approximately 95 % of the phosphate backbone was comprised of Q^2 species while the other 5 % consisted of Q^1 species. Although the results in this thesis show the predominance of Q^2 and Q^1 species, the relative percent distribution differs from what is observed experimentally. The experimental results indicate that the zinc ion acts more as a modifier in the laboratory

glass and tends to break up the network to a greater extent, as indicated by the complete lack of Q^3 and Q^4 species, than in the simulated glass. The reason for this discrepancy in the overall distribution is not known but one possibility may be due to the lack of the covalent contribution in the two body potential model. In order to resolve this issue, employing a three body potential model may improve the results since it considers the covalent character in the phosphorus–oxygen bond (Section 5.5). However, when comparing the Q^i distribution for the simulated $Pb(PO_3)_2$ glass to those obtained experimentally using ^{29}Si MAS NMR for a lead silicate glass, similar results are observed. Dupree et al. [64] found a statistical distribution of 9 %, 27 %, 37 %, 21 % and 5 % for the Q^4, Q^3, Q^2, Q^1, and Q^0 species respectively which is in good agreement with our simulation results (Table 5.1.4.2).

Further studies should be aimed at varying the concentration of the metal oxide in the metaphosphate glasses in order to observe any changes in the Q^i distribution. Generally, one would expect that as the concentration of the metal ion increases the percentage of Q^4 and Q^3 would decrease while the percentage Q^2 and Q^1 species would increase.

5.1.5 RING AND CHAIN STATISTICS

To provide a more detailed understanding of the phosphate backbone structure and more specifically the linkages of the phosphorus ions an analysis of the ring and chain connectivity was carried out. The connectivity study determines the degree of polymerization, the presence of phosphate anions as well as the size and distribution of rings and chains in the phosphate backbone network.

The P-O-P linkages are identified by counting the number of oxygens present around the phosphorus ions within the first P-O coordination shell. The ions, which are connected by similar oxygens, are removed to yield P-P linkages. This information is used to construct a two dimensional map of the phosphate network. Although the map was drawn in two dimension, it represents the three dimensional connectivity of the 960, 896, and 960 phosphorus tetrahedra in the magnesium, zinc and lead metaphosphate glasses respectively. In constructing the phosphate network, the individual anions were separated from the main polymeric backbone. Fused rings were counted such that each ring contained the smallest number of members and then individual branched chains were counted such that the longest possible linear chain remained intact. The same procedure was performed for the phosphate anion units, which were not connected to the main polymeric network. Once all of these individual units were accounted for, a tally of the number and size of all rings and chains were tabulated for both the main phosphate network as well as the phosphate anion structures.

The connectivity studies show that in all three metaphosphate glasses the phosphate network is comprised of linear chains with and without side branches as well as

rings of various sizes. This confirms the results presented in Section 5.1.3, which describes the phosphate backbone consisting of long chains of PO_4 tetrahedra for the three metaphosphate glasses. The existence of long chains of tetrahedra is in agreement with NMR [50], X-ray diffraction [51] and Raman spectroscopy [70] results.

The effect of the modifier on the phosphate backbone may be ascertained from the connectivity study. The modifier will depolymerize the phosphate network, breaking up the characteristic long chains of PO_4 tetrahedra. The degree to which the network breaks up will vary depending on the cation's field strength and size. Since lead has the largest ionic radius and is the strongest modifier of the three metals investigated in this thesis, fewer long chain P-O-P linkages are expected in comparison to the magnesium and zinc metaphosphate glasses. From Table 5.1.5.10 we note that the percentage of chain linkages that are greater than 11 units in length in the lead metaphosphate glass (0.96 %) is considerably less than that found and in the magnesium (3.17 % - see Table 5.1.5.2) and zinc (4.32 % - see Table 5.1.5.6) metaphosphate glasses. Furthermore, the data shows that the longest chain in the main polymeric backbone for the $Pb(PO_3)_2$ glass consists of 19 P-P linkages (Table 5.1.5.10) which is shorter than the chain lengths found in the magnesium (25 P-P - see Table 5.1.5.2) and zinc metaphosphate (30 P-P - see Table 5.1.5.6) glasses. These results are consistent with the field strengths of the metal ions and are in excellent agreement with those obtained experimentally using liquid chromatography and Raman scattering [71]. A structural investigation of a lead iron phosphate glass found that the phosphate backbone consisted primarily of long linear phosphate chains upto 12 P linkages in length. A few chains greater than 12 units in length as well as some cyclic phosphate structures were also identified.

Cyclic ring structures were also observed in the phosphate backbone of the simulated metaphosphate glasses. The distribution of ring structures are summarized in Table 5.1.5.1, Table 5.1.5.5 and Table 5.1.5.9 for the $Mg(PO_3)_2$, $Zn(PO_3)_2$ and $Pb(PO_3)_2$ glasses respectively. Experimental evidence for the presence of ring structures has been reported by Matz et al. [50] for a magnesium metaphosphate glass and by Meadowcroft et al. [72] for a zinc metaphosphate glass using paper chromatography. The effect of the metal ions on the phosphate backbone structure can be observed from the number of ring structures for the three metaphosphate glasses. A similar number of ring structures exists between the magnesium (45) and zinc (51) metaphosphate glasses in comparison to the number (35) in the lead metaphosphate glass. This may be due to their similar field strengths that will result in a similar degree of depolymerization of the phosphate backbone and thus formation of ring structures. The structure of the phosphate backbone in the metaphosphate glasses is shown in Figure 5.1.5.1.

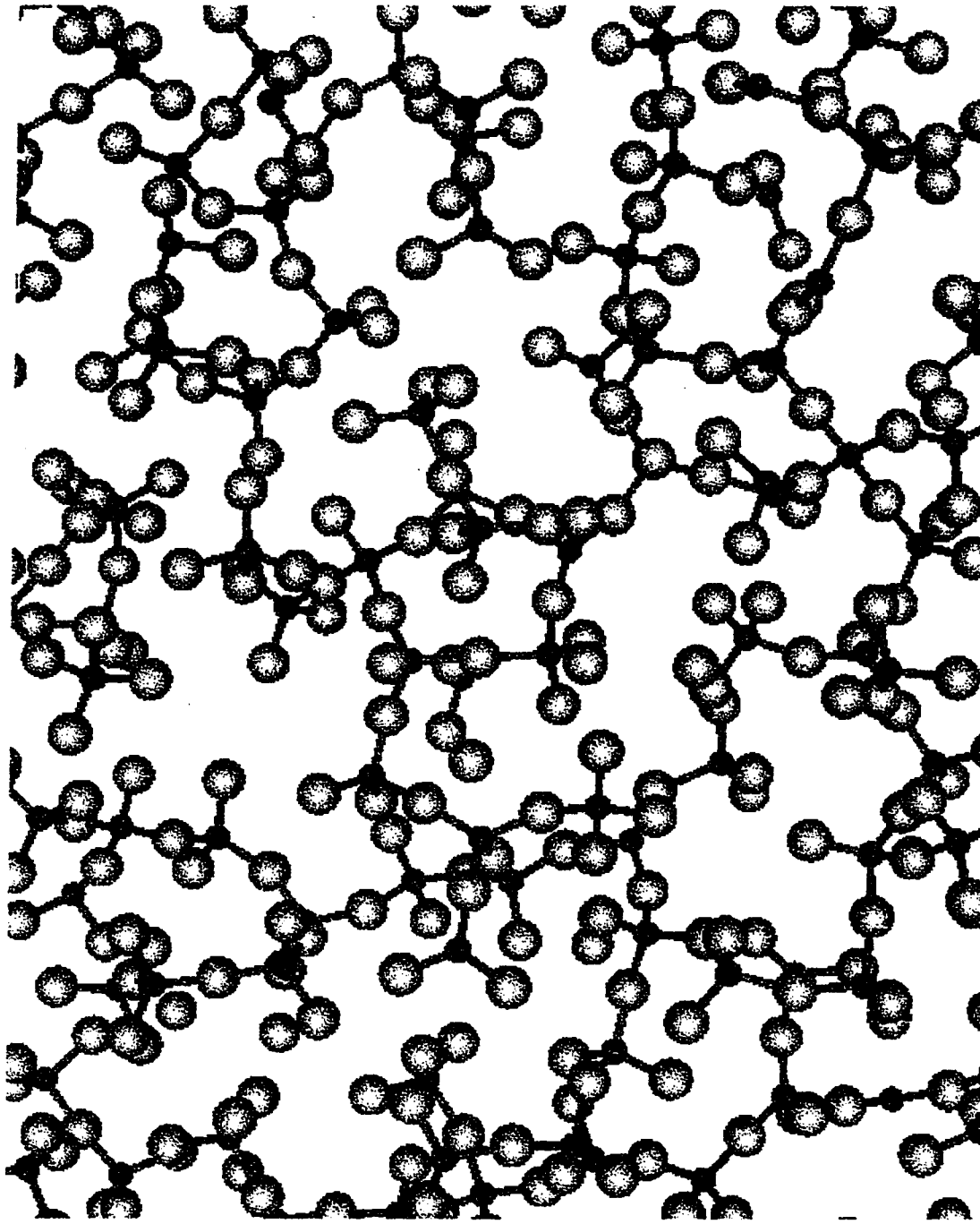

Figure 5.1.5.1 Pictorial representation of the phosphate backbone structure. The small dark grey spheres represent phosphorus and the larger light grey spheres represent oxygens.

Although no experimental data is available in the literature concerning ring size distribution in phosphate glasses, ring analysis for simulated vitreous silica [17] exhibited ring sizes ranging from 4 to 10 which is in excellent agreement with the results obtained in this thesis. Della Valle et al. [73] have collected ring statistics by counting $(SiO)_n$ rings in silica glass and report similar ring sizes varying from 4 to 9 with the 6 membered ring being the most probable size. The predominance of the 6 membered ring has also been observed in the simulated metaphosphate glasses (Table 5.1.5.1, Table 5.1.5.5 and Table 5.1.5.9). The authors did not observe any 2 or 3 membered rings in the silica glass structure. This is in agreement with the results obtained in this thesis in which the smallest ring size was a 4 membered ring found in the magnesium (Table 5.1.5.1) and zinc (Table 5.1.5.5) metaphosphate glasses. The lack of 2 membered rings is in agreement with Zachariasen's network hypothesis (Section 1.1.2), which states that the structure of the phosphate backbone should consist of only corner linked phosphate units. If 2 membered rings were to be present within the phosphate backbone, this would indicate the existence of edge sharing units within the phosphate network. This is consistent with the work of Corbridge et al. [74]. The authors report that the PO_4 tetrahedra are linked toghether by the sharing of corners only and that no cases of tetrahedra sharing an edge have been established in metaphosphate glasses.

Anion structures exist for the three metaphosphate glasses and contain both chain and ring structures. The anion structures are not connected to the main polymeric backbone, we would therefore expect the highest number of anion units to occur in the lead metaphosphate glass because lead is the strongest modifier. Indeed, a greater number of both ring (Table 5.1.5.11) and chain (Table 5.1.5.12) structures are present in the lead metaphosphate glass compared to those in the magnesium and zinc metaphosphate glasses. The lead metaphosphate glass has 12 anion ring structures and 80 anion chains. Contrarily, the magnesium and zinc metaphosphate glass have 2 (Table 5.1.5.3) and 8 (Table 5.1.5.7) ring structures respectively as well as 52 (Table 5.1.5.4) and 41 (Table 5.1.5.8) anion chains respectively. A summary of the ring and chain count for the $Mg(PO_3)_2$, $Zn(PO_3)_2$ and $Pb(PO_3)_2$ glasses is given in Tables 5.1.5.1-5.1.5.12.

Table 5.1.5.1

RING STRUCTURES IN THE $Mg(PO_3)_2$PHOSPHATE BACKBONE

Ring Size (number of Patoms)	Number	Percentage
4	2	4.44
5	9	20.00
6	17	37.78
7	6	13.33
8	2	4.44
9	3	6.67
10	4	8.89
11	2	4.44

Table 5.1.5.2

CHAIN LINKAGES IN THE $Mg(PO_3)_2$PHOSPHATE BACKBONE

Chain Length (number of Patoms)	Number	Percentage
1	88	40.00
2	50	22.73
3	26	11.82
4	13	5.91
5	8	3.64
6	6	2.73
7	11	5.00
8	3	1.36
9	2	0.91
10	2	0.91
11	3	1.36
12	1	0.45
14	1	0.45
15	1	0.45
16	2	0.91
19	1	0.45
25	2	0.91

Table 5.1.5.3

RING STRUCTURES IN THE $Mg(PO_3)_2$ PHOSPHATE ANION UNITS

Ring Size (number of Patoms)	Number	Percentage
5	1	50.00
7	1	50.00

Table 5.1.5.4

CHAIN LINKAGES IN THE $Mg(PO_3)_2$ PHOSPHATE ANION UNITS

Chain Length (number of Patoms)	Number	Percentage
1	7	13.46
2	23	44.23
3	9	17.31
4	3	5.77
5	4	7.69
6	3	5.77
9	1	1.92
10	1	1.92
16	1	1.92

Table 5.1.5.5

RING STRUCTURES IN THE $Zn(PO_3)_2$ PHOSPHATE BACKBONE

Ring Size (number of Patoms)	Number	Percentage
4	1	1.96
5	7	13.73
6	22	43.13
7	8	15.69
8	7	13.73
9	3	6.00
10	1	1.96
11	1	1.96
12	1	1.96

Table 5.1.5.6

CHAIN LINKAGES IN THE $Zn(PO_3)_2$ PHOSPHATE BACKBONE

Chain Length (number of Patoms)	Number	Percentage
1	84	45.41
2	37	20.00
3	26	14.05
4	5	2.70
5	9	4.86
6	1	0.54
7	8	4.32
8	4	2.16
9	2	1.08
12	1	0.54
13	2	1.08
14	2	1.08
15	1	0.54
16	1	0.54
19	1	0.54
30	1	0.54

Table 5.1.5.7

RING STRUCTURES IN THE $Zn(PO_3)_2$ PHOSPHATE ANION UNITS

Ring Size (number of Patoms)	Number	Percentage
5	5	62.50
6	1	12.50
8	1	12.50
9	1	12.50

Table 5.1.5.8

CHAIN LINKAGES IN THE $Zn(PO_3)_2$ PHOSPHATE ANION UNITS

Chain Length (number of Patoms)	Number	Percentage
1	7	17.07
2	18	43.90
3	8	19.51
4	2	4.88
5	1	2.44
6	1	2.44
7	1	2.44
9	1	2.44
10	1	2.44
12	1	2.44

Table 5.1.5.9

RING STRUCTURES IN THE $Pb(PO_3)_2$ PHOSPHATE BACKBONE

Ring Size (number of Patoms)	Number	Percentage
5	11	32.35
6	13	38.24
7	4	11.76
8	3	8.03
9	1	2.94
10	1	2.94
11	1	2.94

Table 5.1.5.10

CHAIN LINKAGES IN THE $Pb(PO_3)_2$ PHOSPHATE BACKBONE

Chain Length (number of Patoms)	Number	Percentage
1	84	40.00
2	42	20.19
3	27	12.98
4	13	6.40
5	13	6.40
6	6	2.88
7	5	2.40
8	4	1.92
9	1	0.48
11	6	2.88
14	1	0.48
19	1	0.48

Table 5.1.5.11

RING STRUCTURES IN THE $Pb(PO_3)_2$ PHOSPHATE ANION UNITS

Ring Size (number of Patoms)	Number	Percentage
5	6	50.00
6	2	16.67
7	2	16.67
8	1	8.33
9	1	8.33

Table 5.1.5.12

CHAIN LINKAGES IN THE $Pb(PO_3)_2$ PHOSPHATE ANION UNITS

Chain Length (number of Patoms)	Number	Percentage
1	36	37.14
2	16	22.86
3	9	12.86
4	6	8.57
5	7	10.00
6	3	4.28
7	1	1.43
11	1	1.43
14	1	1.43

5.2 SUMMARY OF THE PHOSPHATE BACKBONE STRUCTURE

The phosphate backbone structure was shown to be similar in the magnesium, zinc and lead metaphosphate glasses. By investigating the PDFs, CDFs as well as the O-P-O and P-O-P it was found that the fundamental unit in the phosphate backbone for the three metaphosphate glasses is the PO_4 tetrahedral unit which are interconnected by bridging oxygen ions to form the phosphate backbone network. Nonbridging oxygen ions and Q^2 species dominated the phosphate backbone structure in the three metaphosphate glasses. Ring and chain analysis indicated that the backbone is made up of long chains of tetrahedral units as well as ring structures. This has provided some insight into the effect of the modifier on the short range structure of the metaphosphate glasses. However, a more detailed analysis of the role of the cation modifier on the glass structure can be obtained by investigating the short range order around the cation modifiers. This will be the focus of the next section.

5.3 INVESTIGATION OF THE METAL NETWORK – MODIFIER EFFECT

This section will discuss the short range order of the metal network and the effect of the network modifying cations on the structure of the three metaphosphate glasses. The different modifiers will result in different local bonding characteristics such as coordination numbers, interionic bond distances and bond angles all of which will have an impact on the structure of the metal network. The modifier's effect on the metaphosphate glass structure is described in terms of their pair and cumulative distribution functions, bond angle distributions and by determining the types of oxygen species found within the metal network. In order to examine the modifier's environment, the first coordination shell of the metal ion was considered. In a typical network former, the cutoff for the first coordination shell is evident since it is indicated by the null value in the cation-oxygen pair distribution function between the first and second coordination peaks. However, in the case of modifier cations such as magnesium, zinc and lead, there is some overlap between the first and second coordination shells. Therefore, in order to make a valid comparison with other modeling studies and experimental data, it is important to define the extent of the first coordination shell for the modifiers. The cutoff distance, which defines the extent of the first coordination shell, occurs at the minimum distance between the first and second coordination peaks in the PDFs. This definition is also important since the coordination of each metal will change depending on the cutoff distance chosen.

Different experimental techniques have been used to study the structure of metaphosphate glasses. Unfortunately, the information obtained is contradictory with

respect to the local order around the modifier ions. For instance, Kanazawa [41] has found, using X-ray spectroscopy, that the magnesium ions in a magnesium metaphosphate glass have an average coordination number of 6.0 whereas Matz et al. [50] using neutron diffraction experiments report an average coordination number of 4.0. Such discrepancies have also been observed in zinc metaphosphate glasses [57]. The next section will shed some light on the discrepancies observed experimentally by employing computer simulation techniques.

5.3.1 THE METAL-OXYGEN PAIR

To establish the effect of the cation modifiers on the metaphosphate glass structures, the metal-oxygen (M-O) pair and cumulative distribution functions were investigated. Figures 5.3.1.1a, 5.3.1.1b and 5.3.1.1c show the PDFs for the M-O pair in the magnesium, zinc and lead metaphosphate glasses respectively. The average interionic bond distances were determined to be 2.1 Å for Mg-O, 2.0 Å for Zn-O and 2.4 Å for Pb-O using a spherical cutoff of 2.7 Å for the magnesium and zinc metaphosphate glasses and 3.0 Å for the lead metaphosphate glass respectively.

The M-O interionic bond distances obtained from the simulations are in excellent agreement with experimental results found in the literature. For example, in a study of various metaphosphate glasses using X-ray and neutron diffractions, Hoppe et al. [40] report an average Mg-O and Zn-O interionic bond distance of 2.00 Å and 1.95 Å respectively. Musino et al. [51] have studied lead metaphosphate glass using X-ray diffraction and report the Pb-O interionic bond distance to be 2.48 Å.

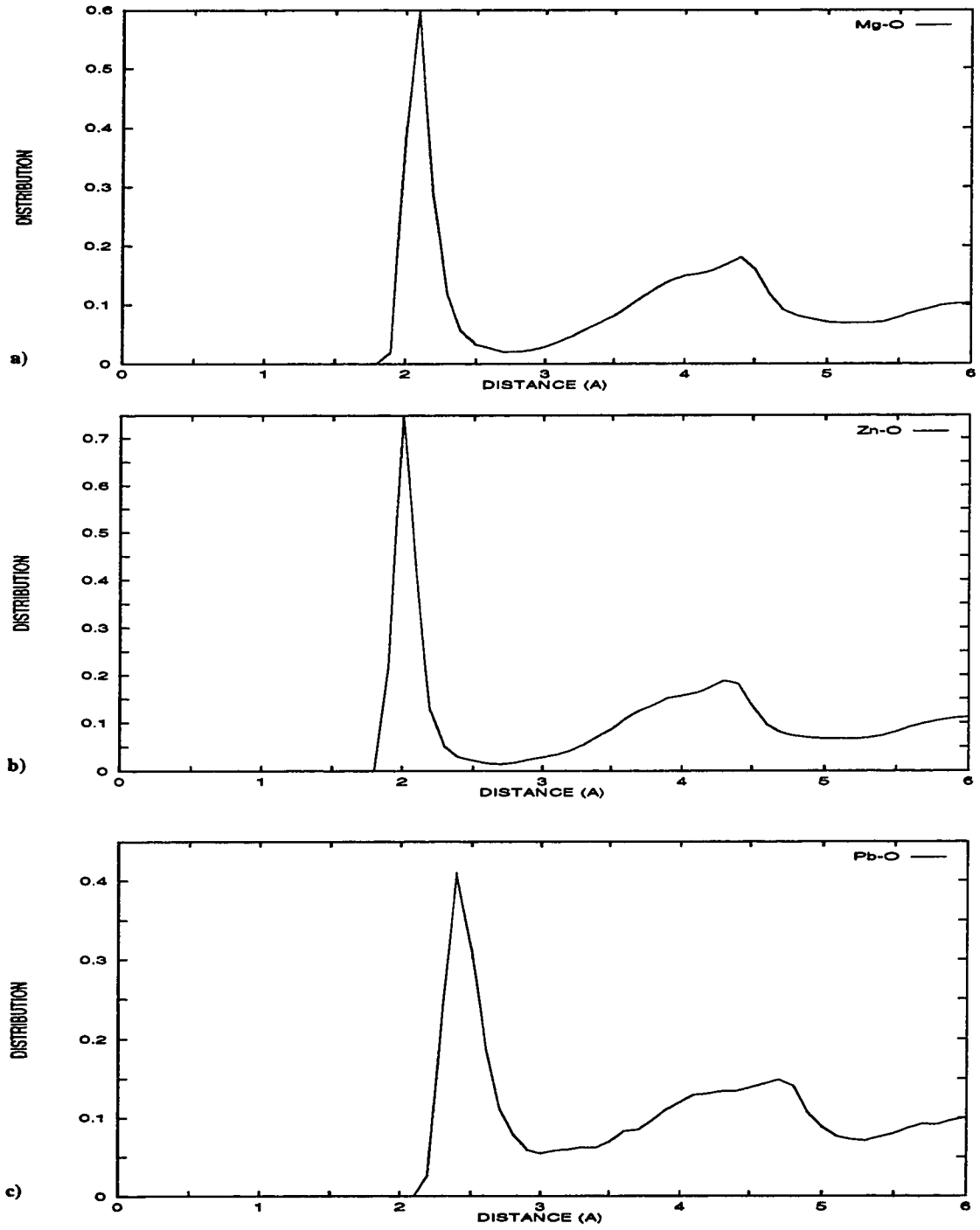

Figure 5.3.1.1 Pair distribution functions for the M-O pair in the a) $Mg(PO_3)_2$, b) $Zn(PO_3)_2$ and c) $Pb(PO_3)_2$ glasses.

The results from the simulation are also in excellent agreement with calculated values obtained using the ionic radii for the M-O pair [40]. Hoppe et al. [40] report the calculated Mg-O and Zn-O interionic bond distances to be 1.92 Å and 1.95 Å respectively.

A common feature in the three PDFs (Figure 5.3.1.1) is the overlap between the first and second coordination peaks, indicating that a clear differentiation between the first and second coordination shells cannot be made. The overlap between the two peaks is more pronounced in the case of the lead metaphosphate glass, suggesting a more defined first coordination shell for the magnesium and zinc ions. Their pair distribution functions show a sharp first peak (FWHM = 0.2 Å) in comparison to the broader peak (FWHM = 0.3 Å) observed for the lead-oxygen pair. The broader distribution in the $Pb(PO_3)_2$ glass indicates the diversity of local environments which the lead ion can occupy in comparison to the more preferred local environments of the magnesium and zinc ions.

The similarities between the Mg-O and Zn-O local environments have also been reported by Matz et al. [50] who studied the structure of various metaphosphate glasses (Zn, Mg, Ca, Sr, and Ba) using neutron diffraction experiments. The authors reported that the atomic distribution functions of the magnesium and zinc metaphosphate glasses show three well defined maxima, the first corresponding to the P-O pair and the third to the O-O pair. The feature that characterizes these metaphosphate glasses (Mg and Zn) is the existence of a small additional peak at r = 0.2 nm located between the first and third peaks. This peak was attributed to the metal-oxygen interionic bond distance, 1.98 Å and 1.92 Å, in the $Mg(PO_3)_2$ and $Zn(PO_3)_2$ glasses respectively.

The short range structure of a glass is similar to that of the crystal counterpart. There are however subtle differences in the interionic bond distances, bond angles and geometric arrangements. Nevertheless, the crystal structure provides a basis for studying the structure of glasses. Comparing the structural data obtained for the simulated metaphosphate glasses to those of the corresponding crystals, similarities were observed. For example, the average Mg-O bond length in crystalline magnesium tetrametaphosphate is 2.09 Å [54] which is in good agreement with the value of 2.1 Å obtained for the simulated magnesium metaphosphate glass. The Zn-O bond length in the zinc metaphosphate crystal has been reported to be 2.09 Å [53] which is also in excellent agreement with the value reported for the zinc metaphosphate glass in this thesis. To our knowledge no data is available on a lead metaphosphate crystal.

The cumulative distribution functions for the M-O pair also describes the local environments of the metal ions. Figures 5.3.1.2a, 5.3.1.2b, and 5.3.1.2c show the CDFs for the Mg-O, Zn-O and Pb-O pairs respectively. The average coordination number obtained for magnesium at a cutoff of 2.7 Å, was 4.3. Using the same cutoff distance a comparable coordination number of 4.1 was found for zinc (Figure 5.3.1.2b). An average coordination number of 5.5 was found for the lead ions, using a cutoff of 3.0 Å. A larger radial cutoff distance was used for the lead metaphosphate glass because the broader corresponding PDF. The strong modifying ability of the lead ion in comparison to the magnesium and zinc ions will contribute to the higher coordination number observed since it will depolymerize the phosphate network to a greater extent. As the phosphate network is depolymerized, bridging oxygen ions are converted to nonbridging oxygen ions thus increasing the number of oxygens available for bonding to the metal network (this will be

described in more detail in Section 5.3.4). The relationship between the number of NBOs and M-O coordination numbers has also been discussed by Uchino et al. [55] in their study of binary alkali metaphosphate glasses using Ab initio molecular orbital calculations.

The similar coordination number for the magnesium and zinc ions may be attributed to their comparable field strengths. The metal ions will interact in a similar fashion with the nearest neighbor oxygen ions resulting in a similar degree of depolymerization of the phosphate network and thus similar coordination numbers are observed. The importance of field strength on the metal coordination number has also been reported in the literature [75,76].

The coordination numbers obtained for M-O pairs in this thesis are in excellent agreement with the recent X-ray and neutron diffraction studies by Hoppe et al. [40] who report an average metal-oxygen coordination number of 4.3 and 4.0 in the magnesium and zinc metaphosphate glasses respectively. Matz et al. [50] have reported similar coordination numbers (4.0 for Mg and 3.75 for Zn) using neutron diffraction. The lead coordination number reported in this thesis agrees very well with the value of 5.04 reported by Musino et al. [51] using X-ray diffraction.

It is interesting to note that the CDF for the Mg-O and Zn-O pairs (Figure 5.3.1.2a and 5.3.1.2b) show a plateau that extends to 3.2 Å, supporting the similar environments for the Mg and Zn ions. In contrast, the CDF for the Pb-O pair (Figure 5.3.1.2c) does not show a plateau, due to the broad peak found in the corresponding PDF, indicating that the Pb ions have a greater variety of local environments than the Mg or Zn ions. This is consistent with the results from the M-O PDFs as well as with experimental data [77, 78].

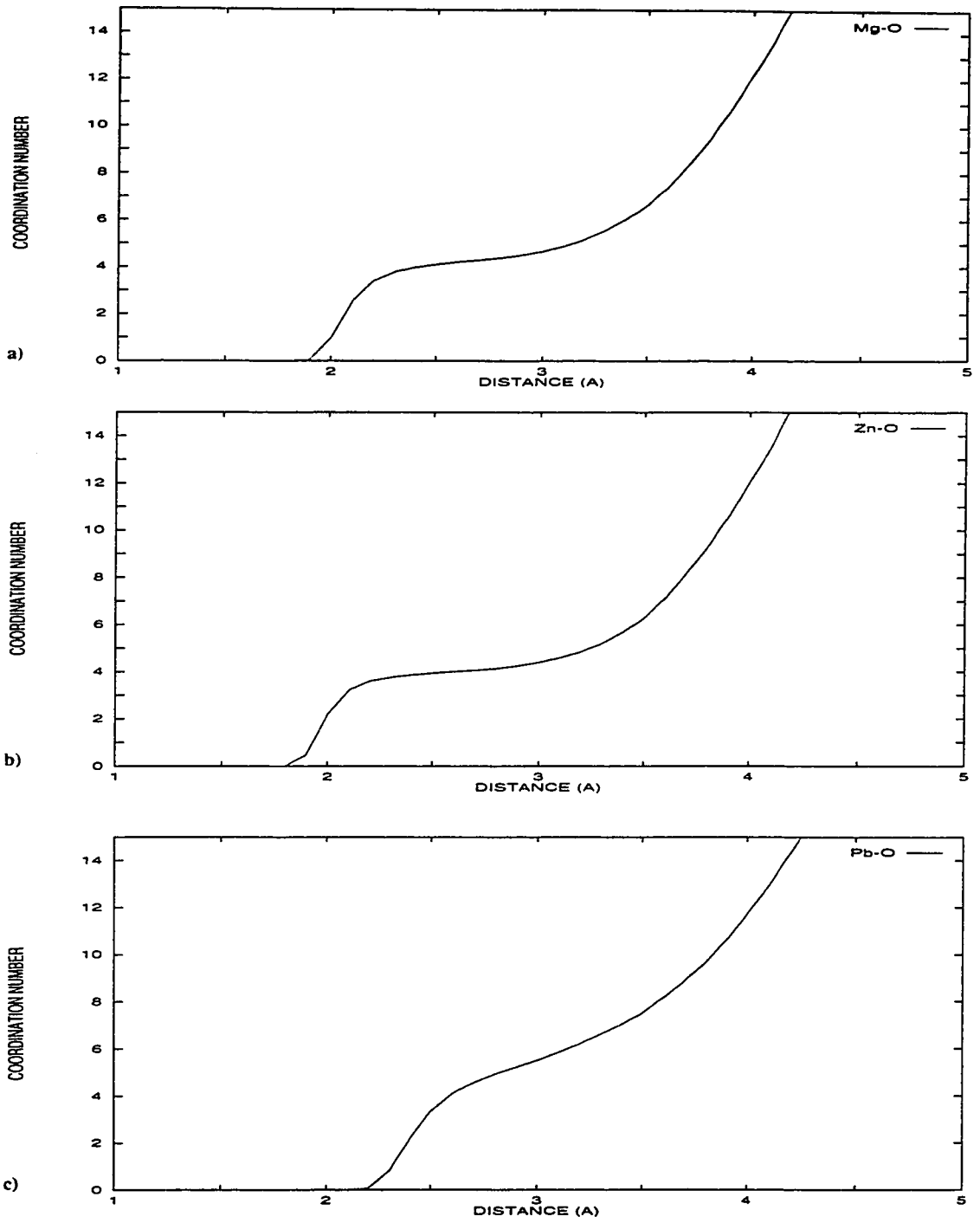

Figure 5.3.1.2 Cumulative distribution functions for the M-O pair in the a) $Mg(PO_3)_2$, b) $Zn(PO_3)_2$ and c) $Pb(PO_3)_2$ glasses.

The probability distributions of the oxygen neighbors surrounding the Mg, Zn and Pb ions for each metaphosphate glass are shown in Figure 5.3.1.3. The range of coordination numbers varies from 3 to 6 for both the Mg-O and Zn-O pair. The most likely coordination number for the Mg and Zn ions is four. Figure 5.3.1.3a shows a significantly higher percentage of 5 coordinated species for the Mg ion (31.5 %) in comparison to the percentage (19.9 %) for the Zn ion shown in Figure 5.3.1.3b. This is explained by considering the field strength values of the Mg (0.51) and Zn (0.59) ions. The stronger modifying ability of the Mg ion will break up the phosphate network to a greater extent and create more NBOs than zinc (further discussion in Section 5.3.4). This will increase the possibility of higher coordinated species to form within the metal network. Furthermore, the similar distribution of coordination numbers for the Mg and Zn ions reveals that these modifiers have similar local environments.

The probability distribution of oxygen neighbors surrounding Pb ions (Figure 5.3.1.3c) shows predominantly 5 and 6 coordinated structures. The stronger modifying ability and significantly larger ionic radii of the lead ion produces the higher coordination numbers observed in the lead metaphosphate glass. The diverse distribution of coordination numbers in the lead metaphosphate glass clearly indicates a greater number of possible local environments for the lead modifier. This is in contrast to the fewer, more preferred, environments of the Mg and Zn ions. This is consistent with the observations from the PDFs and CDFs of the M-O pair.

A summary of the metal-oxygen interionic bond distances and coordination numbers obtained from the simulation is shown in Table 5.3.1.1 along with a comparison to experimental data.

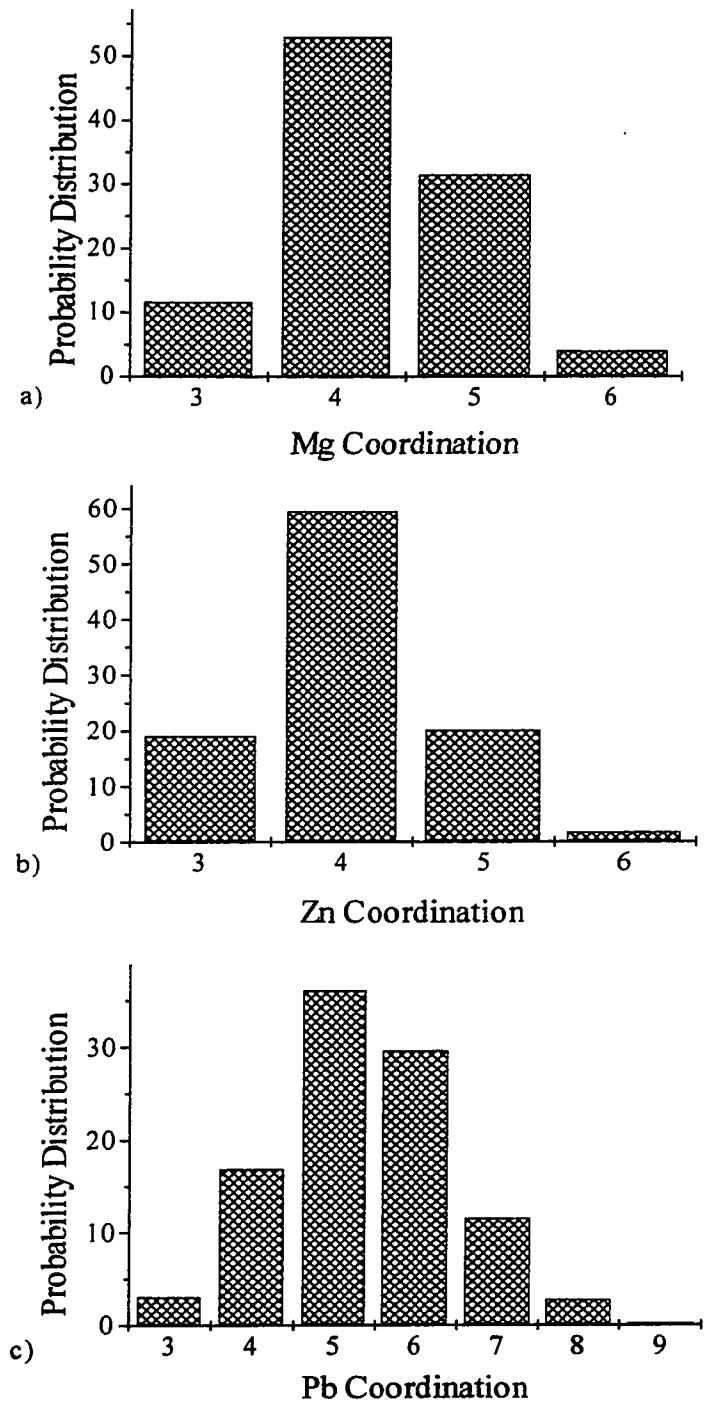

Figure 5.3.1.3 Histograms of the probability versus coordination number for the metal ions in the a) $Mg(PO_3)_2$, b) $Zn(PO_3)_2$, and c) $Pb(PO_3)_2$ glasses.

Table 5.3.1.1

A SUMMARY OF METAL COORDINATION NUMBERS, N

AND BOND DISTANCES, r

Reference	Glass	r_{Me-O} (Å)	N_{Me-O}	Technique
Musino	$Zn(PO_3)_2$	1.996	4.74	X-ray
et al. [51]	$Pb(PO_3)_2$	2.484	5.04	diffraction
Matz	$Mg(PO_3)_2$	1.975	4.00	Neutron
et al. [50]	$Zn(PO_3)_2$	1.920	3.75	diffraction
Hoppe	$Mg(PO_3)_2$	2.00	4.3	X-ray and
et al. [40]	$Zn(PO_3)_2$	1.95	4.0	Neutron diffraction
Bionducci	$Zn(PO_3)_2$	1.94	3.93	Neutron, X-ray
et al. [57]				diffractions EXAFS
Matsubara	$Zn(PO_3)_2$	1.96	4.87	X-ray
et al. [56]				Scattering
This	$Mg(PO_3)_2$	2.1	4.3	MD
thesis	$Zn(PO_3)_2$	2.0	4.1	
	$Pb(PO_3)_2$	2.4	5.5	

5.3.2 THE METAL-METAL AND METAL-PHOSPHORUS PAIR

The metal-metal (M-M) pair distribution functions are shown in Figure 5.3.2.1a, 5.3.2.1b and 5.3.2.1c for the $Mg(PO_3)_2$, $Zn(PO_3)_2$ and $Pb(PO_3)_2$ glasses respectively. The first coordination peaks in the three PDFs are broad, asymmetric and do not return to a null value, revealing the disordered arrangement for the three metal networks. The average M-M bond distance was found to be 3.1 Å (cutoff = 3.2 Å) and 3.0 Å (cutoff = 3.4 Å) for the Mg-Mg and Zn-Zn pairs respectively. Using X-ray diffraction Musino et al. [51] report an average Zn-Zn bond distance of 3.27 Å for a zinc metaphosphate glass which is in good agreement with the value reported in this thesis. The Zn-Zn bond distance obtained from the MD simulation is also in agreement with the corresponding bond length (3.25 Å) found in the $Zn(PO_3)_2$ crystal [53]. Metal-metal bond lengths for the magnesium or lead metaphosphate crystals have not been reported in the literature.

The MD simulation shows that the environment of the Pb-Pb pair differs significantly from that of the magnesium or the zinc pairs. The average Pb-Pb interionic bond distance was found to be 3.7 Å within a spherical cutoff of 4.3 Å (Figure 5.3.2.1c). Although no experimental data reports the Pb-Pb bond distance for a lead metaphosphate glass, Rabinovich [79] report a Pb-Pb bond distance of 3.9 Å in a 30 mol % $PbO.SiO_2$ glass which is in excellent agreement with the value reported in this thesis. The first coordination peak in the Pb-Pb PDFs (Figure 5.3.2.1c) is composed of several maxima indicating that there are several different environments for the lead ion, in contrast to the Mg-Mg and Zn-Zn PDFs which show a maximum and a small shoulder (Figure 5.3.2.1a and 5.3.2.1b).

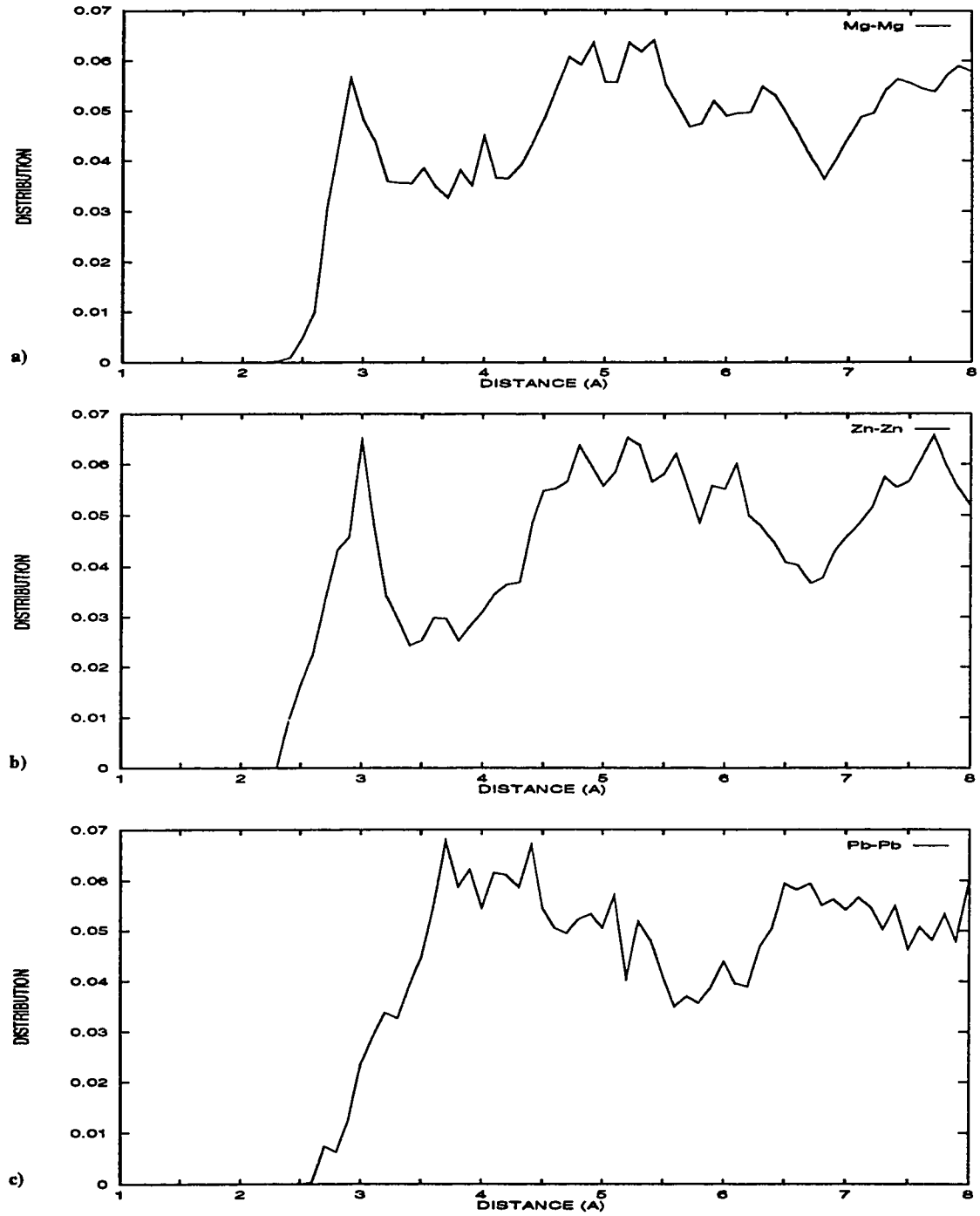

Figure 5.3.2.1 Pair distribution functions for the M-M pair in the a) $Mg(PO_3)_2$, b) $Zn(PO_3)_2$ and c) $Pb(PO_3)_2$ glasses.

The shoulder in Figure 5.3.2.1a appears at longer bond distances (3.1 Å) from the maximum of the Mg-Mg pair. This is in contrast to the shoulder at 2.7 Å in the zinc metaphosphate glass indicating some shorter Zn-Zn interactions from the primary maximum (Figure 5.3.2.1b). The shoulders observed in the PDFs may be attributed to both corner and edge sharing structures found within the magnesium and zinc metal networks. Evidence of edge sharing structures was obtained from the M-O-M bond angles (Section 5.3.3) and by viewing the metaphosphate glasses pictorially. An example of an edge sharing structure in the zinc metaphosphate glass is shown in Figure 5.3.2.2.

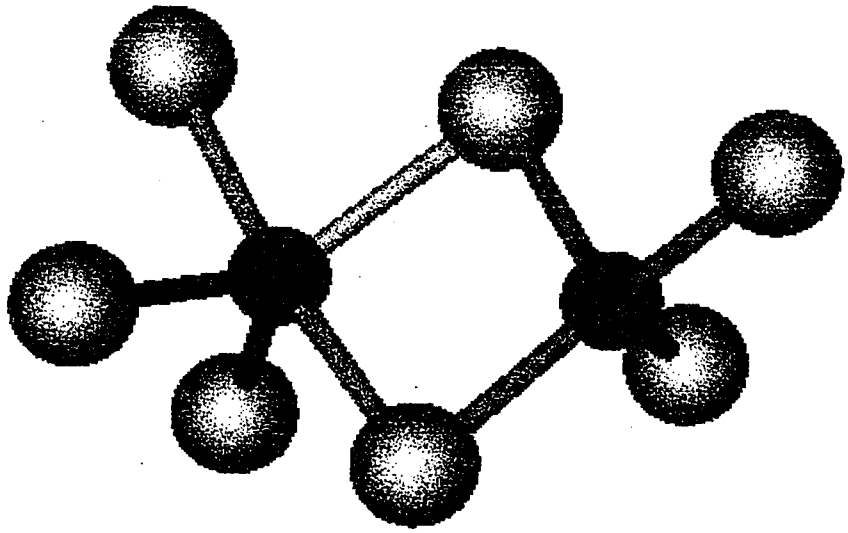

Figure 5.3.2.2 Pictorial representation of an edge sharing structure in the zinc metaphosphate glass. The dark grey spheres represent zinc and the light grey spheres represent oxygen.

The cumulative distribution functions for the Mg-Mg, Zn-Zn and Pb-Pb pairs are shown in Figure 5.3.2.3a, 5.3.2.3b and 5.3.2.3c respectively. The average CN for Pb is 1.0 nearest neighbor lead ions within 4.3 Å. This is in excellent agreement with the value of 1.11 determined by Musino et al. [51] using X-ray diffraction. The coordination values for the Mg-Mg and Zn-Zn are 0.2 (cutoff = 3.2 Å) and 0.3 (cutoff = 3.4 Å) respectively. The similar coordination numbers for the Mg-Mg and Zn-Zn pair supports previous results (Section 5.3.1 and 5.3.2) that the modifiers have similar local environments in comparison to the variety of local environments possible for the lead ion. Takahashi [80] has also reported the similar structural behavior between the Mg and Zn ions in contrast to the Pb ion. The author has studied the effect of various metals and their field strengths on the physical properties of phosphate glasses. Accordingly, the Mg and Zn ions were found to have a similar effect while the lead ion was classified in a separate category.

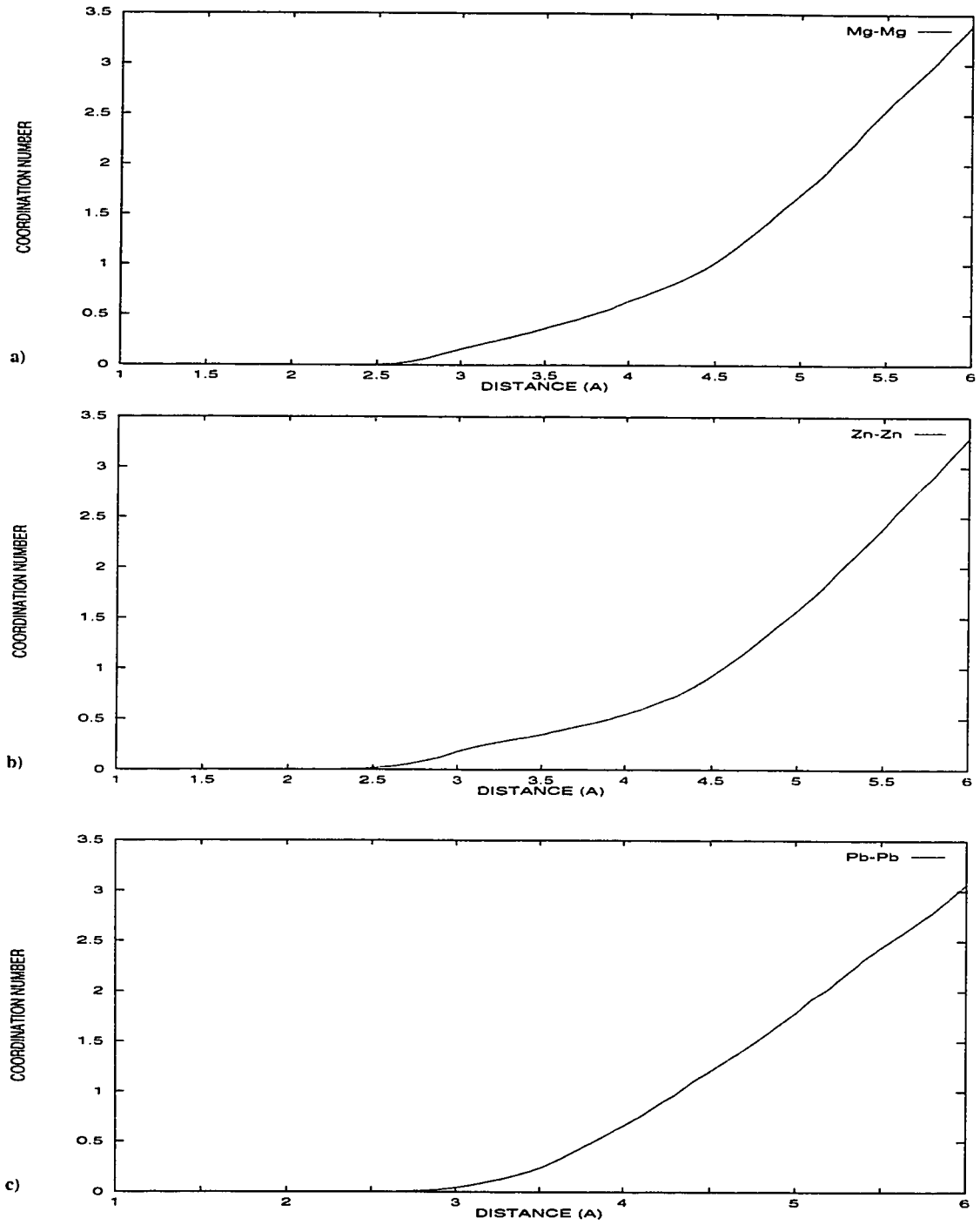

Figure 5.3.2.3 Cumulative distribution functions for the M-M pair in the a) $Mg(PO_3)_2$, b) $Zn(PO_3)_2$ and c) $Pb(PO_3)_2$ glasses.

The PDFs and CDFs of the metal-phosphorus (M-P) pair are important because they describe the linkage between the metal network and the phosphate backbone and consequently provide information on the effect of the modifier on the phosphate backbone structure. The PDFs of the M-P pairs are shown in Figure 5.3.2.4 for the three metaphosphate glasses and show sharp maxima for the first peak, representing the average bond distance, at 3.4 Å, 3.3 Å, and 3.6 Å for the Mg-P, Zn-P and Pb-P pairs respectively. The Zn-P and Pb-P interionic bond distances are in excellent agreement with the values found experimentally (3.19 Å and 3.62 Å respectively) by Musino et al. [51]. A broader pair distribution function for the Pb-P pair is observed with a FWHM of 0.7 Å compared to the narrower pair distribution function for the Mg-P and Zn-P pair both with a FWHM of 0.4 Å. The narrower distribution indicates a more defined first coordination shell for the magnesium and zinc ions. The pair distributions are consistent with the field strength of each modifier. Since lead is the strongest modifier, it will disrupt the phosphate backbone more than the Mg or Zn ions, causing them to occupy a greater number of possible local environments, which translates into a broader Pb-P PDF (Figure 5.3.2.4c).

A relationship can also be made between the M-P bond distance and the M-O coordination number. This is because the M-P pair includes a nonbridging oxygen ion resulting in a M-O-P bonding arrangement. As seen in Section 5.3.1, the type of metal incorporated into the glass structure will affect the M-O CN depending on the field strength of the modifier. A strong modifier such as Pb will create a higher number of NBOs resulting in a higher M-O CN. A higher M-O CN will necessarily increase the M-P interionic bond distance since the greater number of oxygen ions surrounding a metal ion will require the phosphorus ions to position themselves further away.

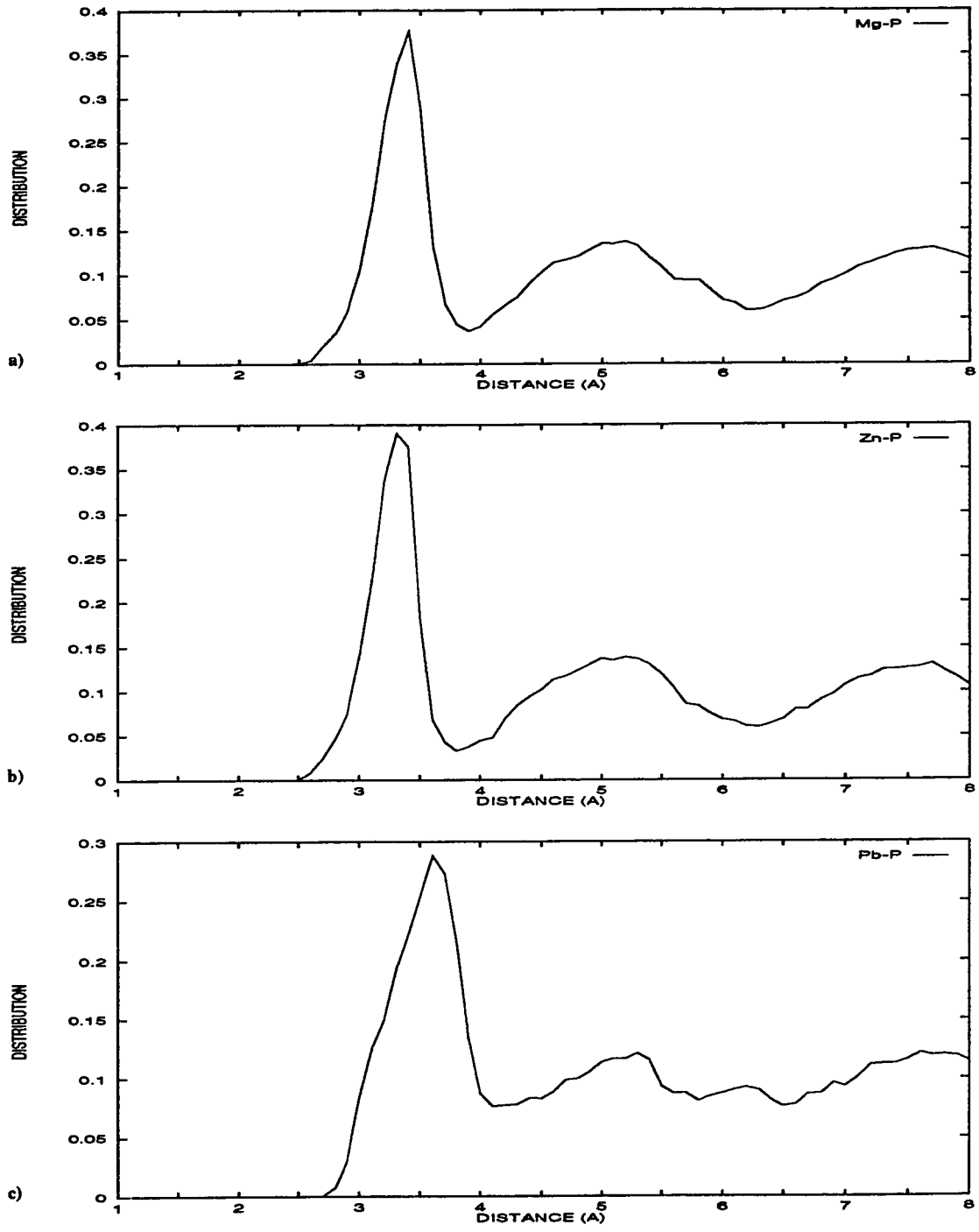

Figure 5.3.2.4 Pair distribution functions for the M-P pair in the a) $Mg(PO_3)_2$, b) $Zn(PO_3)_2$ and c) $Pb(PO_3)_2$ glasses.

This relationship is clearly seen from the results reported in this thesis. The M-O CN decreases from 5.5 to 4.3 to 4.1 and is accompanied by a decrease in the M-P interionic bond distance from 3.6 Å to 3.4 Å to 3.3 Å for the lead, magnesium and zinc metaphosphate glasses respectively.

The coordination numbers for the M-P pair were obtained from the M-P CDFs shown in Figure 5.3.2.5. An average M-P CN of 4.4, 4.0 and 5.3 was determined within a spherical cutoff of 3.9, 3.8 and 4.1 Å in the magnesium, zinc, and lead metaphosphate glasses respectively. A greater number of local environments for the lead ion may be inferred from the Pb-P CDF (Figure 5.3.2.5c) since it does not show a plateau. This is not the case for both the Mg-P and Zn-P CDFs. The M-P CNs obtained from the MD simulations are consistent with the field strength values of the modifier ions. The lead ions will disrupt the phosphate backbone to a greater extent than the Mg and Zn ions resulting in a high Pb-P CN (5.3). Zinc having the weakest ability to disrupt the phosphate backbone exhibits the lowest M-P CN (4.0). Musino et al. [51] have studied zinc and lead metaphosphate glasses using X-ray diffraction and their results reveal similar structural characteristics to the M-P CDFs obtained from the simulations. For example, the authors report an average Zn-P coordination number of 3.03 and a Pb-P coordination number of 4.54.

The coordination numbers obtained for the M-P pairs in conjunction with the M-O CNs (Section 5.3.1) suggests that the metal ions position themselves between the long phosphate chains. This is because the M-P CNs are very similar to the corresponding M-O CNs, such that every oxygen ion that is bonded to a modifier, will also be bonded to a phosphorus ion. Such structural arrangements were also reported experimentally [50].

The results from the M-P PDFs and CDFs indicate that the local environments between the magnesium and zinc ions are more similar in comparison to the lead ions environment. This can be attributed to the similar field strength values and ionic radii of the Mg and Zn ions which will break up the phosphate backbone network to a comparable extent resulting in similar M-P bond distances and coordination numbers.

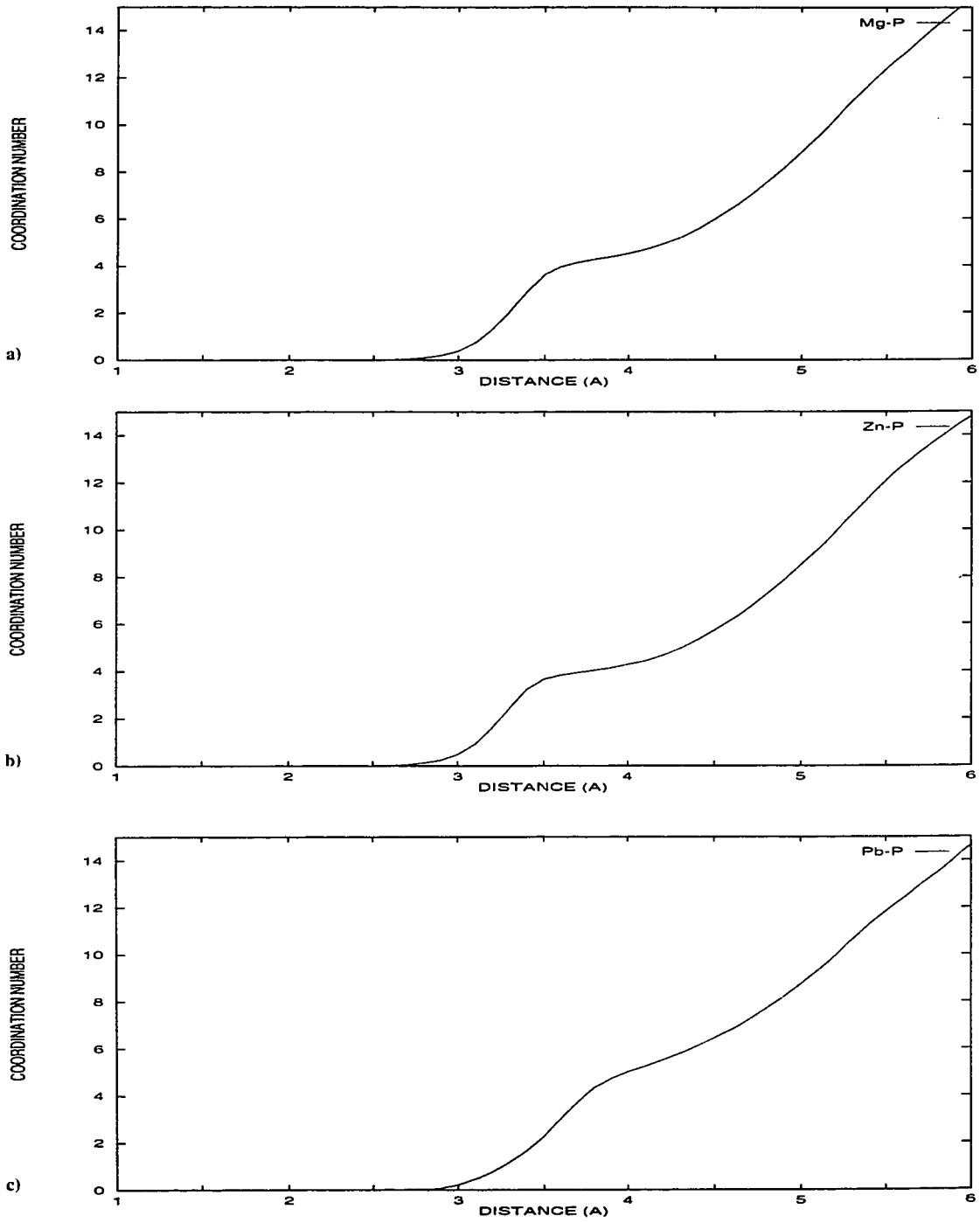

Figure 5.3.2.5 Cumulative distribution functions for the M-P pair in the a) $Mg(PO_3)_2$, b) $Zn(PO_3)_2$ and c) $Pb(PO_3)_2$ glasses.

5.3.3 O-M-O AND M-O-M BOND ANGLE DISTRIBUTIONS

To further quantify the local environment of the metal ions, the O-M-O and M-O-M bond angle distributions (BADs) were calculated for the three metaphosphate glasses. These bond angle distributions represent time averaged values, that is they were run through the MD simulation for an additional 10 000 time steps which accounts for the vibrational motion present in the network. The O-M-O bond angle distributions are shown in Figure 5.3.3.1a, 5.3.3.1b and 5.3.3.1c for the magnesium, zinc and lead metaphosphate glasses respectively. The magnesium and zinc metaphosphate glasses show two O-M-O bond angles. The first appears at 55^0 and a second broader and more intense peak at 89^0 for the magnesium metaphosphate glass while bond angles at 55^0 and 94^0 were observed in the zinc metaphosphate glass. In addition to similar bond angles, the magnesium and zinc metaphosphate glasses also exhibit similar FWHM of 6^0 and 24^0 for the first and second peaks respectively.

The presence of two peaks, at 56^0 and 80^0, is also observed in the lead metaphosphate glass but have broader distributions with FWHMs of 7^0 and 28^0 respectively. The broader distribution reflects the variety of Pb local environments as well as the range of coordination numbers (Section 5.3.1).

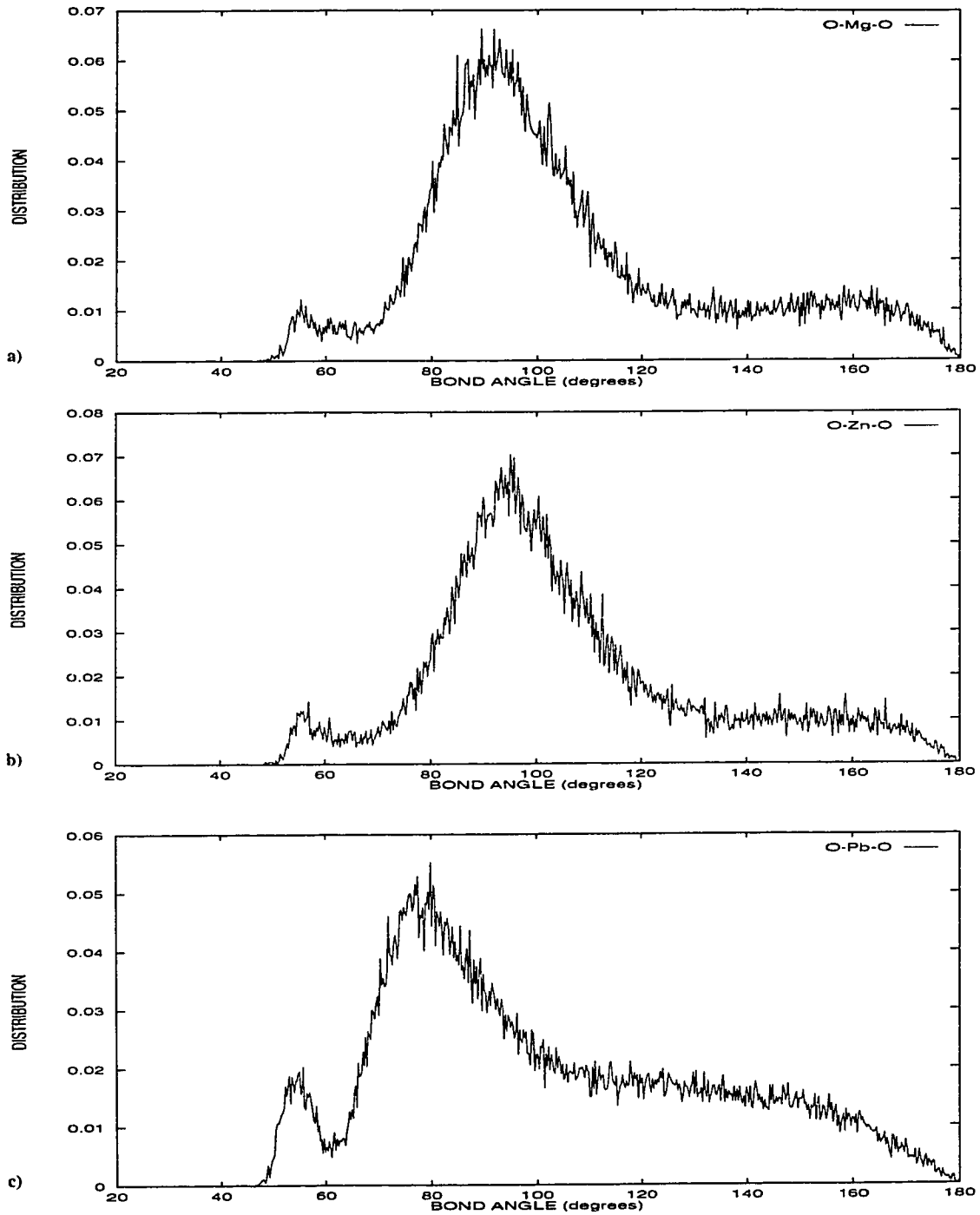

Figure 5.3.3.1 Time averaged O-M-O bond angle distributions for the a) $Mg(PO_3)_2$, b) $Zn(PO_3)_2$ and c) $Pb(PO_3)_2$ glasses.

The larger angle at approximately 90^0 observed in the magnesium and zinc BADs represent both edge and corner sharing oxygen structures found within the metal networks. Furthermore, the angle is associated with the distorted 4 coordinated structures which predominate the magnesium and zinc metal networks. Therefore, the tetrahedral geometry postulated for magnesium and zinc in the literature [50,51] is not possible. The higher coordinated structures (5 and 6) found within the metal networks also possessed a bond angle of approximately 90^0. These results were confirmed by viewing the metaphosphate glasses pictorially.

The lower peak at 80^0 in the lead metaphosphate glass (Figure 5.3.3.1c) is less intense than the corresponding peak in either the magnesium or zinc metaphosphate glasses. The lowered angle is due to the distribution of higher coordination numbers (7, 8 and 9 odd coordinated structures) observed for the Pb-O pair which will result in a lowered average O-M-O bond angle. The intensity of the peak at 80^0 is reduced because of the broad range of coordinated structures that do not show similar bond angles. The numerous bond angles observed in the lead network translates to a broader peak and indicates that the lead ions have various local environments in comparison the magnesium and zinc ions. Furthermore, the angle at 80^0 corresponds to both edge and corner sharing oxygen structures within the lead network.

The peak at smaller bond angles in Figure 5.3.3.1 has a similar distribution in the magnesium and zinc metaphosphate glasses. This bond angle at approximately 55^0 may be attributed to metal-phosphorus edge sharing oxygen structures (M-O-P-O). This arrangement acts as a link between the metal and phosphate networks and is formed by the addition of the metal modifier, which depolymerizes the phosphate backbone and creates NBOs. The lead metaphosphate glass demonstrates a higher probability of finding the metal-phosphorus edge sharing oxygen structures as indicated by a more intense peak at 54^0. This is consistent with the field strength of the lead ion, which renders it the strongest modifier of the three metals investigated in this thesis and therefore creates a higher number of NBOs (Section 5.3.4) and thus edge sharing structures become more probable. An example of the metal-phosphorus edge sharing structures affiliated with the lower bond angle in the three metaphosphate glasses is illustrated in Figure 5.3.3.2.

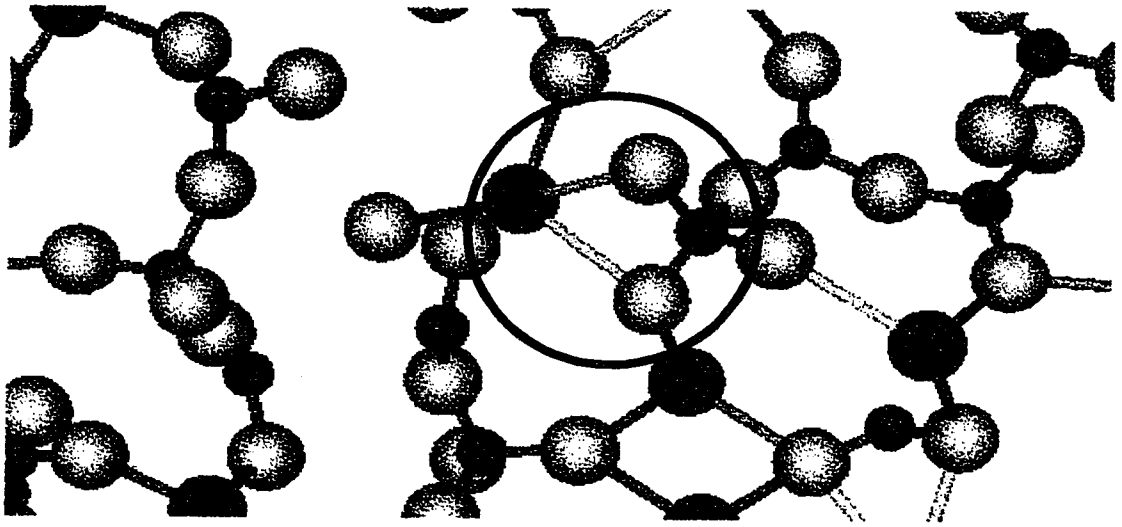

Figure 5.3.3.2 Edge sharing oxygen ions (M-O-P-O) in the $Pb(PO_3)_2$ glass. The larger dark grey spheres represent lead, the smaller dark grey spheres represent phosphorus and the light grey spheres oxygen.

Figures 5.3.3.3a, 5.3.3.3b, 5.3.3.3c show the M-O-M time averaged bond angle distributions for $Mg(PO_3)_2$, $Zn(PO_3)_2$ and $Pb(PO_3)_2$ glasses respectively. The lead metaphosphate glass showed the broadest distribution centered at 87^0 with a FWHM of 53^0 while the magnesium and the zinc metaphosphate glasses have average M-O-M bond angles of 81^0 and 86^0 with a FWHM of 42^0 and 46^0 respectively. The broader BAD seen in the lead metaphosphate glass indicates a greater number of environments for the lead ion in comparison to the number for the magnesium and zinc ions. In addition, the M-O-M bond angle accurately predicts the O-M-O bond angle attributed to edge sharing structures within the metal network as well as the M-M bond distances discussed in Section 5.3.2.

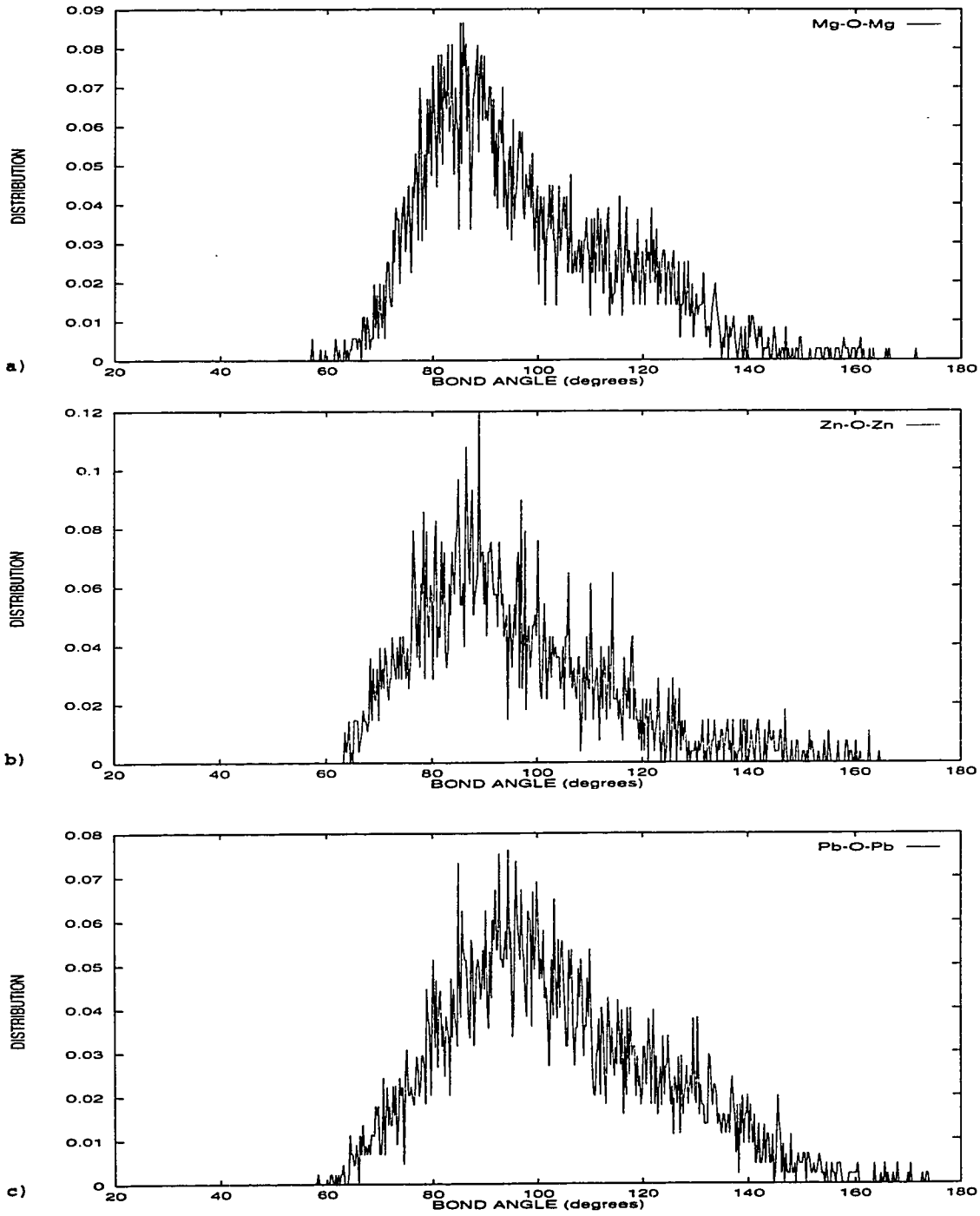

Figure 5.3.3.3 Time averaged M-O-M bond angle distributions for the a) $Mg(PO_3)_2$, b) $Zn(PO_3)_2$ and c) $Pb(PO_3)_2$ glasses.

5.3.4 TYPES OF OXYGEN IONS SURROUNDING THE METAL NETWORK

To interpret the changes in the local environment of each modifier it is useful to know the type of oxygens surrounding each metal ion. The data presented in Table 5.3.4.1 is a tabulation of the speciation of oxygens in the first phosphorus-oxygen coordination shell with respect to the metal network. The results are obtained by first counting the number of oxygens surrounding the metal ion within the first M-O coordination shell. If the oxygens surrounding the metal ions are connected to one phosphorus, it is labeled as a NBO, if it is connected to another phosphorus ion, it is labeled as a BO, the free oxygens are those which are connected to the metal network but not to the phosphate network. Table 5.3.4.1 shows that over 90 % of the oxygens connected to the modifier have at least one phosphorus neighbor within a distance of 3.0 Å. The high percentage of NBOs indicates that the metal ions form linkages between the long phosphate chains. This substantiates the results presented in Section 5.3.2 in which the similar CNs for the M-O and M-P pairs also indicated that the metal ions position themselves between the phosphate chains. The ability of the metal ions to position themselves between the phosphate chains has been reported by Martin [62]. The high percentage of NBOs in metaphosphate glasses has also been observed using ^{31}P MAS NMR by Brow et al. [67]. The authors studied the short range order of zinc polyphosphate glasses and have concluded that as the concentration of zinc increases, the metals position themselves interstitially between the phosphate chains hence increasing the number of NBOs.

The results obtained for the $Mg(PO_3)_2$ glass indicate that 99.4 % of the oxygens surrounding magnesium ions are connected to the phosphate network (phosphorus), 0.4 %

of the oxygens surrounding magnesium are surrounded by two phosphorus ions while 0.2 % of the oxygens are only connected to Mg ions. These results are similar to those obtained for the $Zn(PO_3)_2$ glass (Table 5.3.4.1) and confirms previous conclusions stated in this thesis (Sections 5.1.4, 5.1.5 and 5.3) that the $Mg(PO_3)_2$ and $Zn(PO_3)_2$ glasses have similar structural features. In contrast, the results obtained for the $Pb(PO_3)_2$ glass do not show any free oxygens and show the highest percentage of NBO (99.7 %) species.

Table 5.3.4.1

TYPES OF OXYGENS SURROUNDING INDIVIDUAL METAL IONS

MODIFIER	% FREE	% NBO	% BO	% EXTRA
Mg	0.2	99.4	0.4	0.0
Zn	0.5	98.9	0.6	0.0
Pb	0.0	99.7	0.3	0.0

These results are consistent with the field strength values of the cation modifiers. The lead ion will disrupt the phosphate network more extensively than the Mg or Zn ions, thus creating the highest percentage of NBOs. Zinc being the weakest modifier has the lowest percentage of NBOs. The relative percentage of NBOs for the three metaphosphate glasses is consistent with the results of the M-O and M-P coordination numbers (Sections 5.3.1 and 5.3.2). Since the $Pb(PO_3)_2$ glass has the highest M-P coordination number it is

reasonable that it has the highest percentage of NBOs since it forms the most M-O-P linkages by breaking up the phosphate network. The zinc metaphosphate glass has the lowest M-P coordination number thus resulting in fewer linkages to the phosphate network and consequently the fewest number of NBO species (Table 5.3.4.1).

A summary of the results pertaining to the speciation of oxygen ions in the first metal-oxygen coordination shell with respect to the phosphate network is presented in Table 5.3.4.2. These results were obtained by first counting the number of oxygen ions within the first P-O coordination shell (2.1 Å). The oxygen ions surrounding phosphorus ions and which are also bonded to a metal ion are tabulated. The values reported in Table 5.3.4.2 indicate the percentage of oxygens (n) which are part of the phosphate backbone but are also attached to a modifier. For example, n = 2 indicates that there are two metals surrounding a backbone oxygen while n = 3 reveals that there are three metals surrounding a central oxygen ion which is also connected to the phosphorus network. Table 5.3.4.2 shows that over 50 % of the oxygens surrounding phosphorus are not attached to a modifier (% n = 0) and most probably remain as bridging oxygen ions. The addition of a modifier depolymerizes the phosphate network by converting phosphorus bridging oxygen ions (BO) to nonbridging oxygen ions (NBO). The relationship between the number of NBOs and the extent of possible local environments surrounding the metal ion has been reported in the literature [81,82]. For example, Minser et al. [82] report that a greater number of NBOs causes an increase in the depolymerization of the backbone structure which also causes an increase in the variety of possible local environments for the metal ion.

Table 5.3.4.2

TYPES OF OXYGENS RELATED TO THE METAL BACKBONE SURROUNDING INDIVIDUAL PHOSPHORUS IONS

Metal	% n = 0	% n = 1	% n = 2	% n = 3	% n = 4
Mg	55.7	35.1	9.1	0.1	0.0
Zn	57.1	35.3	7.5	0.1	0.0
Pb	50.7	30.9	16.9	1.5	0.0

Consequently one would expect a greater number of nonbridging oxygen ions in the lead metaphosphate glass (due to its lower field strength). This is shown to be the case since the percentage of n = 1, n = 2, and n = 3 oxygens which totals 49.3 % is higher than the percentages found for the magnesium (44.3 %) and zinc metaphosphate glasses (42.9 %).

Tables 5.3.4.1 and 5.3.4.2 show that nonbridging oxygens predominantly surround the environment of the metal ions. This emphasizes the fact that the metal ions are found between the long phosphate chains, predominantly as corner sharing oxygen structures.

5.4 SUMMARY OF THE METAL NETWORK ANALYSIS

The structural investigation of the metal network for the three metaphosphate glasses showed that the local environments of the magnesium and zinc ions were most similar and can be attributed to their similar field strength values and ionic radii. The lead ion has been shown to have several local environments that it can occupy compared to the preferred environments observed for the Mg and Zn ions, this consequently makes the lead metal network more disordered than the magnesium or zinc networks. This can be attributed to the strong modifier strength of the lead ion, which will disrupt the phosphate backbone structure to a greater extent thus creating more NBO species and a wider distribution of possible environments for the lead ions. The short range geometry of the metal ions were observed both pictorially and from the bond angle distribution. The magnesium and zinc ions were found to consist of distorted four coordinated structures while the lead ion consisted of both distorted five and six coordinated structures. It was demonstrated that the structural characteristics of the metal network could in part be predicted by the field strength of the cation modifier.

5.5 THE THREE BODY POTENTIAL MODEL

Despite the success of the two body potential model in describing the short range order of the three metaphosphate glasses, improvements may be made by introducing a bond directionality term that accounts for the partial covalent character of the P-O bond. The term acts to restrict the deviation of the tetrahedral angle (O-P-O) from its theoretical value of 109.5^0. The application of a three body potential model to silicate glasses has been shown to be very successful [31,33]. Improvements in the short range order was achieved by a reduction in the number of bond defects, narrowed O-Si-O bond angle and a reduced Si-O-Si bond angle. A three body potential model for phosphates and a structural model that accounts for the double bond present in the basic PO_4 structural unit has yet to be developed.

Therefore, this section discusses the development of the adjustable potential parameters required to employ a three body model for phosphate structures. This was achieved by developing the parameters such that the correct crystal structure for P_2O_5 was obtained (Section 5.5.1). In addition, the structural properties obtained for the P_2O_5 glass using the three body potential model will be compared those obtained using the two body potential model as a means of validating the potential parameters (Section 5.5.2).

5.5.1 THE STRUCTURE OF CRYSTALLINE P_2O_5

The validity of the potential parameters was determined by comparing the crystalline structure obtained from the MD simulation (MD crystal) at 300 K to the P_2O_5 crystal structure acquired from crystallographic data (static crystal) [49,83]. The P_2O_5 static crystal represents the crystal, which has not been run through the MD calculations and contains the original atomic positions. The set of adjustable parameters developed for SiO_2 by Feuston and Garofalini [31] were used as a reference but were adjusted such that the correct ion-ion bond distances were obtained for the P-P and P-O pairs. This was achieved by comparing pair and cumulative distribution functions as well as viewing the crystal pictorially.

The room temperature pair distribution functions of the P-O bond for the P_2O_5 static crystal is shown in Figure 5.5.1.1. The PDF shows two distinct sharp peaks at 1.49 Å and 1.56 Å [49]. The PDF for the P-O bond in the MD crystal is also shown in Figure 5.5.1.1. As with the static crystal, two peaks were observed, at 1.41 Å and 1.56 Å, associated with the first oxygen coordination shell of the phosphate tetrahedra. The PDF for the MD crystal emphasizes that the developed potential parameters can model the two bond lengths present in crystalline P_2O_5. The peak at shorter bond distances represents the phosphorus-oxygen double bond (P=O) while the peak at longer bond distances is associated with phosphorus-oxygen single bonds (P-O) present in the PO_4 tetrahedral unit. In addition to achieving the simulation of the two bond lengths, a distinct separation exists between the two peaks in the MD crystal indicating a high degree of short range order.

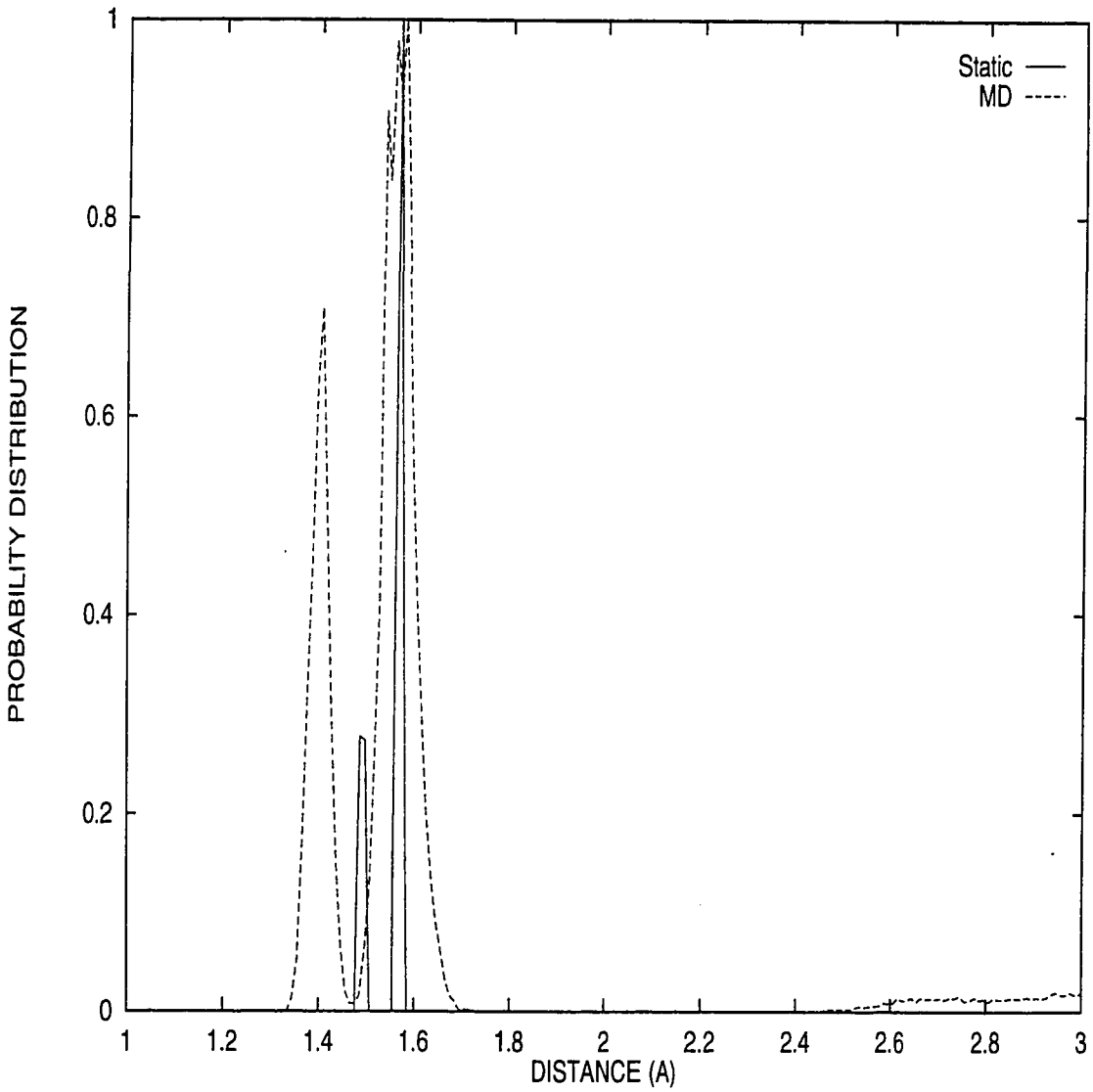

Figure 5.5.1.1 Pair distribution functions for the P-O pair in the P_2O_5 static and MD crystals.

The CDF for the P-O pair is shown in Figure 5.5.1.2 for both the static and MD crystals. The average coordination number, determined from crystallographic data, is 4.0 (cutoff = 1.6 Å). This is inferred from the fact that crystalline P_2O_5 is made up of PO_4 tetrahedrons [49,85]. The CDF for the static crystal clearly reflects a high degree of short range order by the plateau that extends to long distances (3.1 Å). The CDF for the MD crystal is in excellent agreement with crystallographic data indicating a high degree of short range order and also shows an average coordination of 4.0 (cutoff = 1.7 Å). Furthermore, both the static crystal and the MD crystal show a second coordination number of 1.0 representing the lone double bonded oxygen surrounding each phosphorus ion. This is consistent with the structure of the phosphate tetrahedra which has one unlinked oxygen atom (P=O) [84].

The pair distribution functions of the P-P bonds for the static and MD crystals are shown in Figure 5.5.1.3. The PDF for the static crystal shows two sharp peaks at approximately 3.0 Å, while a broader single peak exists at 3.1 Å for the MD crystal. The average coordination number for the P-P pair was found to be 4.0 (cutoff = 3.0 Å) for the static crystal as demonstrated by the CDF in Figure 5.5.1.4. The average coordination number for the MD crystal of 4.0 (cutoff = 3.3 Å) is in excellent agreement with crystallographic data thus supporting the validity of the developed potential parameters.

The accurate simulation of the bond lengths and coordination numbers for the P-O and P-P pairs indicated that the developed potential parameters could accurately reproduce the P_2O_5 crystal structure. Table 5.5.1.1 presents a comparison of the structural features derived from the pair and cumulative distribution functions for the P_2O_5 (i) static crystal (derived from crystallographic data) and (ii) MD crystal.

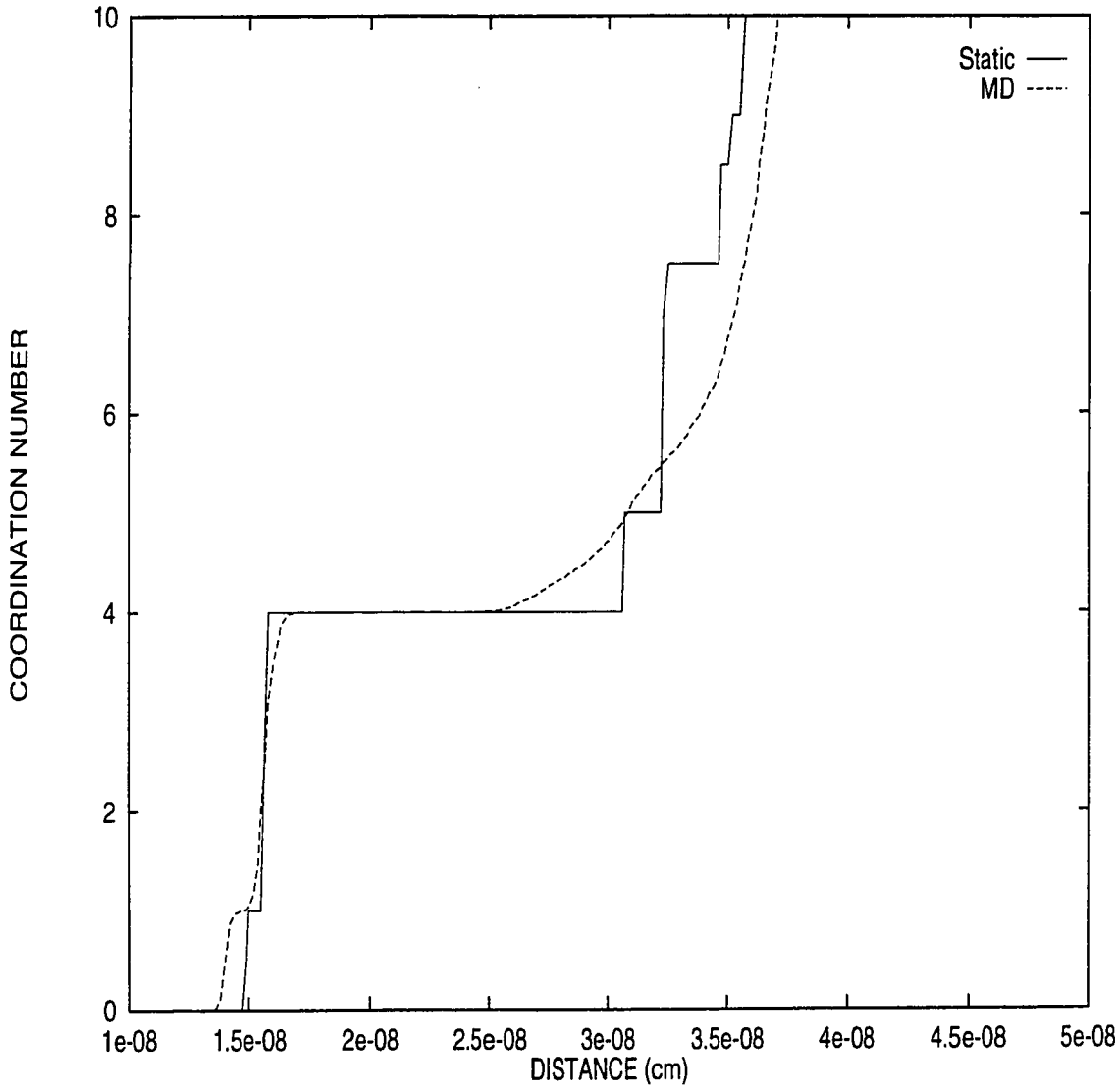

Figure 5.5.1.2 Cumulative distribution functions for the P-O pair in the P_2O_5 static and MD crystals.

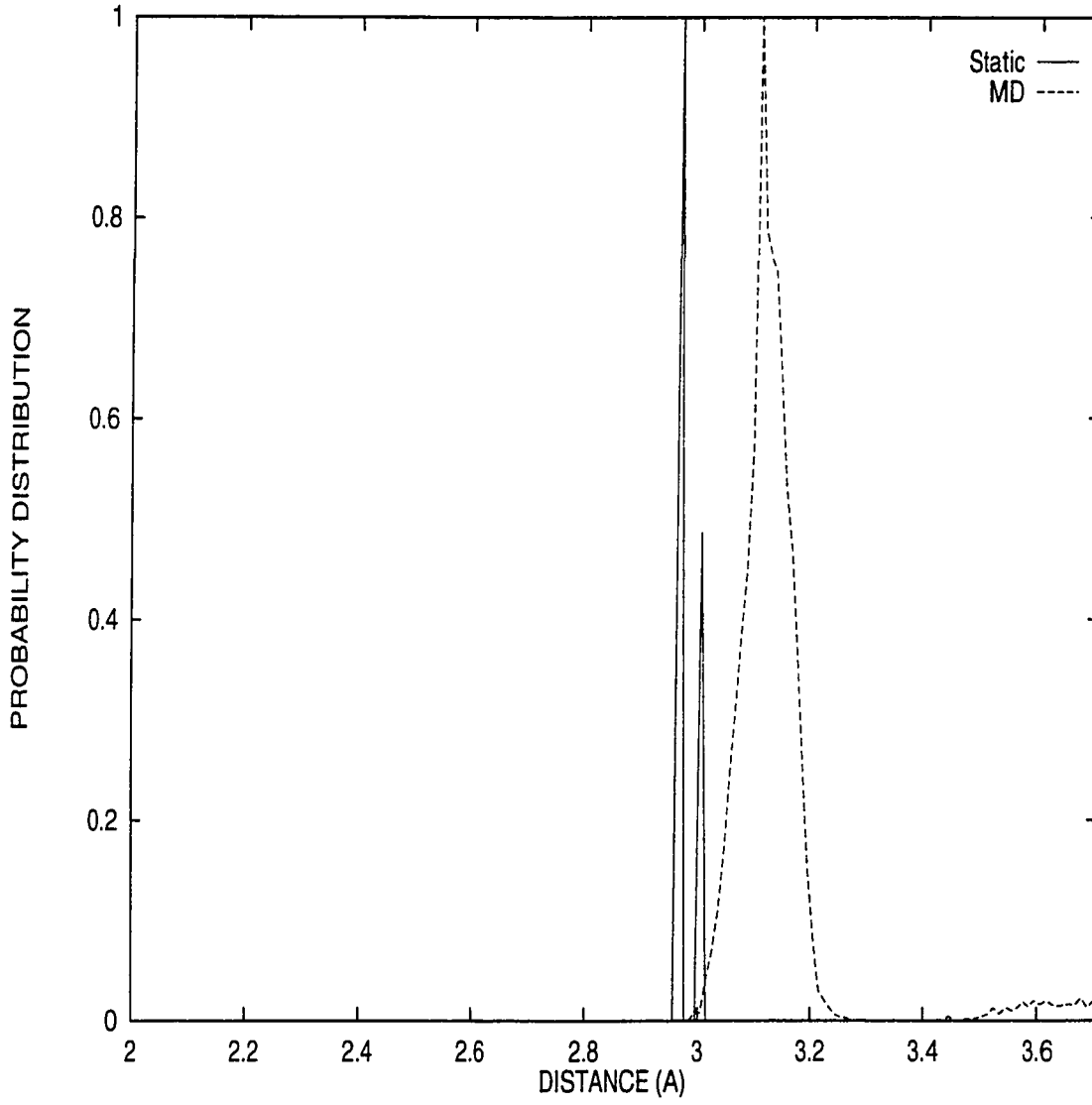

Figure 5.5.1.3 Pair distribution functions for the P-P pair in the P_2O_5 static and MD crystals.

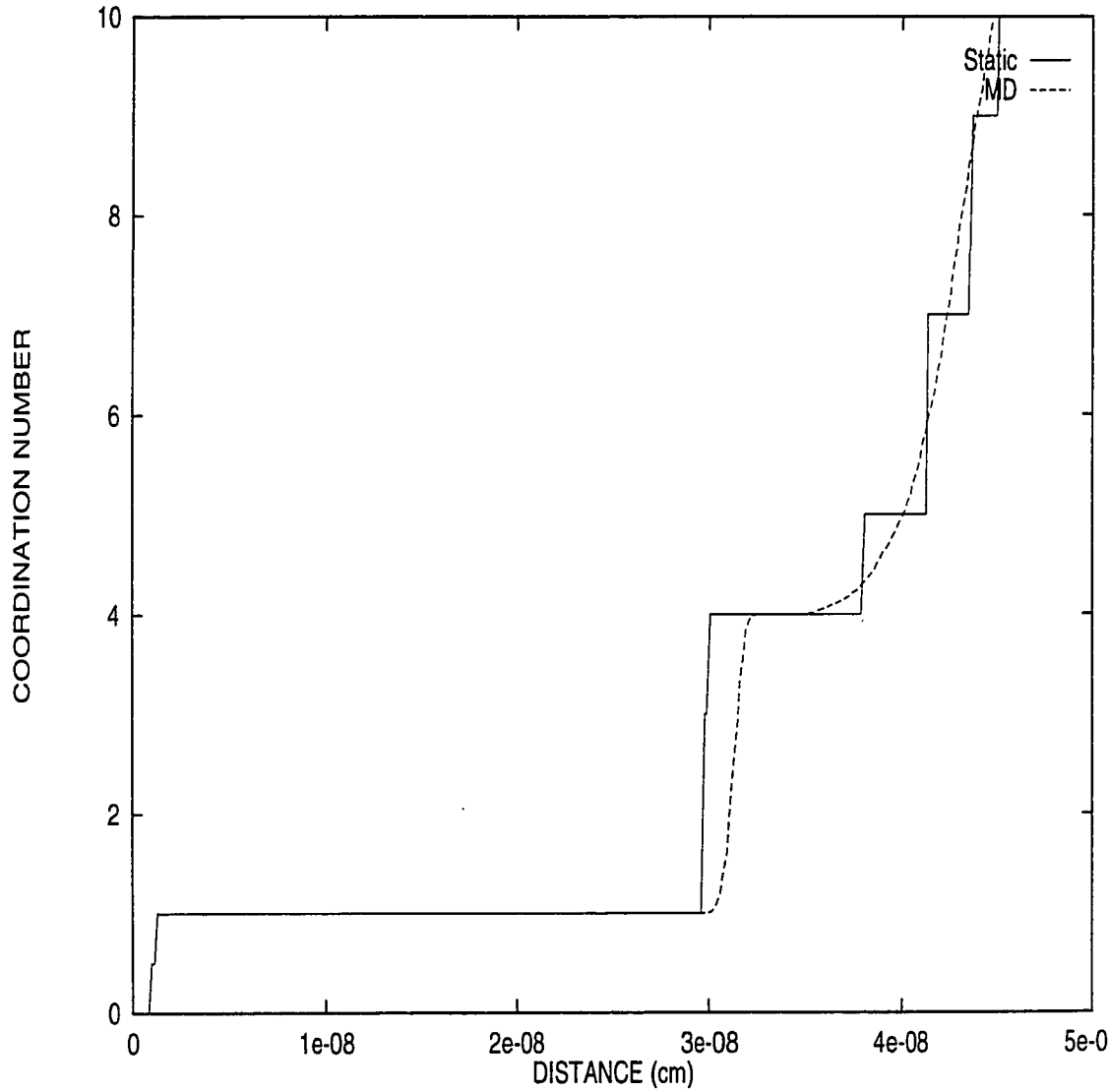

Figure 5.5.1.4 Cumulative distribution functions for the P-P pair in the P_2O_5 static and MD crystals.

Table 5.5.1.1

A COMPARISON OF BOND LENGTHS AND COORDINATION NUMBERS IN CRYSTALLINE P_2O_5

Structural feature	Static crystal	MD crystal
P-O (Å)	1.56	1.56
P=O (Å)	1.49	1.41
P-O CN	4.0	4.0
P=O CN	1.0	1.0
P-P (Å)	3.0	3.1
P-P CN	4.0	4.0

In Figure 5.5.1.5 pictorial representations of the P_2O_5 a) static crystal structure and b) MD crystal structure are shown. These figures clearly demonstrate that the static and MD crystals have similar structural features. Figure 5.5.1.5b reveals that the double bonded oxygens nearest neighbors, are bridging oxygen ions. This is consistent with the structure obtained from crystallographic data (Figure 5.5.1.5a) as well as from experimental data. The position of the double bonded oxygen in the P_2O_5 crystal structure has been reported by Hoppe et al. [84]. The authors report that the double bonded oxygen (DBO) position is not arbitrary and that its nearest inter-tetrahedral atomic neighbor are not phosphorus atoms but rather bridging oxygen atoms.

Having established that the derived potential parameters can accurately simulate the P_2O_5 crystal, we proceeded with the simulation of the P_2O_5 glass.

a)

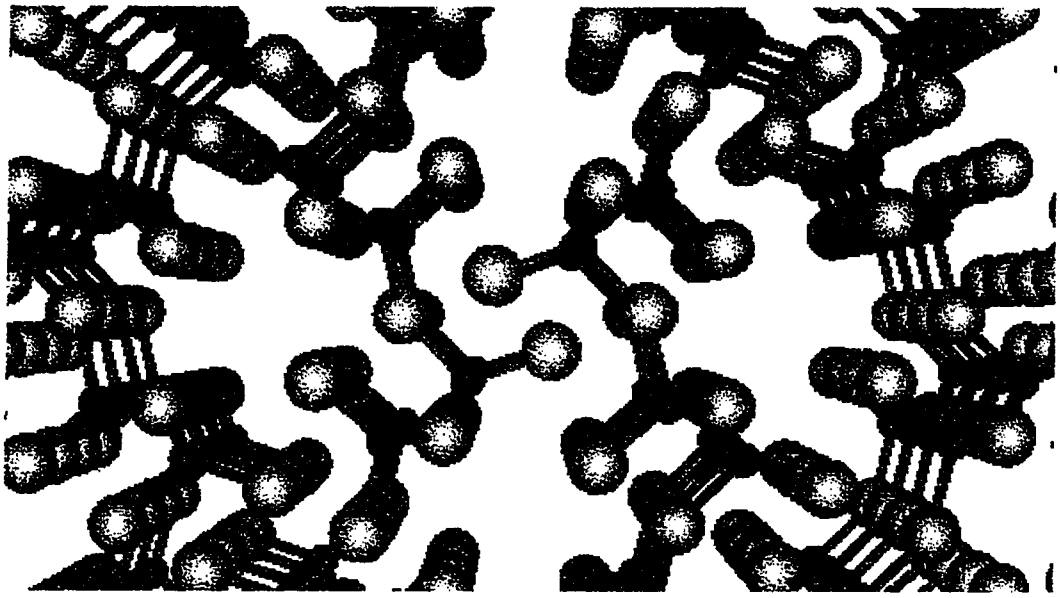

b)

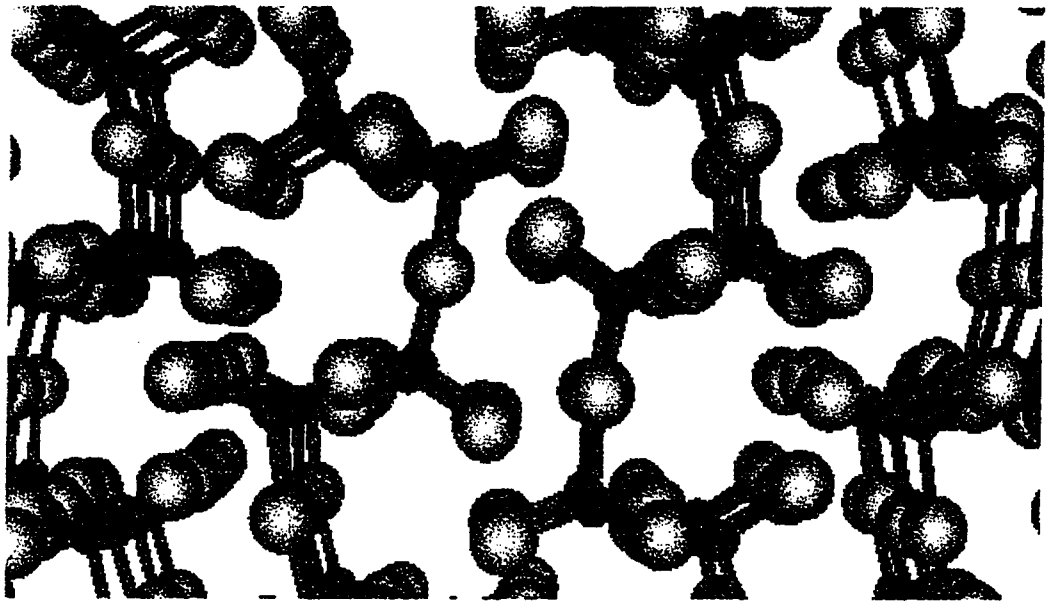

Figure 5.5.1.5 Structure of the P_2O_5 a) static crystal and b) MD crystal. The small dark grey spheres represent phosphorus and the larger light grey spheres represent oxygen.

5.5.2 THE STRUCTURE OF VITREOUS P_2O_5

In this section the structural properties of vitreous P_2O_5 simulated using both the two and three body potential models are presented. The structural properties obtained using the three body potential model will be compared to existing experimental results and to results obtained from the two body MD simulation as a means of validating our potential parameters. The structure of the simulated room temperature glasses were analyzed in terms of their pair and cumulative distribution functions, number of bond defects and by identifying the types of oxygen ions found in the phosphate glass. A radius of 1.9 Å and 3.4 Å was used as the cutoff for defining the first coordination shell of the P-O and P-P pair respectively in both the two and three body potential models.

Figure 5.5.2.1 shows a comparison of the pair distribution functions for the P-O pair obtained using the two and three body potential models. The striking feature of the PDF obtained using the two body potential model is the absence of a peak at 1.4 Å. In contrast, the PDF obtained using the three body potential model shows two peaks at 1.4 Å and 1.6 Å. These results are in excellent agreement to theoretical values determined by Van Wazer [1]. The author has reported two phosphorus-oxygen bond distances at 1.39 ± 0.02 Å and 1.62 ± 0.02 Å in vitreous P_2O_5. To account for his observations the author has attributed the peak at 1.39 Å to the P=O bond and the peak at 1.62 Å to the P-O bond. Okura et al. [86] have also reported the presence of two phosphorus-oxygen bond distances in vitreous P_2O_5 at 1.51 Å and 1.62 Å using Ab initio calculations.

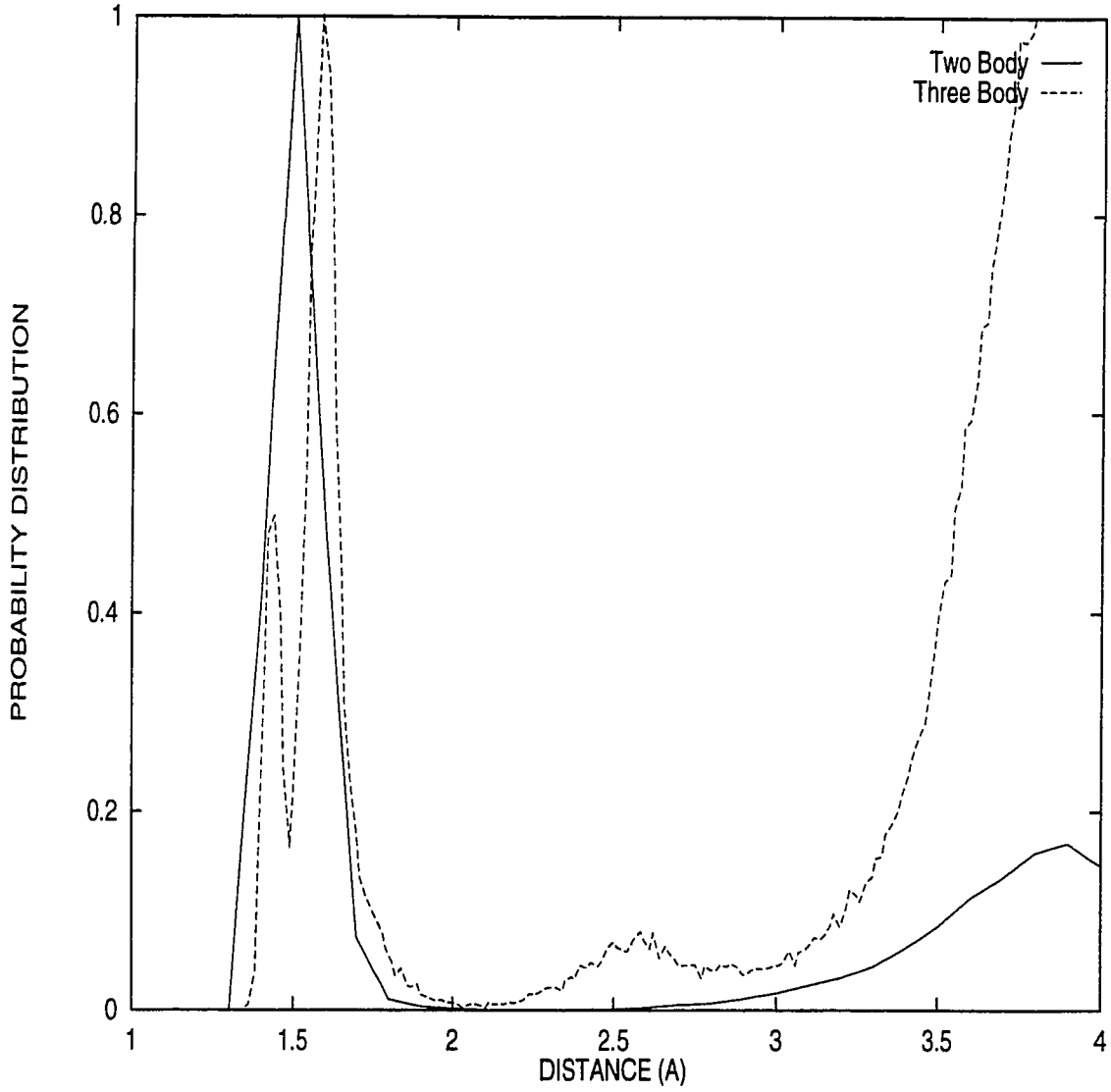

Figure 5.5.2.1 Pair distribution functions for the P-O pair in the P_2O_5 glass using the two and three body potential models.

Raman [87,88] and infrared [89] spectra of vitreous P_2O_5 show two significant peaks at 640 and 1390 cm^{-1} which have been assigned to the P-O and P=O stretching respectively. Similar experimental results were reported by Thorpe et al. [90] thus confirming the presence of both bond distances in the P_2O_5 glass.

In addition, a comparison of peak areas for the P-O and P=O peaks (Figure 5.5.2.1) revealed a ratio of 1:4. This ratio correctly corresponds to the relative percentage of double bonds in the PO_4 tetrahedral unit, which is 25 %, further emphasizing the validity of the developed potential parameters. The ratio of 1:4 has also been reported by Van Wazer [1] who concluded from radial distribution functions that ¼ of the bonds in vitreous P_2O_5 were attributed to double bonded oxygens. Therefore, the three body potential model successfully simulates the P-O and P=O bonds present in the tetrahedral unit. This is a significant improvement from the two body potential model for describing the local order around phosphorus.

Figure 5.5.2.2 shows the P-O cumulative distribution functions using the two and three body potential models. The average coordination number for the P-O pair was found to be 4.1 using the three body potential model, which is in excellent agreement with experimental data for alkali metaphosphates [40,50,51]. Furthermore, Van Wazer [1] reports an average coordination number of 4.2 for the P-O pair in vitreous P_2O_5 and similar results have also been reported by Galeener et al. [87,88]. Okura et al. [86] have determined using Ab initio calculations that the basic structural unit in pure P_2O_5 glass is a PO_4 tetrahedron implying an average coordination of 4 for phosphorus. The CDF obtained using the two body potential model yields a higher average coordination number of 4.3.

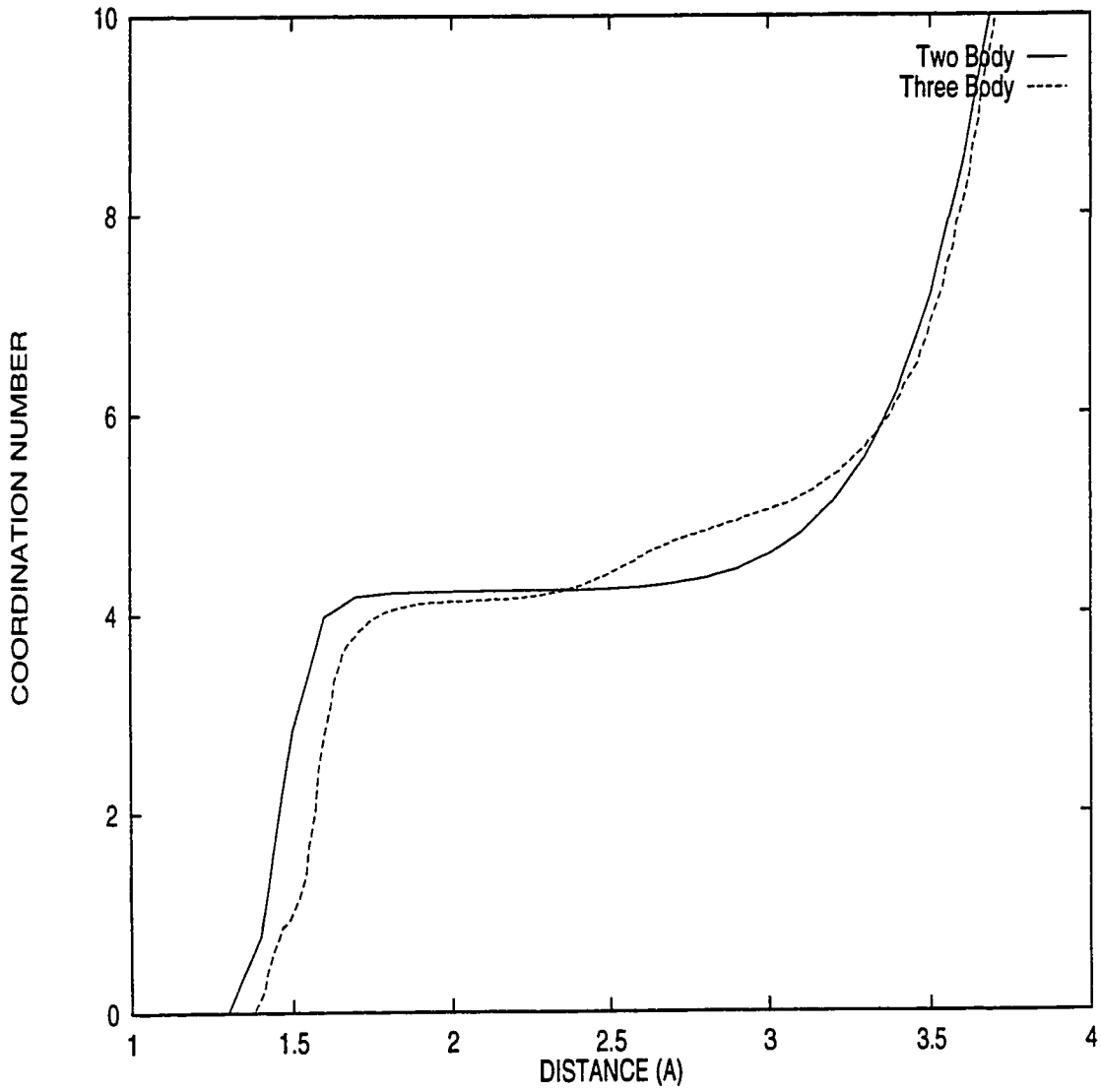

Figure 5.5.2.2 Cumulative distribution function for the P-O pair in the P_2O_5 glass using the two and three body potential models.

Feuston and Garofalini have shown [31] that most two body potentials fail to accurately reproduce the high degree of short range order found in the laboratory glass. The main difference between the two body and three body potential model simulations are the presence of a larger number of bond defects (odd coordinated structures) using the two body potential model. Figure 5.5.2.3 shows the percentages of odd coordinated phosphorus ions obtained using both the two and three body potential models. The two body potential model produces a significantly higher percentage (26 %) of odd coordinated phosphorus in comparison to the three body potential model (10 %). In addition, the bond defects present in the P_2O_5 glasses are of a different nature for each potential model. Only odd 5 coordinated structures were found using the three body potential model whereas odd 5 and 6 coordinated structures were present in the glass simulated using the two body potential model. These results reveal the improvement in the short range order of the phosphorus ions using three body potential model. However, the number of bond defects reported for the three body potential should be reduced to a more acceptable value of 1-2 % as reported by Newell et al. [33]. This can be achieved by further parameterization of the adjustable parameters.

The room temperature pair distribution functions for the P-P pair obtained using the two and three body potential models are shown in Figure 5.5.2.4. An average P-P bond distance of 3.2 Å with a FWHM of 0.14 Å was found in the P_2O_5 glass obtained from the three body potential model. This is in contrast to the bond distance of 3.0 Å and FWHM of 0.25 Å obtained from the two body potential model. The narrower distribution obtained from the three body model indicates a higher degree of short range order in the P_2O_5 glass.

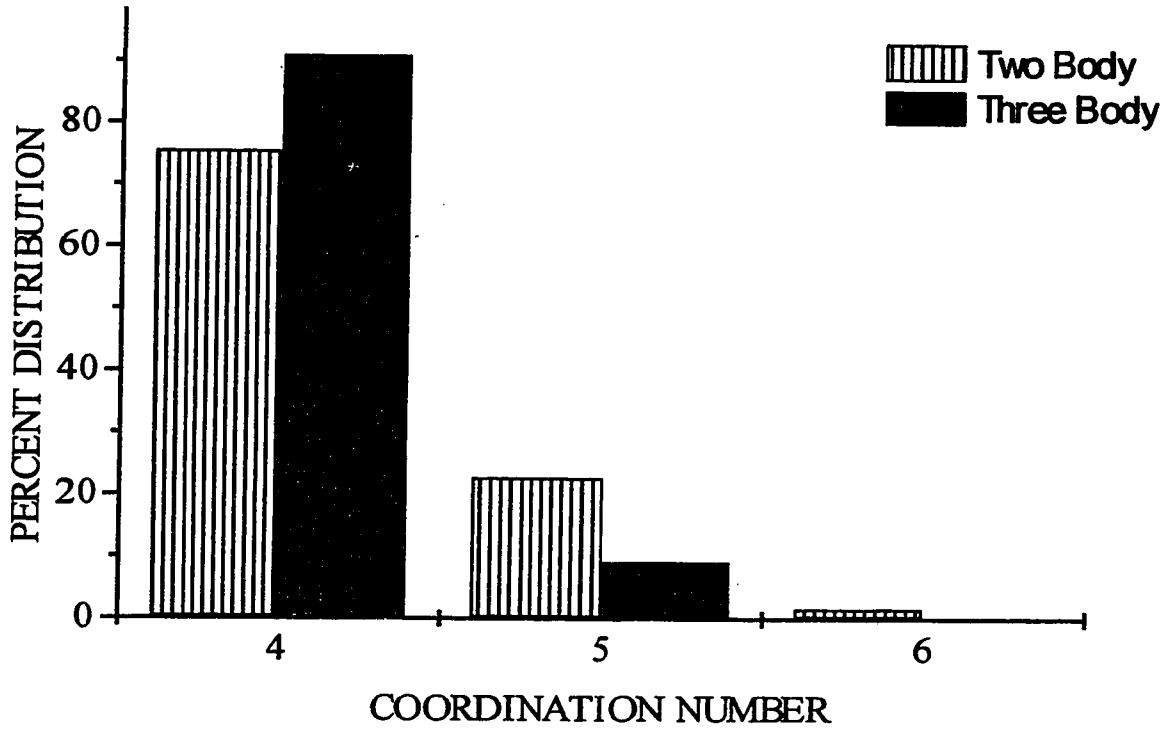

Figure 5.5.2.3 Types of coordinated oxygens in the P_2O_5 glass using the two and three body potential models.

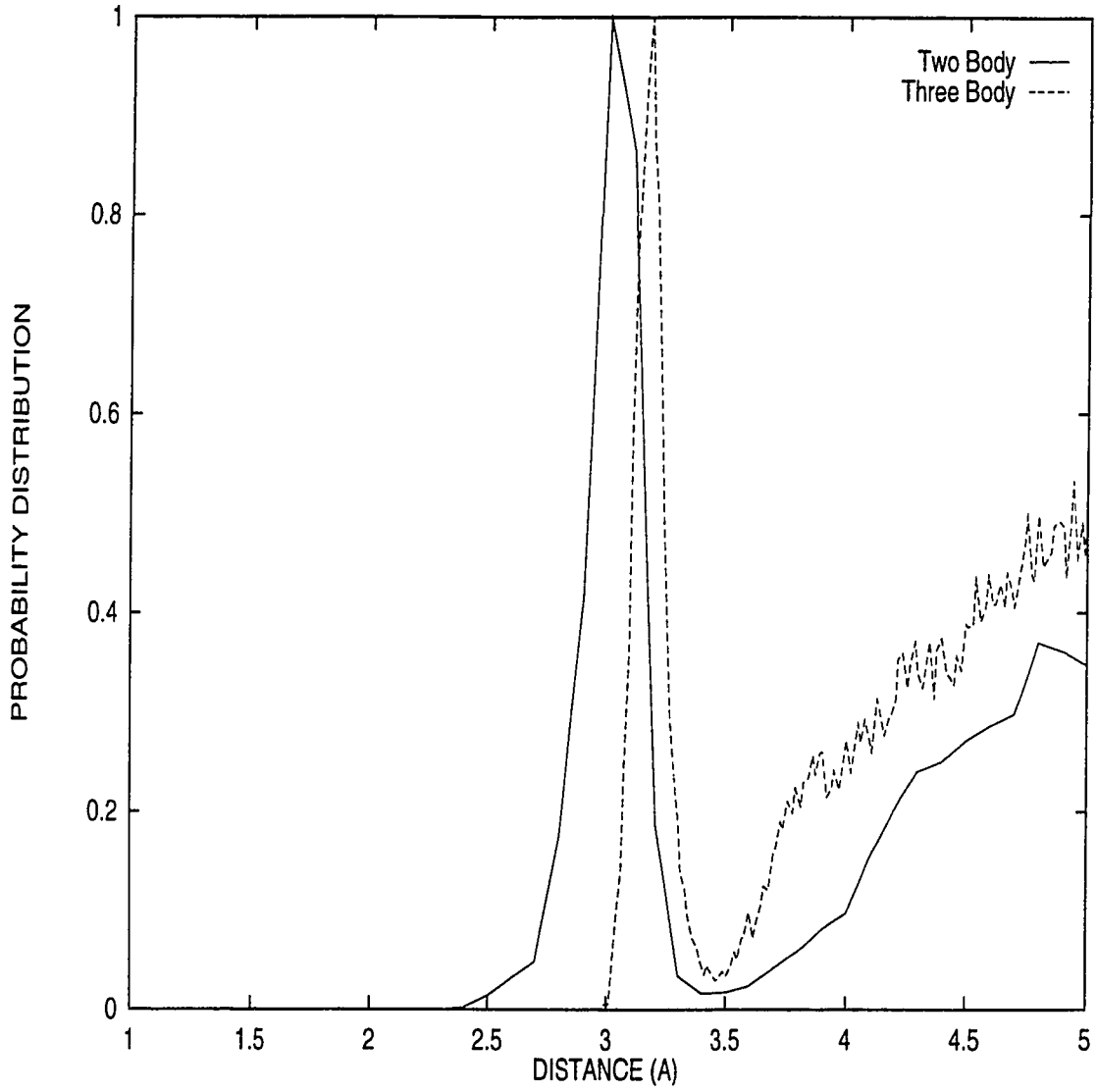

Figure 5.5.2.4 Pair distribution function for the P-P pair in the P_2O_5 glass using the two and three body potential models.

The cumulative distribution functions for the P-P bond in the P_2O_5 glass using the two and three body potential models are shown in Figure 5.5.2.5. The average coordination number was found to be 3.2 and 4.3 for the glasses simulated using the two and three body potential models respectively. The difference between these coordination numbers is due to the shift in the corresponding P-P peak position observed in the PDFs (Figure 5.5.2.4).

Although the pair and cumulative distribution functions for the two body potential model agreed fairly well with experimental data, the P-O-P bond angle was too broad in comparison to experimental data. The broad distribution revealed that the two body potential model failed to reproduce accurately the high degree of short range order observed in the laboratory glass. Figure 5.5.2.6 shows the P-O-P bond angle distribution for the P_2O_5 glass using both the two and three body potential models. The P-O-P bond angle which is the angle bridging the individual phosphate tetrahedra was found to possess a maximum at 170^0 with a FWHM of 17^0 using the three body potential model. The FWHM for the P-O-P bond angle is in excellent agreement with the value found for Si-O-Si (14^0) using a three body potential model. Using the two body potential model the P-O-P bond angle was found to have maximum at 154^0 with a FWHM of 33^0. The three body potential model gave a much narrower bond angle distribution demonstrating that the model introduced less randomness in the connectivity of the individual phosphate tetrahedra.

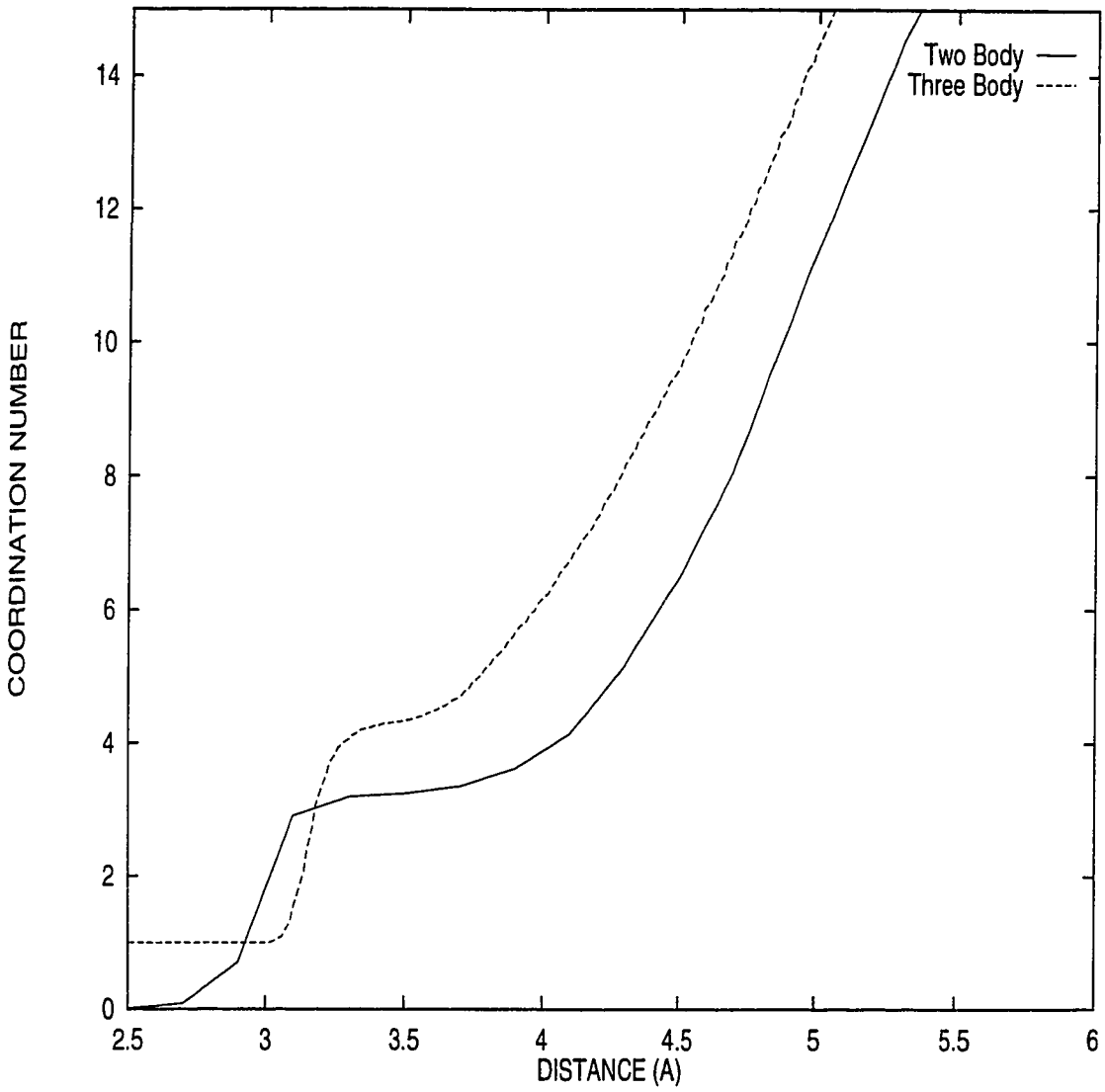

Figure 5.5.2.5 Cumulative distribution function for the P-P pair in the P_2O_5 glass using the two and three body potential models.

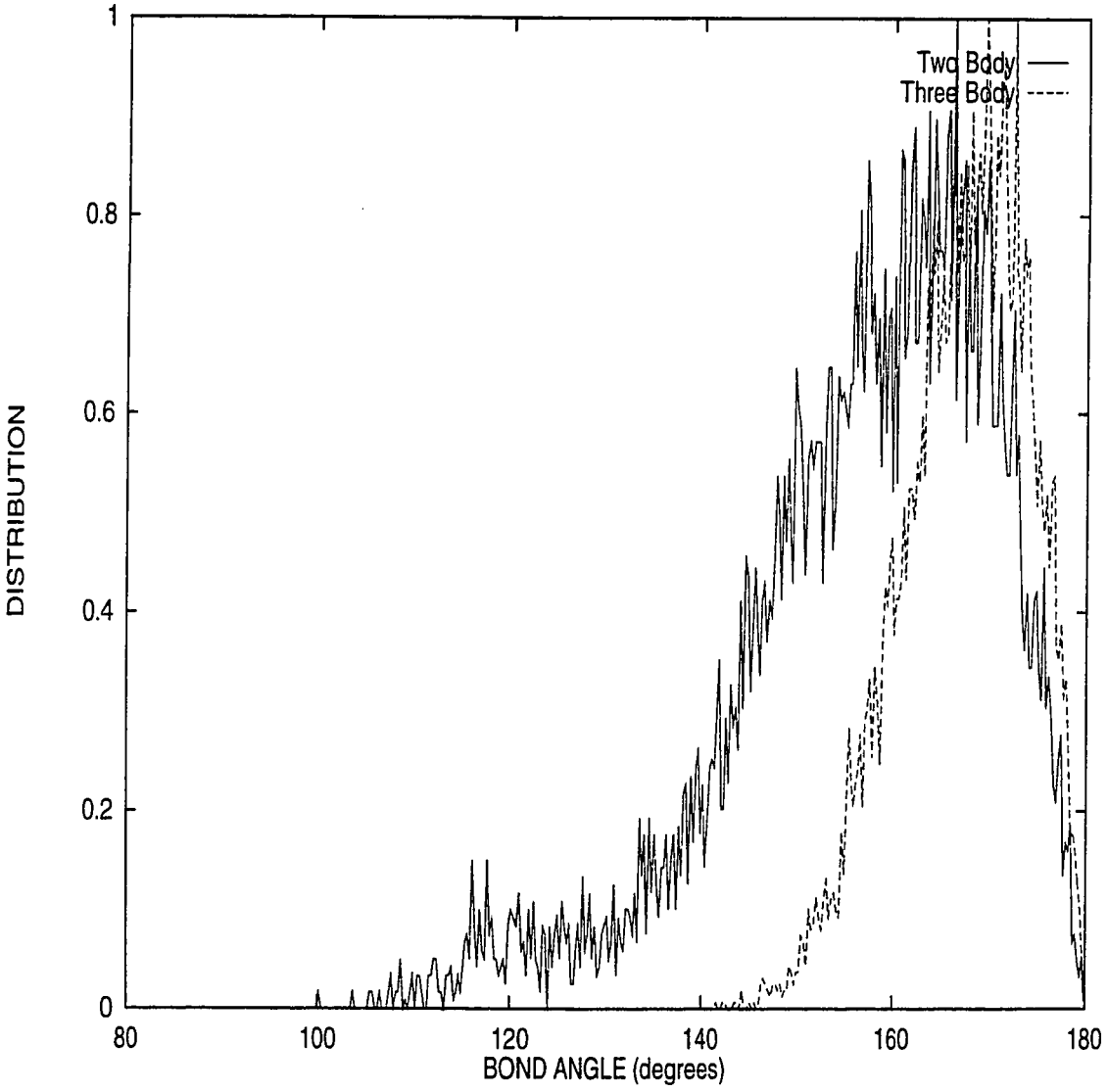

Figure 5.5.2.6 P-O-P bond angle distributions using the two and three body potential models.

The O-P-O bond angle distribution obtained using the three body potential model shown in Figure 5.5.2.7 indicates two maxima, at 108^0 and at 92^0. This is in contrast to the single maximum at 109^0 obtained using the two body potential model (Figure 5.5.2.7). The primary maxima are close to the theoretical tetrahedral bond angle of 109.5^0 and exhibit a narrow distribution with a FWHM of 15^0 for both the two and three body potential models. This was in good agreement with the FWHM for O-Si-O of 13^0 reported by Newell et al. [33] using the same three body potential model. The sharp bond angle distributions in conjunction with the average coordination number of 4.0 indicate the presence of well defined phosphate tetrahedra within the glass structures. The tetrahedra are a reflection of the presence of short range order. However, parameterization should be performed to further narrow the O-P-O bond angle distribution. In a study of sodium trisilicate glass Newell et al. reduced the O-Si-O bond angle distribution from 13^0 to 7^0 [33].

The peak at smaller bond angles, in the O-P-O bond angle distribution, obtained using the three body potential model was attributed to odd 5 coordinated structures. The general structure of these odd coordinated species was determined to be "square pyramidal" which can be observed pictorially in Figure 5.5.2.8 and accounts for the angle at 92^0. Future work should involve bringing the O-P-O bond angle closer to its theoretical value of 109.5^0 and to eliminate the peak at smaller bond angles. This would improve the short range order of the phosphorus ions. A summary of the structural properties for the P_2O_5 glass obtained using the two and three body potential models is shown in Table 5.5.2.1.

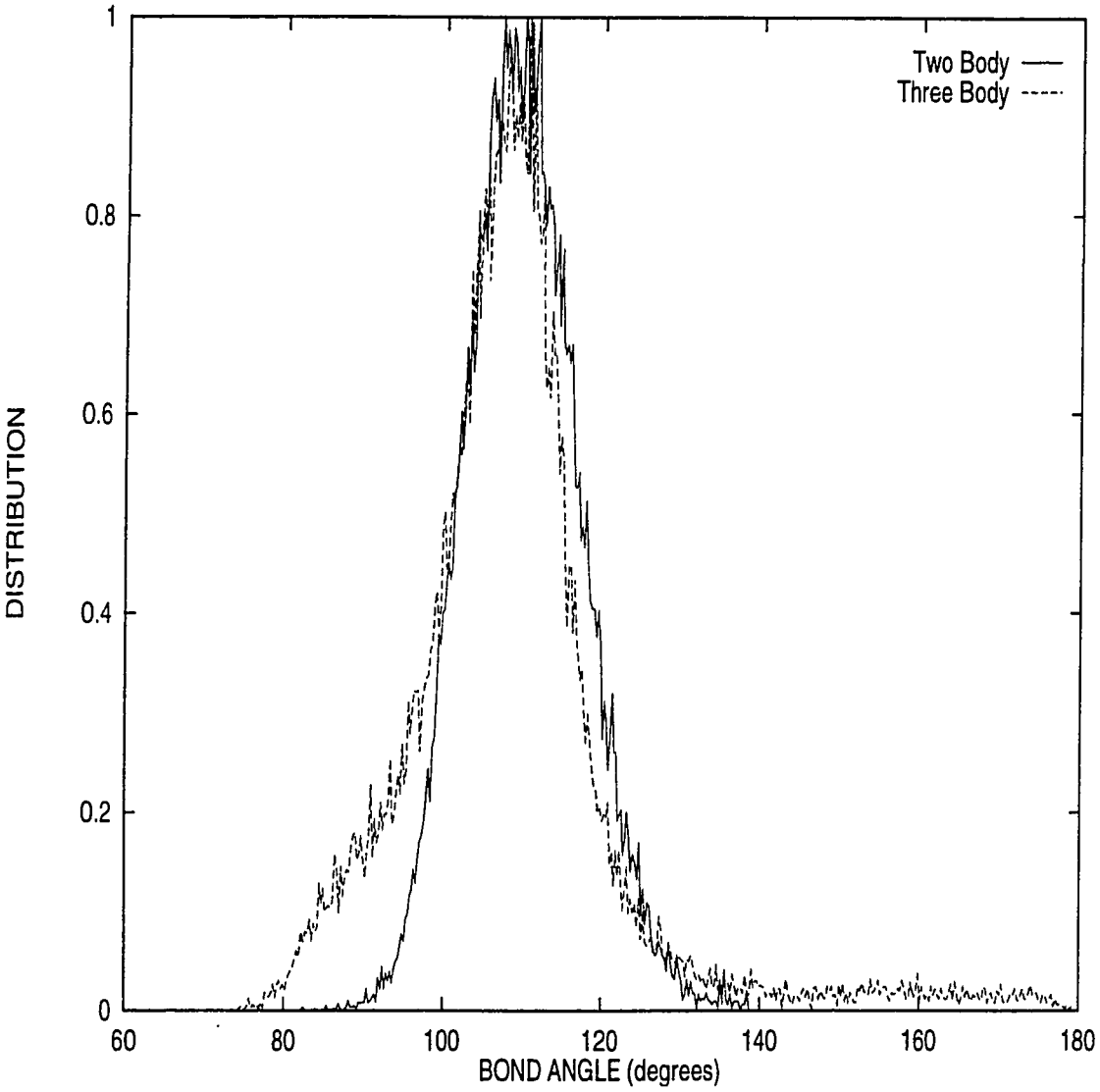

Figure 5.5.2.7 O-P-O bond angle distributions using the two and three body potential models.

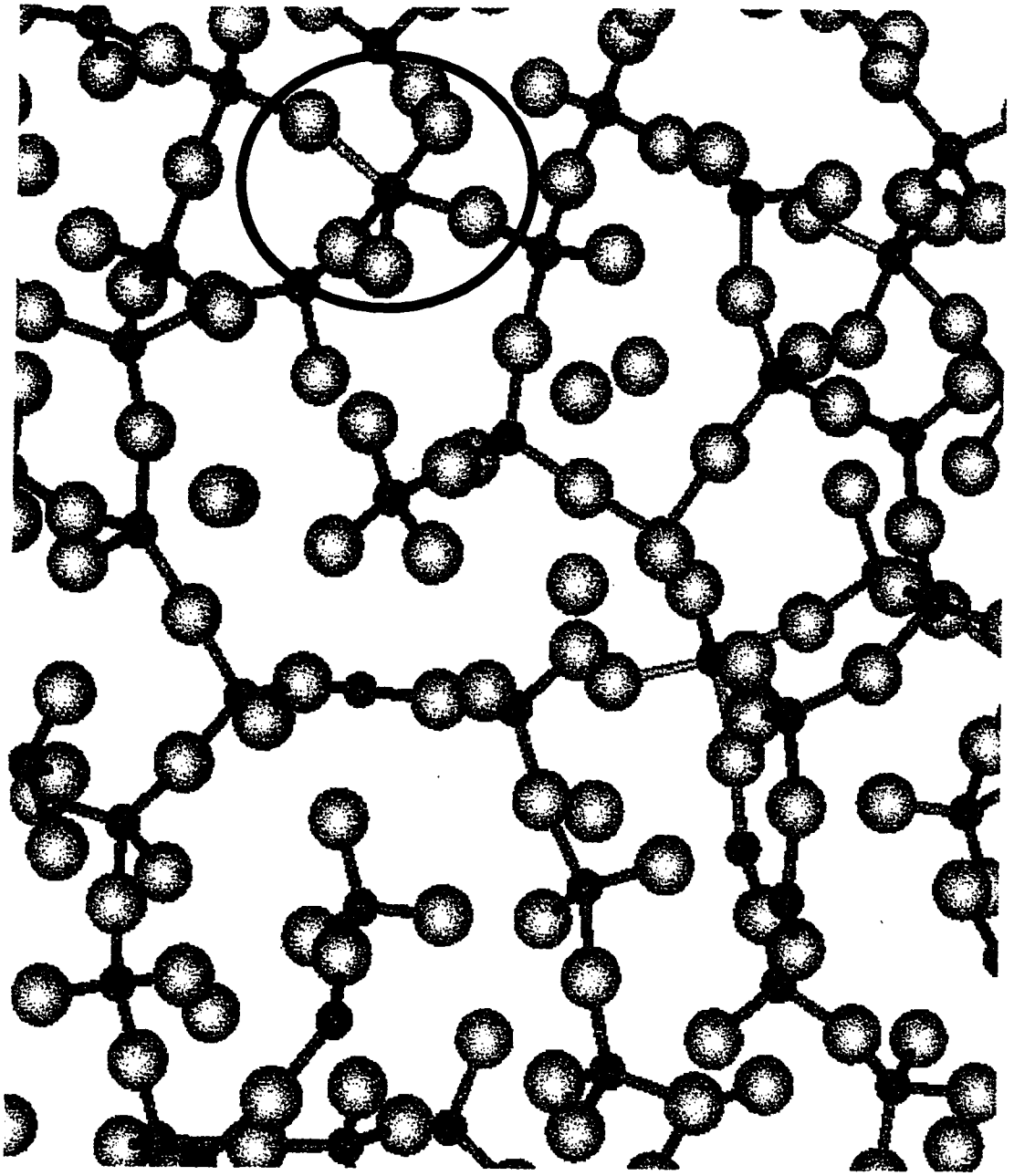

Figure 5.5.2.8 P_2O_5 glass structure simulated using the three body potential model. The small dark grey spheres represent phosphorus and the larger light grey spheres represent oxygen.

Table 5.5.2.1

A COMPARISON BETWEEN THE GLASS STRUCTURES OBTAINED FROM THE TWO AND THREE BODY POTENTIAL MODELS

Structural feature	Two body model	Three body model
P-O (Å)	1.5	1.6
P=O (Å)	-	1.4
P-O CN	4.3	4.1
P-P (Å)	3.0	3.2
P-P CN	3.2	4.3
P-O-P (degrees)	154	170
O-P-O (degrees)	109	108 and 92

The distribution of Q^i species within the P_2O_5 glass calculated using both the two and three body potential models are summarized in Table 5.5.2.2. The Q^i distribution gives further information on the local environment of phosphorus. Similar Q^i distributions were observed using the two models.

Table 5.5.2.2

PERCENT Q^i DISTRIBUTION FOR THE P_2O_5 GLASS

	Q^1	Q^2	Q^3	Q^4
P_2O_5 (2 BODY)	2.5	20.8	45.3	31.3
P_2O_5 (3 BODY)	2.5	22.6	43.2	31.7

The prevalence of Q^3 species was in accordance with the theoretical description of the phosphate glass network in which three of the oxygens are connected to other tetrahedral units to form long linear chains of PO_4 tetrahedra. Hoppe et al. [84] reported similar structural behavior in vitreous P_2O_5 such that the PO_4 groups were connected to adjacent units by three of their four oxygen ions, while the fourth oxygen represented the double bonded oxygen ion. The predominance of Q^3 species in vitreous P_2O_5 was determined by infrared spectroscopy according to Wong [91]. The similarity between the Q^i distributions using both the two and three body potential models was expected since the parameterization of the potential parameters was used to optimize bond distances and coordination numbers but the overall structure of the glass should remain the same [33]. Furthermore, a similar Q^i distribution was observed experimentally by Grimmer et al. [92] using ^{31}P-MAS-NMR on vitreous P_2O_5.

Calculating the ratio of double bonds to single bonds for each type of Q species and finding their sum over all Q species resulted in a value of 1:4.5. This ratio is in excellent agreement with the results obtained from the peak area ratio (1:4) of the PDFs for the P-O bond in the P_2O_5 glass using the three body potential model. This substantiates the accurate simulation of the double bonded oxygen within the tetrahedral unit using the three body potential model.

The final step in establishing the validity of the potential parameters was to investigate the types of oxygens found in the P_2O_5 glass. These results are summarized in Table 5.5.2.3 and reveal the similarity in the overall P_2O_5 glass structure using the two and three body potential models.

Table 5.5.2.3

PERCENTAGE OF THE TYPES OF OXYGENS IN VITREOUS P_2O_5

	4	3	2	1	0
P_2O_5 (2 body)	0.0	0.0	66.5	33.5	0.0
P_2O_5 (3 body)	0.0	0.0	64.0	36.0	0.0

The numbers 4, 3, 2, 1 and 0 represent the total number of phosphorus attached to a central oxygen ion. Therefore, using the three body potential model 64.0 % of the oxygens were bonded to two phosphorus ions (bridging oxygens) in comparison to 66.5 % using the two body potential model. Similarly, 33.5 % and 36.0 % of the oxygens were found to be NBOs using the two and three body potential models respectively. The predominance in the number of bridging oxygen atoms was expected since three of the four oxygen ions of every tetrahedral unit are bonded to other tetrahedral units via bridging corner oxygens.

The overall P_2O_5 glass structure was equivalent using the two and three body potential models, which further validated the adjustable potential parameters.

The ability of the three body potential model in reproducing the P_2O_5 glass structure attests to the success in developing the BMH potential parameters. However, further studies should be aimed at reducing the O-P-O bond angle distribution closer its theoretical value of 109.5^0 as well as reducing the number of bond defects. This will further improve the short range order in phosphate glasses, which will eventually permit the use of the three body potential model to simulate metaphosphate glasses.

5.6 SUMMARY OF THREE BODY MD SIMULATION

The potential parameters required for a three body potential model were developed and they accurately reproduced the crystalline and vitreous structures of P_2O_5 when compared to experimental and theoretical results. A significant improvement in the short range order of the phosphorus ions was observed from the pair distribution functions using the three body potential model since two phosphorus-oxygen interionic bond distances were simulated at the correct distances rather than the averaged single peak obtained from the two body potential model. Furthermore, using the three body potential model, the number of bond defects were significantly reduced from 26 % to 10 % and were limited to only 5 coordinated species. The three body potential model also accurately simulated the PO_4 tetrahedral units whereby each phosphorus ion was coordinated to three bridging oxygen ions and one free oxygen ion. The P-O-P bond angle distribution was narrowed by the use of the three body potential model. Simulations should now be aimed at reducing the O-P-O bond angle distribution and as well as to further reduce the number of bond defects.

CHAPTER 6

6.0 CONCLUSIONS

Experimental methods have been predominantly used to study the short range order of glasses. However, such methods provide only averaged structural information. A detailed understanding of the short range order in glasses is important since it is responsible for the structural behavior and physical properties in glasses. Consequently, there has been increasing interest in employing computational techniques, which can provide more detail at the atomic level regarding the structure of glasses. These techniques have been focused primarily on silicate glasses. In the literature only sparse experimental data is available on metaphosphate glasses and even less is available on computer simulations of these glasses.

In this thesis, we extended the use of computational techniques to the study of metaphosphate glasses. Such glasses were of particular interest since the information in the literature is still lacunar with respect to their structural properties. By applying Molecular Dynamics and using a two body potential model, the simulation of three metaphosphate glasses was achieved, $Mg(PO_3)_2$, $Zn(PO_3)_2$ and $Pb(PO_3)_2$. The structure of the phosphate backbone was first investigated with the help of pair distribution functions, cumulative distribution functions, bond angle distributions, identifying the types of oxygen ions found within the phosphate backbone as well as performing a ring and chain analysis. Such tests provide an indication of the effect of the cation modifier on the phosphate backbone in the metaphosphate glasses.

From these studies the following can be concluded:

(i) The average coordination of the phosphorus ion was found to be 4.0 in the three metaphosphate glasses.

(ii) The basic structural unit in the phosphate backbone is the PO_4 tetrahedra

(iii) These tetrahedra form long linear chains throughout the phosphate backbone in the three metaphosphate glasses.

(iv) The role of the modifier in the metaphosphate glasses has little effect in the overall short range order of phosphorus ions.

The influence of the modifier on metaphosphate glass structure was obtained by investigating the structural properties of the metal network. The addition of the metal oxide leads to a depolymerization of the network by breaking the P-O-P links to form non-bridging oxygen ions. The following observations were made concerning the effect of the modifier on glass structure:

(i) The degree of depolymerization is based on the field strength of the cation modifier. The stronger the modifier (lower field strength), the greater the degree of depolymerization.

(ii) The M-O coordination number was found to be 4.3, 4.1 and 5.5 for magnesium, zinc and lead respectively.

(iii) The lead ion showed a greater number of local environments compared to magnesium or zinc thus rendering it the most disordered metaphosphate glass of the three studied.

(iv) The local environment of the magnesium and zinc ions were most similar based on their similar field strength value and ionic size.

These MD simulations which were performed using a two body potential model agree well with experimental data. However, improvements in the local order of the phosphorus ions may be achieved by employing a three body potential model. This will increase the similarity between the simulated phosphate glass and the laboratory glass. Subsequently, BMH pair potential parameters were developed for P_2O_5 for use in a three body potential model. This relied on the comparison of the short range structure between the original static crystal and the MD crystal. A reasonable set of potential parameters was then used for the three body simulation of vitreous P_2O_5, which showed considerable improvement in the short range order of the phosphorus ions compared to the results obtained from the two body potential model. The simulation of the two phosphorus-oxygen bond lengths was achieved as well as a significant reduction in the number of bond defects. Amelioration in the P-O-P bond angle distributions was also evident using the three body potential model. The short range order of vitreous P_2O_5 was confirmed through a comparison to the structure obtained using the two body potential model as well as to experimental data found in the literature.

Additional parameterization is required to improve the O-P-O bond angle distribution as well as to further reduce the number of bond defects found within the phosphate glass. Eventually, this will permit the application of a three body potential model to simulate metaphosphate glasses and thus improve the understanding of the structure in these glasses and the effect of the modifier.

CHAPTER 7

7.0 FUTURE WORK

In this thesis, an in depth investigation into the short range structure of metaphosphate glasses was performed using computer simulations. The goal was to provide detailed structural analysis such that these metaphosphate glasses can later be exploited for their technological advantages. To achieve this goal any future work will have to be focused on improving the computational procedure and understanding which parameters affect the structural properties of the metaphosphate glasses.

To improve the computational procedure, further parameterization of the adjustable potential parameters is required for the P-O and P-P pair in P_2O_5, using the three body potential model, such that more accurate structural simulations may be performed. In order to do so, an increase in the attractive force for the P-P pair should be achieved as well as an increase in the repulsive forces between the P-O pair. This would reduce the coordination number closer to the theoretical value of 4.0 as well as to reduce the number of bond defects. Having developed a three body potential model that can be used for the simulation of phosphate systems, a more detailed understanding of the short range structure of metaphosphate glasses may be performed. In doing so, it is important to extend the investigation to other metal ions such that the influence of mass and charge may be determined.

The effect of the modifier's mass on the short range structure of metaphosphate glasses can be determined by employing a three body potential model for the simulation of alkaline earth metaphosphates ($M(PO_3)_2$ where M = Mg, Ca, Sr and Ba). The choice of

these modifiers will allow a systematic analysis since the charge will remain constant. In addition, such a study will permit the comparison between the anomalous metaphosphate glasses to the normal metaphosphate glasses.

Also, the structure of metaphosphate glasses is dependent on the different valence states of the metal ions. In order to account for the effect of these valence states on the structure of the metaphosphate glasses, it is important to control all other variables that may also influence glass structure. In general, the study of Na^{+}, Mg^{+2} and Al^{+3} are good choices because of their similar mass and ionic radii. It is also possible to investigate Cs^{+}, Ba^{+2} and La^{+3} metaphosphate glasses. The masses of these ions are the same to within 5% and consequently any differences seen in their local structure can be ascribed to the cation charge.

A compositional study of metaphosphate glasses would also increase our understanding of the modifier effect on glass structure. One would expect that as the concentration of metal increases the percentage of NBOs would also increase. This would necessarily influence the depolymerization of the phosphate backbone as well as the coordination number for the modifier. One can also study mixed alkali glasses to see if the local geometry of a particular metal ion is affected by the introduction of a second metal cation into the glass structure. It would be interesting to see if the four coordinated structure preferred by the Mg or Zn ions remains four coordinated or if it changes because of the presence of a second modifier. This would be especially important in lead-iron phosphate glasses, which are becoming useful in nuclear waste immobilization. Experimental studies on such glasses have been performed but to our knowledge no computational studies have been reported.

CHAPTER 8

8.0 REFERENCES

1. J. R. Van Wazer, in Phosphorus and Its Compounds, Vol.1 Chemistry, Interscience Publishers Inc., New York (1958) 717-719.
2. R. J. Araujo and N. F. Borrelli, in Optical Properties of Glasses, D.R. Uhlmann and N. J. Kreidl, eds. American Ceramic Society, (1990).
3. G. B. Rothenberg, in Glass Technology – Recent Developments, Noyes Data Corporation, London (1976).
4. B. C. Sales and L. A. Boatner, "Lead-iron phosphate glass: A stable storage medium for high level nuclear waste", Science **5** 45-48 (1984).
5. M. J. Weber, "Science and technology of laser glass", J. Non-Cryst. Solids **123(1-3)** 208-222 (1990).
6. R. C. Ropp, in Inorganic Polymeric Glasses, Elsevier, New York (1992).
7. G. B. Rouse, Jr., P. J. Miller and W. M. Risen, Jr., "Mixed alkali glass spectra and structure", J. Non-Cryst. Solids **28** 193-207 (1978).
8. G. Pashina, G. Piccaluga and M. Magini, "X-ray diffraction study of Na^+ ions coordination in sodium borate glasses", J. Chem. Phys., **81** 6201-6206 (1984).
9. A. Musino, G. Piccaluga and G. Pinna, "Short range order in AgI-$AgPO_3$ glasses by x-ray diffraction", J. Chem. Phys. **89 (2)** 1074-1077 (1988).
10. G. Walter, R. Kranold, W. Gocke and N. Enenkel, "Investigation of single-phase glasses using small angle x-ray scattering techniques", J. Appl. Cryst. **24** 616-623 (1991).

11. G. D. Khattak, E. E. Khawaja, L. E. Wenger, D. J. Thompson, M. A. Salim, A. B. Hallak and M. A. Daous, "Compositional –dependent loss of phosphorus in the formation of transition-metal phosphate glasses", J. Non-Cryst. Solids **195** 1-12 (1996).

12. D. G. Minser, B. Walden and W. B. White, "Structure of alkali-zinc silicate glasses by raman spectroscopy", Comm. Amer. Ceram. Soc. **67**, C 47-49 (1984).

13. J. Koo, B. S. Bae and H. K. Na, "Raman spectroscopy of copper phosphate glasses", J. Non-Cryst. Solids **212** 173-179 (1997).

14. G. N. Greaves, "EXAFS and the structure of glass", J. Non-Cryst. Solids, **71** 203-217 (1985).

15. P. A. O'Day, J. J. Rehr, S. I. Zabinsky and G. E. Brown Jr., "Extended x-ray absorption fine structure (EXAFS) analysis of disorder and multiple-scattering in complex crystalline solids", J. Amer. Chem. Soc. **116** 2938-2949 (1994).

16. C. R. A. Catlow and J. M. Thomas, "Modelling of catalysts and its relation to experimental problems", Phil. Trans. R. Soc. Lond. A **341** 255-268 (1992).

17. B. Vessal, "Simulation studies of silicates and phosphates", J. Non-Cryst. Solids **177** 103-124 (1994).

18. A. Paul, in Chemistry of Glasses, Chapman and Hall, London (1990).

19. H. Scholze, in Glass: Nature, Structure and Properties, Springer-Verlag, New York (1991).

20. W. H. Zachariasen, "The atomic arrangement in glass", J. Am. Chem. Soc. **54** 3841-3851 (1932).

21. C. J. Phillips, in Glass: The Miracle Maker, Pitman Publishing Corporation, New York (1941).

22. M. B. Volf, in Chemical Approach to Glass, Elsevier, New York (1984).

23. L. V. Woodcock, C. A. Angell and P. Cheeseman, "Molecular dynamics studies of the vitreous state: Simple ionic systems and silica", J. Chem. Phys. **65** 1565-1577 (1976).

24. B. Vessal, M. Leslie and C. R. A. Catlow, "Molecular dynamics simulation of silica glass", Mol. Sim. **3** 123-136 (1989).

25. T. F. Soules, "A molecular dynamic calculation of the structure of sodium silicate glasses", J. Chem. Phys. **71(11)** 4570-4578 (1979).

26. S. K. Mitra, M. Amini, D. Fincham and R. W. Hockney, "Molecular dynamics simulation of silicon dioxide glass" Phil. Mag. B **43(2)** 365-372 (1981).

27. S. H. Garofalini, "Molecular dynamics simulation of the frequency spectrum of amorphous silica", J. Chem. Phys. **76** 3189 (1982).

28. B. Vessal, M. Amini, M. Leslie and C. R. A. Catlow, "Potentials for molecular dynamics simulations of silicate glasses", Mol. Sim. **5** 1-7 (1990).

29. R. Fernández-Perea, F. J. Bermejo and E. Enciso, "Molecular dynamics on a realistic model for a strong glass", Phys. Rev. B **53(10)** 6215-6224 (1996).

30. J. M. Delaye, V. Louis-Achille and D. Ghaleb, "Modeling oxide glasses with Born-Mayer-Huggins potentials: effect of composition on structural changes", J. Non-Cryst. Solids **210** 2232-242 (1997).

31. B. P. Feuston and S. H. Garofalini, "Empirical three body potential for vitreous silica"" J. Chem. Phys. **89(9)** 5818-5824 (1988).

32. S. K. Mitra and R. W. Hockney, "Molecular dynamics simulation of the structure of soda silica", Phil. Mag. B **48(2)** 151-167 (1983).

33. R. G. Newell, B. P. Feuston and S. H. Garofalini, "The structure of sodium trisilicate glass via molecular dynamics employing three-body potentials", J. Mat. Res. **4(2)** 434-439 (1989).

34. J. M. Haile, in Molecular Dynamics Simulation, Elementary Methods, John Wiley and Sons Inc. New York (1992).

35. D. E. C. Corbridge, in The Structural Chemistry of Phosphorus Compounds. Topics in Phosphorus Chemistry Vol. 3, Wiley, New York (1966).

36. J. R. Van Wazer and K. A. Holst, "Structure and Properties of the Condensed Phosphates. I. Some General Considerations of Phosphoric Acids", J. Amer. Chem. Soc. **72(2)** 639-644 (1950).

37. J. R. Van Wazer, "Structure and Properties of the Condensed Phosphates. II. A Theory of the Molecular Structure of Sodium Phosphate Glasses", J. Amer. Chem. Soc. **72(2)** 644-647 (1950).

38. J. R. Van Wazer, "Structure and Properties of the Condensed Phosphates. III. Solubility, Fractionation and Other Solubilty Studies", J. Amer. Chem. Soc. **72(2)** 647-655 (1950).

39. J. R. Van Wazer and D. A. Campanella, "Structure and Properties of the Condensed Phosphates. IV. Complex Ion Formation in Polyphosphate Solutions", J. Amer. Chem. Soc. **72(2)** 655-663 (1950).

40. U. Hoppe, G. Walter, R. Kranold, D. Stachel and A. Barz, "The dependence of structural peculiarities in binary phosphate glasses on their network modifier content", J. Non-Cryst. Solids **192&193** 28-31 (1995).

41. T. Kanazawa, "Structural characteristics of $MgO-P_2O_5$ glasses", J. Non-Cryst. Solids **52** 187-194 (1982).

42. H. Kawazoe, "Coordination number and chemical shift in $K_{\alpha 1-2}$ emission of Mg^{2+} in oxide glasses", J. Non-Cryst. Solids **42** 281-286 (1980).

43. M. P. Allen and D. J. Tildesley, in Computer Simulation of Liquids, Claredon Press, Oxford (1990).

44. J. E. Stanworth, "The ionic structure of glass", J. Soc. Glass Technol. **32** 366-372 (1948).

45. S. K. Mitra, "Molecular dynamics simulation of silicon dioxide glass", Phil. Mag. B **45(5)** 529-548 (1982).

46. L. Verlet, "Computer experiments on classical fluids. I. Thermodynamic properties of Lennard-Jones molecules", Phys. Rev. **159(1)** 98-103 (1967).

47. T. F. Soules, "Molecular dynamics calculations of glass structure and diffusion in glass", J. Non-Cryst. Solids **49** 29 (1982).

48. C. A. Elyard, P. L. Bayton and H. Rawson, "The properties of binary phosphate glasses", Glastechn. Ber. **6** 36-43 (1959).

49. D. W. J. Cruickshank, "Refinements of structures containing bond between Si, P, S or Cl and O or N. VI P_2O_5 Form III", Acta Cryst. **17** 679-680 (1964).

50. W. Matz, D. Stachel and E. A. Goremychkin, "The structure of alkaline earth metaphosphate glasses investigated by neutron diffraction", J. Non-Cryst. Solids **101** 80-89 (1988).

51. A. Musino, G. Pashina, G. Piccaluga and G. Pinna, "Short range order of metaphosphate glasses by x-ray diffraction", J. Non-Cryst. Solids **177** 97-102 (1994).

52. P. K. Gupta, "Non-crystalline solids: glasses and amorphous solids", J. Non-Cryst. Solids **195** 158-164 (1996).

53. M.T. Avenbuch-Pouchot, A. Durif and M. Bagieu-Beucher, "Structure d'un polyphosphate de zinc, $Zn(PO_3)_2$", Acta Cryst. C **39** 25-26 (1983).

54. A. G. Nordand K. B. Lindberg, "The crystal structure of magnesium tetrametaphosphate, $Mg_2P_4O_{12}$", Acta Chem. Scand. A **29(1)** 1-6 (1975).

55. T. Uchino and Y. Ogata, "Ab initio molecular orbital calculations on the electronic structure of phosphate glasses. Binary alkali metaphosphate glasses", J. Non-Cryst. Solids **191** 56-70 (1995).

56. E. Matsubara, K. Sugiyama, Y. Waseda, M. Ashizuka and E. Ishida, "Structural analysis of zinc metaphosphate glass by anomalous x-ray scattering", J. Mat. Sci. Letters **12** 14-16 (1989).

57. M. Bionducci, G. Licheri, A. Musino, G. Nvarra, G. Piccaluga and G. Pinna, "The structure of a Zn(II) metaphosphate glass. I. The cation coordination by a combination of x-ray and neutron diffraction, EXAFS and x-ray anomalous scattering", Z. Naturforsh. **51a** 1209-1215 (1996).

58. U. Hoppe, "A structural model for phosphate glasses", J. Non-Cryst. Solids **195** 138-147 (1996).

59. L. Cervinka, J. Bergerova and M. Trojan, "An x-ray study of phosphate glasses of the composition $[M(PO_3)_2]_n$ (M = Zn, Cu, Mn, Ca and Mg)", J. Non-Cryst. Solids **192&193** 121-124 (1995).

60. G. J. Exarhos, P. J. Miller and W. M. Risen Jr., "Interionic vibrations and glass transitions in ionic oxide metaphosphate glasses", J. Chem. Phys. **60(11)** 4145-4155 (1974).

61. B. N. Nelson and G. J. Exarhos, "Vibrational spectroscopy of cation-site interactions in phosphate glasses", J. Chem. Phys. **71(7)** 2739-2747 (1979).

62. S. W. Martin, "Review of the structures of phosphate glasses", Eur. J. Solid State Inorg. Chem. **28** 163-205 (1991).

63. R. Gresh, W. Muller-Warmuth and H. Dutz, "X-ray photoelectron spectroscopy of sodium phosphate glasses", J. Non-Cryst. Solids **34** 127-136 (1979).

64. R. Dupree, N. Ford and D. Holland, "An examination of the ^{29}Si environment in the $PbO-SiO_2$ system by magic angle spinning nuclear magnetic resonance. Part I. Glasses", Phys. Chem. Glasses **28(2)** 78-84 (1987).

65. T. M. Alam and R. K. Brow, "Local structure and connectivity in lithium phosphate glasses: a solid state ^{31}P MAS NMR and 2D exchange investigation", J. Non-Cryst. Solids **223** 1-20 (1998).

66. R. K. Brow, C. C. Phifer, G. L. Turner and R. J. Kirkpatrick, "Cation effects on ^{31}P MAS NMR chemical shifts of metaphosphate glasses", J. Am. Ceram. Soc. **74(6)** 1287-1290 (1991).

67. R. K. Brow, D. R. Tallant, S. T. Myers and C. C. Phifer, "The short range structure of zinc polyphosphate glass", J. Non-Cryst. Solids **191** 45-55 (1995).

68. R. K. Brow, "An XPS study of oxygen bonding in zinc phosphate and zinc borophosphate glasses", J. Non-Cryst. Solids **194** 267-273 (1996).

69. A. Lai, A. Musinu, G. Piccaluga, S. Puligheddu, "Structural evolution in zinc and lead phosphate glasses by X-ray diffraction and ^{31}P MAS NMR spectroscopy", Chem. Phys. Glasses **38(4)** 173-179 (1997).

70. Y. S. Bobovich, "An investigation of the structure of glassy phosphates using raman spectra", Optics and Spectroscopy **11** 492-497 (1961).

71. B. C. Sales, R. S. Ramsey, J. B. Bates and L. A. Boatner, "Investigation of the structural properties of lead-iron phosphate glasses using liquid chromatography and raman spectroscopy", J. Non-Cryst. Solids **87** 137-158 (1986).

72. T. R. Meadowcroft and F. D. Richardson, "Structural and thermodynamic aspects of phosphate glass", Trans. Faraday Soc. **60** 54-70 (1964).

73. R. G. Della Valle and H. C. Andersen, "Molecular dynamics simulation of silica liquid and glass", J. Chem. Phys. **94** 5056-5063 (1991).

74. D. E. C. "The structural chemistry of phosphates", Bull. Soc. Fr. Mineral. Cristallogr., **94** 7-20 (1971).

75. C. Nelson, T. Furukawa and W. B. White, "Transition metal ions in glasses: network modifiers or quasi-molecular complexes", Mat. Res. Bull. **18** 959-966 (1983).

76. R. E. Tischer, "Effect of compression and compositional changes on the nature of chromium sites in simple glasses", J. Chem. Phys. **48(9)** 4291-4299 (1968).

77. G. H. Sigel, Jr., "Vacuum ultraviolet absorption in alkali doped fused silica and silicate glasses", J. Phys. Chem. Solids **32** 2373-2383 (1971).

78. D. F. Mullica, H. O. Perkins, D. A. Grossie, L. A. Boatner and B. C. Sales, "Structure of dischromate-type lead pyrophosphate, $Pb_2P_2O_7$", J. Solid State Chem. **62** 371-376 (1986).

79. E. M. Rabinovich, "Review lead in glasses", J. Mater. Sci. **11** 925-948 (1976).

80. K. Takahashi, in Advances in Glass Technology, Plenum Press, New York 366-376 (1962).

81. G. W. Brady, "Structure of sodium metaphosphate glass", J. Chem. Phys. **28(1)** 48-50 (1958).

82. D. G. Minser, B. Walden and W. B. White, "Structure of alkali-zinc silicate glasses by raman spectroscopy", Comm. Amer. Ceram. Soc. **67** C47-49 (1984).

83. C. H. MacGillavry, H. C. J. de Decker, L. M. Nijland, "Crystal structure of the third form of phosphorus pentoxide", Nature **164** 448-449 (1949).

84. U. Hoppe, "A structural model for phosphate glasses", J. Non-Cryst. Solids **195** 138-147 (1996).

85. M. Feike, C. Jager and H. W. Spiess, "Connectivities of coordination polyhedra in phosphate glasses from ^{31}P double-quantum NMR spectroscopy", J. Non-Cryst. Solids **223** 200-206 (1998).

86. T. Okura, N. Aoki and T. Kanazawa, "Molecular orbital study for short and medium range order of P_2O_5 glass", J. Non-Cryst. Solids **95&96** 427-432 (1987).

87. F. L. Galeener, J. C. Mikkelsen, Jr., "The Raman spectra and structure of pure vitreous P_2O_5", Solid State Communications **30** 505-510 (1979).

88. F. L. Galeener, J. C. Mikkelsen Jr., R. H. Geils and W. J. Mosby, "The relative Raman cross sections of vitreous SiO_2, GeO_2, B_2O_3 and P_2O_5", Appl. Phys. Lett. **32(1)** 34-36 (1978).

89. W-B. Chang, Z-Z. Jin and X-W. Zou, "Calculated infrared and Raman spectra of P_2O_5 glass", Physics Letters A **159** 361-364 (1991).

90. M. F. Thorpe and F. L. Galeener, "Central force model for the high frequency vibrational bands of glasses", J. Non-Cryst. Solids **35&36** 1197-1202 (1980).

91. J. Wong, "Vibrational spectra of vapor-deposited binary phosphosilicate glasses", J. Non-Cryst. Solids **20** 83-100 (1976).

92. A-R. Grimmer and G-U. Wolf, "^{31}P-MAS-NMR studies on crystalline and vitreous polymorphs of phosphorous pentoxide P_2O_5", Eur. J. Solid State Inorg. Chem. **28** 221-232 (1991).